



Study of digital compensation techniques for 50G-PON optical access networks

Flávio André Nogueira Sampaio

► To cite this version:

Flávio André Nogueira Sampaio. Study of digital compensation techniques for 50G-PON optical access networks. Signal and Image processing. Ecole nationale supérieure Mines-Télécom Atlantique, 2023. English. NNT : 2023IMTA0345 . tel-04089838

HAL Id: tel-04089838

<https://theses.hal.science/tel-04089838>

Submitted on 5 May 2023

HAL is a multi-disciplinary open access archive for the deposit and dissemination of scientific research documents, whether they are published or not. The documents may come from teaching and research institutions in France or abroad, or from public or private research centers.

L'archive ouverte pluridisciplinaire **HAL**, est destinée au dépôt et à la diffusion de documents scientifiques de niveau recherche, publiés ou non, émanant des établissements d'enseignement et de recherche français ou étrangers, des laboratoires publics ou privés.

THESE DE DOCTORAT DE

L'ÉCOLE NATIONALE SUPERIEURE MINES-TELECOM ATLANTIQUE
BRETAGNE PAYS DE LA LOIRE - IMT ATLANTIQUE

ECOLE DOCTORALE N° 648
Sciences pour l'Ingénieur et le Numérique
Spécialité: Mathématiques et Sciences et Technologies de
l'Information et de la Communication

Par

Flávio André NOGUEIRA SAMPAIO

**Etude des techniques de compensation numérique
pour les réseaux d'accès optique 50G-PON**

Thèse présentée et soutenue à Plouzané, IMT Atlantique, le 02/03/2023
Unité de recherche : LABSTICC
Thèse N° : 2023IMT0345

Rapporteurs avant soutenance :

Christophe Peucheret Professeur, ENSSAT, FOTON
Christelle Aupetit-Berthelemot Professeure, ENSIL-ENSCI, Université de Limoges

Composition du Jury :

Président :	Stéphane Azou	Professeur, ENIB, LAB-STICC
Examineurs :	Christophe Peucheret	Professeur, ENSSAT, FOTON
	Christelle Aupetit-Berthelemot	Professeure, ENSIL-ENSCI, Université de Limoges
	Frédéric Lehmann	Professeur, Telecom SudParis, Samovar
	Ghaya Rekaya-Ben Othman	Professeure, Telecom Paris, MIMOPT
	Naveena Genay	Ingénieure de recherche, Orange Innovation
Dir. de thèse :	Raphaël Le Bidan	Enseignant-chercheur, IMT Atlantique
Co-dir. de thèse :	Yves Jaouën	Professeur, Telecom Paris

Invité :

Erwan Pincemin, Ingénieur de recherche, Orange Innovation

Acknowledgements

I would like to express my gratitude to my supervisors. I wish to thank Naveena Genay, Erwan Pincemin, and Yves Jaouën for their technical advice, resources, and effort to ensure the best condition for developing the thesis. Also, I want to thank my supervisor Raphaël Le Bidan. I am grateful for the privilege to learn from him, for his welcome at Brest, for the time he dedicated to this thesis and for all the lessons about digital communication and the method to solve problems, to always go deep without leave any detail behind.

I want to thank my colleagues from Orange for their hospitality in Lannion, the technical support, and the encouragement that was important for my formation as a person and professional. Thanks, Minqi Wang (more precisely 王旻琦) and Anas El Ankouri, for their friendship, help, standing together as a team in the good and the difficult times, and most of all, for their sincere friendship. I also thank Gaël Paul Simon and Fabienne Saliou for their advice and help in integrating into the work and life in Brittany. To Philippe Chanclou I express my sincere thanks for agreeing with this immense opportunity, his attention to the work, the resources destined for the thesis and his recognition of this work. I also wish to thank my colleagues: Jeremy Potet, Fabien Scagnelli, David Patient, Clara Catanese, Reda Ayassi, Eric Pitard, Frédéric Miet, Régine Angoujard Miet, Dylan Chevalier, Georges Gaillard, Sylvain Barthomeuf, Fabrice Bougart, Nicholas Brochier, and Christophe Billant.

I would like to thank Mathilde Gay and Laurent Bramerie for the opportunity to work in the FOTON laboratory.

I want to thank the precursors of this journey and lifetime friends Vinicius Nunes Henrique Silva, Luiz Anet Neto, and Tadeu Nagashima for the first opportunity, their trust, patience, and your outstanding presence under challenging moments that allowed me to keep going forward.

For the great moments outside work, I want to thank the Krampouz Ultimate club for their hospitality, and the great memories during the trainings and championships especially my cherish friends Tangui Le Bourdonnec, Emilien Corbin, Anna Le Coadou and Noémie Guillerme.

Finally, I would like to thank my parents, my brother, and my uncles for their unconditional support in my life choices and for their effort to be present even at long distances.

Résumé en Français

Motivation

Au cours des années suivantes, les débits requis pour les réseaux d'accès sont immenses en raison de l'augmentation massive des appareils connectés et des applications gourmandes en bande passante. Les réseaux optiques passifs (PON) sont le choix classique pour les travaux d'accès car ils allient un faible coût et une capacité de débit de transmission élevée. Les chercheurs de l'industrie travaillent au sein des groupes de normalisation ITU-T et IEEE à augmenter la capacité d'un canal optique 10 Gbit/s à 25 Gbit/s, 50 Gbit/s et même 100 Gbit/s. Cette thèse se concentre sur les techniques de compensation numérique pour le 50G-PON parce que c'est l'évolution qui devrait être déployée en premier sur le terrain et que le canal optique est gravement impacté par la dispersion chromatique, le chirp, la limitation de la bande passante et l'atténuation.

- Nous avons utilisé deux modèles qui se rapprochent des conditions réelles d'un PON basé sur la modulation d'intensité et la détection directe (IM/DD), un modèle petit signal construit dans MATLAB© et un modèle grand signal via VPI Transmission Maker™.
- Nous avons étudié la compensation de l'interférence intersymbole (ISI) via l'égalisation linéaire et l'égalisation à retour de décision (LE et DFE respectivement) basées sur le critère d'erreur quadratique moyenne minimale (MMSE), et montré comment prédire les performances de l'égaliseur au moyen d'équations simples, sur la base d'un modèle du canal.
- Nous avons également considéré l'utilisation d'un récepteur optimal au sens du maximum de vraisemblance (MLSE) pour compenser les distorsions linéaires et non linéaires. Les trois récepteurs compensateurs de distorsions ont été optimisés pour avoir une complexité minimale et pour correspondre aux exigences de performance de la prochaine génération PON recommandées par l'ITU-T.
- Enfin, nous avons réalisé des transmissions hors ligne expérimentales dans le laboratoire 50Gbit/s d'Orange. Les mesures expérimentales ont conforté le modèle IM/DD simulé, et les trois récepteurs basés sur DSP ont été évalués en conditions réelles.

Organisation du Manuscrit

Le manuscrit est décomposé en 6 chapitres, une introduction et une conclusion et des annexes.

L'introduction générale, présente succinctement les différentes générations de réseaux optiques passifs et la structure du manuscrit au travers de quelques lignes descriptives de chaque chapitre.

Le chapitre 1 décrit brièvement les besoins et l'évolution des réseaux d'accès optiques. Le principal objectif de ce chapitre c'est de présenter les options de mise en œuvre des PON 50G et les exigences du système, en particulier la sensibilité cible du récepteur. Dans ce chapitre c'est spécifié pourquoi les réseaux optiques passifs (PON) sont une réponse technique appropriée et propose une description de leur évolution chronologique, génération par génération en précisant comment chacune d'elles permet de fournir des connexions de qualité à mesure que les débits binaires, la bande passante et les appareils connectés augmentent. Ensuite les normes relatives à ces évolutions du PON ainsi que les feuilles de route qui sont établies par les trois grandes organisations d'entreprises qui les érigent à savoir, le groupe Full Service Access Network (FSAN), l'Union Internationale des Télécommunications (ITU) et le groupe de travail Ethernet 802.3 de l'Institute of Electrical and Electronic Engineers (IEEE). Cette rétrospective permet de conforter le sujet de la thèse qui s'intègre dans une récente préconisation sur le 50G-PON avec une ONU compatible avec des DSP, capable d'égalisation côté récepteur.

Le modèle de canal optique basée sur la modulation d'intensité et la détection directe (IM/DD) est présenté au chapitre 2. Les caractéristiques opérationnelles du laser à semi-conducteur, de la fibre et de la photodiode, intégrant les phénomènes pénalisants et bruits, sont bien décrites par les expressions dérivées des équations de Maxwell. Elles sont utilisées pour représenter la physique et la forme d'onde en temps continu. Sont pris en compte deux régimes de fonctionnement, petit et grand signal permettant, d'adapter les modèles développés. Les fonctions de transfert sont également détaillées. Le besoin d'égalisation est introduit du point de vue de la bande passante limitée et de la présence d'encoches d'évanouissement dans la réponse en régime en fréquence en régime de petit signal, y compris l'émetteur (DML ou EML), la fibre optique dispersive, et la photodiode. Des simulations d'un lien selon plusieurs configurations envisageables ont été effectuées en utilisant les logiciels VPI et/ou Matlab. Les réponses en fréquence et impulsionnelles du canal sont fournies en régime des petits signaux, comparées et analysées en prenant en compte les interférences inter-symboles. La bibliographie est souvent rappelée pour situer les résultats obtenus. Ensuite les performances simulées pour chacune des configurations sont données et la solution avec l'EML ne répond pas exactement aux préconisations du fait d'une ISI trop importante.

Le troisième chapitre expose la théorie et la mise en œuvre des égaliseurs numériques pour traiter les dégradations IM/DD identifiées dans le chapitre précédent. Tout d'abord, une théorie de prédiction de performance en closed form, en supposant que la réponse du canal est connue, du fonctionnement de l'égaliseur basée sur le critère d'erreur quadratique moyenne minimale (MMSE) et leurs applications à l'égaliseur linéaire (LE) sont présentées. Puis une détermination adaptative des coefficients de taps basée sur la version adaptative du MMSE, basé sur le algorithme moindre carré moyen (LMS-LE) est utilisé. Les performances des systèmes considérés (EML ou DML à l'émetteur, au récepteur bandes passantes de 18.75 GHz et 37.5 GHz) sont ensuite évalués après transmission et égalisation avec le LMS-LE. Pour minimiser la complexité d'égalisation et maximiser la performance du récepteur basée sur des techniques de compensation de

distorsions sont présentées. Puis l'égaliseur LMS-LE est appliquée aux scénarios de simulation présentés. Son apport a été discuté et démontré par rapport à un lien qui en est dépourvu, montrant qu'il gère très bien les impacts linéaires de la limitation de la bande passante en présence de bruit. Toutes les configurations proposées respectaient la sensibilité et le budget optique requis avec une égalisation linéaire dont les limites ont été évaluées. Il a été vérifié que le retard ajouté par le MMSE-LE est négligeable pour les applications HS-PON compatibles DSP (exigences ITU-T).

Le chapitre 4 suit exactement la même structure que le chapitre 3 mais est maintenant appliqué à un égaliseur à retour de décision (DFE) Le DFE complémente l'égaliseur linéaire vu au chapitre 3 pour faire face à l'ISI (interférence inter symbole) résiduelle du canal 50G IM/DD. Dans un premier temps la structure et le principe de fonctionnement du MMSE-DFE sont proposés. Puis l'égaliseur à rétroaction basée sur le critère MMSE-DFE, les expressions mathématiques pour sa prédiction en closed form et l'implémentation adaptative en utilisant le algorithme adaptative (LMS-DFE) est présenté. La méthode d'optimisation pour déterminer le nombre de coefficients minimum dans les filtres d'anticipation et de rétroaction du MMSE-DFE pour respecter la sensibilité de récepteur recommandée et un taux de erreur à 10^{-2} (prise en compte de codes correcteurs d'erreurs LDPC) pour le HS-PON est bien détaillée en s'appuyant sur un logigramme complet. Tout ceci est ensuite appliqué au lien descendant HS-PON à 50 Gbits/s avec des émetteurs EML et DML et un récepteur à base d'APD à bande passante définie, comme dans le chapitre précédent. Il est montré que pour atteindre la sensibilité recommandée par l'UIT-T, seulement 2 coefficients sur le filtre FF et un sur le filtre FB sont suffisants. La dernière partie compare les prédictions sous forme fermée obtenues aux performances simulées du LMS-DFE et du LMS-LE sur le 50G HS-PON basé sur EML et DML.

Le cinquième chapitre s'intéresse aux méthodes de compensation des distorsions non linéaires introduites par les composants d'extrémités des blocs émetteurs et récepteurs, qui ne sont pas corrigées par ce qui a été développé dans les chapitres précédents. Il s'agit d'utiliser à la réception des techniques d'estimation de la séquence de vraisemblance maximale (MLSE). Ici, deux métriques de branche différentes, basées sur l'estimation d'un linéaire canal et bruit gaussien, ou basé sur l'extraction des statistiques de l'échantillon par la construction de histogrammes, sont comparés. Après avoir introduit les généralités nécessaires à ce chapitre, deux versions de MLSE sont introduites et évaluées à travers les simulations de canaux optiques basées sur EML et DML. La première est basée sur un modèle de canal gaussien linéaire et la seconde sur la fonction de distribution de probabilité conditionnelle (PDF) des séquences reçues. Le MLSE-GEN présente plus d'avantages que le MLSE-LIN en termes de complexité et de performances d'égalisation. Il est plus adapté pour compenser les distorsions non linéaires du canal HS-PON et atteindre les performances requises par l'ITU-T.

Le chapitre 6 porte sur quelques comparaisons expérimentales des performances des différents égaliseurs. L'égalisation est effectuée hors ligne après la conversion analogique-numérique dans un oscilloscope en temps réel. Après avoir étudié par simulation le régime petit signal pour donner les caractéristiques physiques du HS-PON et le modèle grand signal pour analyser l'impact du canal sur les transmissions au plus près de la réalité, il est proposé dans le sixième chapitre de montrer expérimentalement les performances qui ont pu être atteintes avec le lien IM/DD à 50Gbit/s. Les tendances obtenues en mesures sont dans la même logique que les simulations. Il apparaît que le SNR du canal optique impacte beaucoup les performances des égaliseurs et qu'il sera nécessaire de privilégier un récepteur par rapport aux autres, en prenant en compte les complexités bien entendu.

Le dernier chapitre est la conclusion qui synthétise l'ensemble du travail effectué pendant la thèse et propose des perspectives envisagées à ce travail.

Contributions scientifiques

Les parties du travail de recherche décrites dans cette thèse ont conduit à la publication des articles suivants :

Publications en tant que premier auteur:

An analysis of linear digital equalization in 50Gbit/s HS-PONs to compensate the combined effect of chirp and chromatic dispersion

F. A. N. Sampaio E. Pincemin, N. Genay, L. A. Neto, R. Le Bidan, Y. Jaouen. In 2021 Conference on Lasers and Electro-Optics Europe & European Quantum Electronics Conference (CLEO/Europe-EQEC), virtual conference, 2021.

Study of Minimum Mean Square Error Optimal Equalizers for 50Gbit/s High Speed Passive Optical Networks

F. Sampaio, N. Genay, E. Pincemin, R. Le Bidan, Y. Jaouen, and F. Bourgart, in OSA Advanced Photonics Congress, paper SpF1E.2, virtual conference, 2021.

Publications en tant que deuxième auteur:

Low Bandwidth APD Receiver Assessment with Fixed FIR Filter and SOA for Multi-Rate and Several Wavelengths of Class N1 and C+ of Higher Speed PONs

G Gaillard, F Saliou, J Potet, G. Simon, P. Chanclou, F. N. Sampaio, in European Conference and Exhibition on Optical Communication, Mo4C. 2, Basel, Switzerland, 2022.

5G & optics in 2020-where are we now? what did we learn?

Fabienne Saliou, Luiz Anet Neto, Gael Simon, Flavio Nogueira Sampaio, Anas El Ankouri, Minqi Wang, Philippe Chanclou, 2020 European Conference on Optical Communications (ECOC), Brussels, Belgium, 2020.

Mots clés: égalisation, modulation d'intensité, réseau optique passif, traitement des signaux numériques.

Abstract

Over the following years, the required bit rates for access networks are immense due to the massive increase of connected devices and bandwidth-hungry applications. Passive Optical Networks (PON) are the conventional choice for access works because they ally low cost and have high transmission rate capacity. As industry researchers from ITU-T and IEEE target increasing the single channel capacity from 10 Gbit/s to 25Gbit/s, 50Gbit/s, and 100 Gbit/s, this thesis focuses on digital compensation techniques for the 50G-PON since the optical channel is critically impaired by chromatic dispersion, chirp, bandwidth limitation, and attenuation. The work was organized as follows:

- We used two models that approximate the real conditions of a PON based on Intensity Modulation and Direct Detection (IM/DD), a small-signal model constructed in MATLAB[®] and a large signal model via VPI Transmission Maker[™].
- Intersymbol Interference (ISI) compensation through Minimum Mean Square Error (MMSE) linear and decision feedback equalization (LE and DFE, respectively). Furthermore, we predicted the equalizers performance through closed-form equations.
- Maximum Likelihood Sequence Estimation (MLSE) to compensate for linear and nonlinear distortions. Then the three DSP-based receivers were optimized to have minimal complexity and to meet the performance requirements of the next PON generation recommended by ITU-T.
- Finally, we realized experimental offline transmissions in Orange's 50Gbit/s laboratory. The experimental measurements confronted the simulated IM/DD model, and the three DSP-based receivers were evaluated in practice.

Keywords: equalization, intensity modulation, passive optical network, digital signal processing.

List of acronyms

ACS	Add-Compare-Select
AWGN	Additive White Gaussian Noise
ADC	Analog-to-Digital Converter
ASIC	Application-specific integrated circuit
AGC	Automatic Gain Control
APD	Avalanche Photodiode
BCE	Best Channel Estimation
BER	Bit Error Ratio
BM	Branch Metric
BMR	Branch Metric Register
CD	Chromatic Dispersion
CMR	Cumulated Metric Register
DSP	Digital Signal Processing
DAC	Digital-to-Analog Converter
DML	Directly Modulated Laser
DMT	Discrete Multitone
EAM	Electro-Absorption Modulator
EML	Externally Modulated Laser
ER	Extinction Ratio
FFT	Fast Fourier Transform
FB	Feedback
FF	Feedforward
FFE	Feedforward Equalizer
FIR	Finite Impulse Response
FSM	Finite State Machine
FSE	Fractionally Spaced Equalizer

FSR	Fractionally Spaced Receiver
FM	Frequency Modulation
FSAN	Full Service Access Network
HS-PON	Higher Speed Passive Optical Networks
IM	Intensity Modulation
IMDD	Intensity Modulation and Direct Detection
IM	Intensity modulator
ITU-T	International Telecommunications Union
ISI	Intersymbol Interference
IFFT	Inverse Fast Fourier Transform
LD	Laser Diode
LMS	Least Mean Square
LMS-DFE	Least Mean Square Decision Feedback Equalizer
LMS-LE	Least Mean Square Linear Equalizer
LS	Least Square
MFB	Matched Filter Bound
MLSD	Maximum Likelihood Sequence Detection
MLSE	Maximum Likelihood Sequence Estimator
MSE	Mean Square Error
MMSE-DFE	Minimum Mean Square Error Decision Feedback Equalizer
MMSE-LE	Minimum Mean Square Error Linear Equalizer
NN	Neural Network
NRZ-OOK	Non-return-to-zero On-Off-Keying
ODN	Optical Distribution Network
OLT	Optical Line Terminal
ONU	Optical Network Unit
OFDM	Orthogonal Frequency Division Multiplexing
PON	Passive Optical Network

PM	Phase Modulation
PTP	Point-to-Point
PIN	Positive-Intrinsic-Negative
PRBS	Pseudorandom Binary Sequence
PAM	Pulse Amplitude Modulation
ROP	Received Optical Power
SOA	Semiconductor Optical Amplifier
SMF	Single-Mode Fiber
SNR	Signal-to-Noise Ratio
SPR	Survivor Path Register
SSE	Symbol Spaced Equalizer
SBS	Symbol-by-Symbol
TWDM	Time and Wavelength Division Multiplexing
TDM	Time Division Multiplexing
VOA	Variable Optical Attenuator
VDA	Viterbi Decoding Algorithm
VE	Viterbi Equalizer
WDM	Wavelength-Division Multiplexing
ZF	Zero Forcing
ZFE	Zero-Forcing Equalizer

Contents

Acknowledgements	i
Résumé	ii
Abstract	vi
List of acronyms	viii
Thesis Publications	xiv
General Introduction	1
1 Context and Motivations.....	3
1.1 Introduction.....	3
1.2 Background and motivation	3
1.2.1 Fixed access optical network.....	4
1.3 Passive optical networks	4
1.4 Overview of ITU-T and IEEE PON systems and standards	6
1.5 Major characteristics of PON devices	8
1.5.1 Modulation and detection.....	9
1.5.2 Major PON requirements	10
1.6 Concluding remarks.....	12
2 Intensity Modulation and Direct Detection based Optical Channel and Receiver Architecture	14
2.1 Introduction.....	14
2.2 Intensity modulation and direct detection.....	14
2.3 Small signal regime transmission model.....	15
2.3.1 Laser transfer function	17
2.3.2 Intensity modulation transfer function	17
2.3.3 Photodetector model.....	19
2.4 The receiver architecture	20
2.4.1 Discrete-time equivalent channel model	21
2.5 50G HS-PON implementation.....	23
2.6 Simulated performance of the 50G-PON	23
2.6.1 Small signal regime simulation parameters	24

2.6.2	Analysis of the unchirped, EML, and DML sources in small signal regime	25
2.6.3	Parameters of the 50G PON channel large signal simulations	26
2.6.4	Performance of 50G PON channel	28
2.7	Concluding remarks	29
3	Digital Filter Based Linear Equalization Techniques to Compensate the 50G-PON Channel Distortions	31
3.1	Introduction	31
3.2	Equalization-based digital filters	31
3.3	The MMSE linear equalizer	32
3.3.1	The criterion of the MMSE-LE	33
3.4	The closed form MMSE-LE	34
3.5	The adaptive LMS-LE	36
3.6	MMSE-LE optimization methodology	37
3.7	Theoretical performance of the MMSE-LE over the 50G-PON	37
3.7.1	Closed form performance prediction	38
3.8	Simulated performance of the LMS-LE over the 50G-PON	43
3.8.1	The EML + 25G Rx	43
3.8.2	The EML + 50G Rx	44
3.8.3	The DML + 25G Rx	45
3.8.4	The DML + 50G Rx	46
3.8.5	Transient analysis of the LMS-LE	46
3.9	Main results of the linear equalizer	47
3.10	Concluding remarks	48
4	Decision Feedback Equalization to improve the 50G-PON Receiver	50
4.1	Introduction	50
4.2	The MMSE decision feedback equalizer	50
4.3	The closed-form MMSE-DFE	51
4.4	The adaptive LMS-DFE	54
4.5	MMSE-DFE optimization methodology	55
4.6	Performance of MMSE-DFE over 50G-PON channels	56
4.6.1	Closed-form prediction	56
4.7	Simulated performance of the LMS-DFE and LMS-LE over the 50G HS-PON based on EML and DML	65

4.7.1	The EML + 25G Rx channel	65
4.7.2	The EML + 50G Rx channel	66
4.7.3	The DML + 25G Rx channel	67
4.7.4	The DML + 50G Rx channel	69
4.7.5	Transient analysis of the LMS-DFE	70
4.8	Main results of the DFE	71
4.9	Concluding remarks.....	72
5	Maximum Likelihood Sequence Estimation: An Optimal Solution for the 50G-PON	74
5.1	Introduction.....	74
5.2	The sequence detection	74
5.2.1	The goal of the MLSE	76
5.3	The variants of the MLSE receiver	77
5.3.1	The linear Gaussian channel-based model MLSE	77
5.3.2	The generalized version of the MLSE	78
5.4	The Viterbi algorithm implementation	80
5.4.1	The MLSE optimization.....	81
5.5	Simulated performance of the MLSE and MMSE receivers over the 50G HS-PON based on EML and DML	82
5.5.1	Channel estimation	82
5.5.2	The EML + 25G Rx based channel.....	85
5.5.3	The EML + 50G Rx based channel.....	86
5.5.4	The DML + 25G Rx based channel.....	88
5.5.5	The DML + 50G Rx based channel.....	89
5.5.6	Performance comparison of the MMSE and MLSE equalizers	91
5.6	Concluding remarks.....	91
6	Experimental Demonstration of the LE, DFE, and MLSE based Receivers.....	92
6.1	Introduction.....	92
6.2	Experimental setup	92
6.3	Receivers optimization methodology	93
6.4	Experimental and simulated performance of the DSP-based receivers over the 50G-PON channel in downstream condition	93
6.4.1	LMS-LE experimental performance over the 50G-PON DS channel	

6.4.2	LMS-DFE experimental performance over the 50G-PON DS channel	96
6.4.3	MLSE experimental performance over the 50G-PON DS channel	97
6.4.4	Experimental performance comparison of the MMSE equalizers and MLSE based receivers	98
6.4.5	Transient analysis of the MMSE and MLSE-based receivers	99
6.4.6	Comparison of small-signal and measured frequency response .	100
6.5	Experimental performance of MLSE and MMSE receivers over the 50G-PON channel in upstream conditions	101
6.6	Concluding remarks	102
7	Conclusions.....	103
	Future perspectives	104
	Appendix A	106
	Appendix B	107
	Appendix C	108
	Appendix D	109
	Bibliography	110

Thesis Publications

Parts of the research work described in this thesis have led to the publication of the following papers:

Publications as the first author

An analysis of linear digital equalization in 50Gbit/s HS-PONs to compensate the combined effect of chirp and chromatic dispersion

F. A. N. Sampaio E. Pincemin, N. Genay, L. A. Neto, R. Le Bidan, Y. Jaouen. In 2021 Conference on Lasers and Electro-Optics Europe & European Quantum Electronics Conference (CLEO/Europe-EQEC), virtual conference, 2021.

Study of Minimum Mean Square Error Optimal Equalizers for 50Gbit/s High Speed Passive Optical Networks

F. Sampaio, N. Genay, E. Pincemin, R. Le Bidan, Y. Jaouen, and F. Bourgart, in OSA Advanced Photonics Congress, paper SpF1E.2, virtual conference, 2021.

Publications as co-author

Low Bandwidth APD Receiver Assessment with Fixed FIR Filter and SOA for Multi-Rate and Several Wavelengths of Class N1 and C+ of Higher Speed PONs

G Gaillard, F Saliou, J Potet, G. Simon, P. Chanclou, F. N. Sampaio, in European Conference and Exhibition on Optical Communication, Mo4C. 2, Basel, Switzerland, 2022.

5G & optics in 2020-where are we now? what did we learn?

Fabienne Saliou, Luiz Anet Neto, Gael Simon, Flavio Nogueira Sampaio, Anas El Ankouri, Minqi Wang, Philippe Chanclou, 2020 European Conference on Optical Communications (ECOC), Brussels, Belgium, 2020.

General Introduction

There is an explosion in the consumption of internet services that forces telecommunications engineers to find solutions that allow for increasing the capacity of transmission systems. Passive Optical Network (PON) enables users and servers to exchange information at higher rates.

Passive optical network systems are becoming more and more deployed worldwide. However, the PONs must allow higher rates and ensure low costs and sufficient transmission quality. Several companies (operators, vendors) work together through standardization bodies to guarantee PON with ever-increasing speeds. In the physical layer, this means an infrastructure based on Intensity Modulation and Direct Detection (IM/DD) with low-cost optical components, higher bandwidths, with recommended performances such as Optical Budget (OB), sensitivity, bit error ratio (BER), latency, and complexity that allow modern and future applications.

Since 1995 PONs started with rates of hundreds of Mbit/s with the APON, evolved to 1Gbit/s with GPON, then to 10Gbit/s with XG-PON, and now speed is at 50Gbit/s with a network known as higher speed PON (HS-PON or HSP), where one of the pivotal technologies is Digital Signal Processing (DSP) [1]. At this bit rate, there are expectations of the introduction of an Analog-to-digital Converter (ADC) capable of converting analog signals into digital signals, an equalizer to compensate the channel distortions, and a more advanced Forward Error Correction (FEC), known as Low Density Parity Check (LDPC), which enables the lowest PON pre-FEC threshold of 10^{-2} compared to previous PON generations.

Assuming the scenario of a PON with an ADC at the end-user side, the main objective of this thesis is to evaluate how digital equalization contributes to 50Gbit/s communications in PONs, mainly through off-line digital signal processing.

This thesis is structured as follows: Chapter 1 introduces the PON, the need for higher bit ratios around the world, the PON standards evolution through time, the major impairments of the optical channel, and the choice of IM/DD over coherent systems in the access networks context, and the essential PON characteristics. Chapter 2 details the IM/DD PON effects from the perspective of a small-signal regime to understand the impact of chirp, chromatic dispersion, bandwidth limitation, and photodiode. Then it presents the channel modeling into an equivalent discrete-time channel model, next the architecture of the DSP-based receiver, and the performances of the 50G-PON channel with Externally Modulated Lasers (EMLs) and Directly Modulated Laser (DMLs) in the small-signal and large-signal regimes. Chapter 3 introduces the digital equalization techniques, especially the Minimum Mean Square Linear Equalization (MMSE-LE). It presents the closed-form and adaptive realization through the Least Mean Square (LMS), the implementation of the Linear Equalizer (LE) based on the Minimum Mean Square Error (MMSE) to calculate the equalizer taps. Next, the theoretical and simulated performance with the EML and the DML setups in the large-signal condition previously presented in Chapter 2 are discussed. Then, Chapter 4 introduces an equalization technique more advanced than the LE. It details the Minimum Mean Square Error Decision Feedback Equalizer (MMSE-DFE) in the same manner as the LE. First, it presents the closed form to obtain the tap coefficients and predict the performance of the DFE, then the LMS version of the DFE followed by the

theoretical and simulated performance of the EML and DML based channels. Also, the DFE and LE are compared. Finally, Chapter 5 presents the MLSE, for which two versions are described. First, the linear version assumes a linear channel impacted by Additive White Gaussian Noise (AWGN). Next, a more generalized version of the MLSE, without linearity or AWGN assumption, is introduced. Afterward, the implementation method and the performance through the EML and DML based channels are evaluated and compared with the LE and the DFE. Then, Chapter 6 shows the assessment of the DSP architecture in an experimental demonstration with 50Gbit/s transmissions, followed by comparisons of measured and simulated results. Finally, most of this work's contents are summarized in Chapter 7.

1 Context and Motivations

1.1 Introduction

Data use increases daily due to the growth of connected devices and applications that requires higher speed traffic. The access networks enterprises allow users to reach the services they want with the required quality for a good experience.

This chapter presents the context of passive optical access networks. Here the structure of optical access networks, applications, and the evolution of standards proposed by the leading industry operators and vendors are discussed. Then, we discuss the overall characteristics and challenges present in Passive Optical Networks (PONs) and the requirements envisaged for the present and next PON generation.

Chapter 1 is organized as follows: section 1.2 introduces the applications, the increasing demand for higher bit rates worldwide, and the bottleneck of access networks. Next, the PON infrastructure and topologies are discussed in section 1.3. Afterward, the historical evolution, deployment, and standards considering downstream and upstream communication are presented in section 1.4. Next, the effects, impairments, requirements, and key-enabling PON technologies are discussed in section 1.5. Section 1.6 discusses the main content of the chapter, especially the next PON generation subject.

1.2 Background and motivation

Since the beginning of the Internet in 1968 [2], the trend has been to improve services and connectivity. Today, access to information is almost effortless. It became easy to research data on any subject, to communicate with people worldwide remotely through Whatsapp, or even listen to a song thanks to the evolution of the Internet. The fast connection allows us to reach immersive applications such as the experience of watching the highlights of the football's world cup 4K or 8K Ultra High Definition (UHD) on Youtube, playing video games, or accessing the metaverse using Virtual Reality (VR).

Furthermore, the increase in connected users and devices is impressive. The prediction from Cisco for 2023 is that nearly two-thirds of the world's population will have access to the Internet. A total of 5.3 billion users and 29.3 billion connected devices are expected [3]. The deployment of the Internet is organized in a hierarchical infrastructure network to meet the demand for connectivity, as shown in figure 1.1.

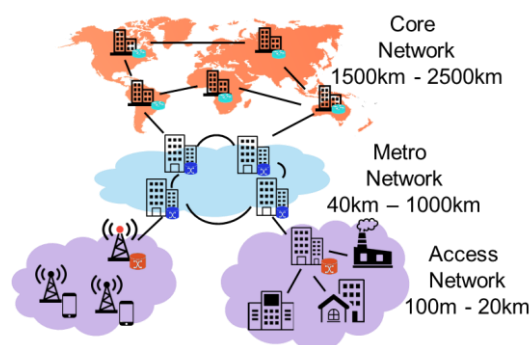


Figure 1.1: The representation of the telecommunication network segments.

The hierarchy architecture has three layers with different topologies and objectives. The core network, also known as the backbone, interconnects cities, countries, and continents and usually spans distances up to 2500km. It provides any-to-any connections with a mesh topology. The metro network uses a ring topology with ranges from 40km to hundreds of kilometers conventionally. Both above mentioned networks use optical fiber and compose the optical transport network. Their objective is to ensure transport, multiplex, switching, and reliability to transport data with terabit rates from client to client [4]–[6]. Finally, the subject of study of the thesis: Access networks connect users of the last mile to the other networks. The links connections have a range of a few meters to 20 kilometers. It connects dispersed users through a capillary-like topology. Compared to optical transport networks, access networks operate at rates of the order of tens of gigabits and must have limited costs since they have a limited number of users sharing the common network elements.

1.2.1 Fixed access optical network

At the beginning of the access network deployment, the communication relied on twisted copper pairs and coaxial cables, as in the digital subscriber lines (DSL) and cable modem connections. However, due to the aging and necessary improvement of quality, as the line rates of DSL grow, the copper-based networks transmission capacity constrained the access networks throughput and costs. To avoid network bottleneck, the operators substitute electrical cables with optical fiber. This trend was noticed generation after generation of networks. Also, the fibers have other advantages over copper since they are not severely impacted by electromagnetic interference (EMI) and hence are more stable and achieve lower latency transmission, which is critical as the bit rate increases. Fiber growth can be noticed in France. The use of fiber in France started in 2007, allowing users to reach a shared connection of 2.5Gbit/s downstream, and today the studies are looking towards the deployment of 50Gbit/s PON.

Actual applications such as Netflix video streaming with 4K streaming enabled requires a connection speed of 16 Mbit/s [7]. For instance, in France, there is a plan for a high bit rate seeking to increase the user bit rate beyond 30 Mbit/s [8]. Hence, access networks need constant improvement as time goes by.

Passive optical access networks evolve generation after generation to deliver quality connections as the higher bit rates, bandwidth, and connected devices increase. The following section will detail the PON and its historical evolution.

1.3 Passive optical networks

A PON is a system used by telecommunications service providers to ensure connectivity to users to deliver services through passive optical devices. figure 1.2 shows the diagram of a PON.

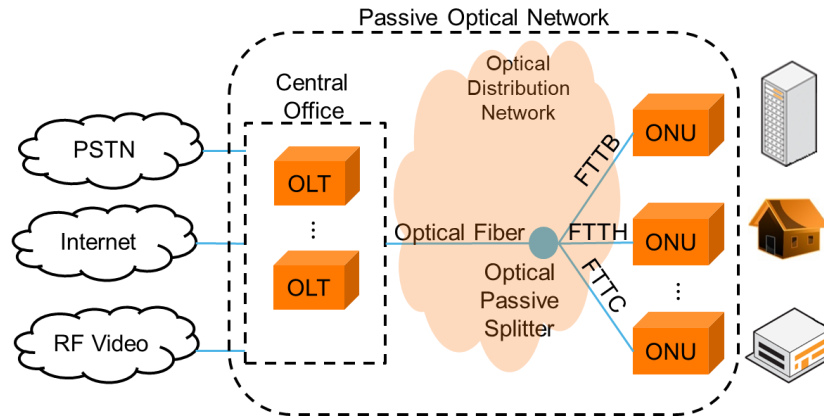


Figure 1.2: The passive optical network.

A PON consists of an Optical Line Terminal (OLT) localized in the operator's Central Office (CO) that sends data through an optical fiber to Optical Network Units (ONUs) installed in the user premises. The PON shares data flow using a passive optical distribution network (ODN) based on a passive optical splitter. Thus a single fiber outgoing from the OLT at the CO is shared between many terminations either individual or shared. The passive split ratio performed by the splitters is commonly 64 but can range from 16 to 128.

The sharing solutions are named FTTx (Fiber to the x), where x represents the end-user premise [9]. The most used options are FTTH (Fiber to the Home), FTTB (Fiber to the Building), and FTTC (Fiber to the Curb). In FTTH each user has its optical termination ONU. In the FTTB or FTTC, the ONUs are shared between several users and feature an individual copper drop. The provided services by the operators are the Internet, the Public Switched Telephone Network (PSTN), and the radiofrequency video (RF video). The constraints of costs for access networks pressured the operators to propose solutions adapted to the user's infrastructure.

The communication between the OLT and ONU is Point-To-Multipoint (PTMP) to ensure broadband access with less expensive infrastructure. Consequently, the optical power is divided by the optical splitter, which ratio is 1 to N, or 1:N, where N is the number of fiber outputs. So far, the PON uses Time-Division Multiplex (TDM) and Time Division Multiplex Access (TDMA) to manage the data traffic. Otherwise, the Wavelength Division Multiplex (WDM) and the combination of TDM and WDM are alternatives.

In the TDM/TDMA PON, over a transmission with N time slots, each slot is allocated to an ONU, and the OLT manage the bidirectional communication that may be Downstream (DS) or Upstream (US), both with frames of 125 μ s.

In the downstream configuration, the OLT broadcasts data from metro networks to each ONU in different recurring timeslots on a single wavelength channel. In other words, in continuous-mode downstream transmission, each ONU identifies and retrieves data from its allowed channel (since the time slot might change from frame to frame DS), as illustrated in figure 1.3 a).

In the upstream (US) configuration, the transmission comes from the ONU to the OLT in burst mode, as depicted in figure 1.3 b). In other words, during the OLT's assigned time slots, the ONU sends data to the OLT. The ONU data are transmitted

and arrive in sequential form without overlap through time multiplexing. Different wavelengths are used over downstream and upstream transmissions [5], [10].

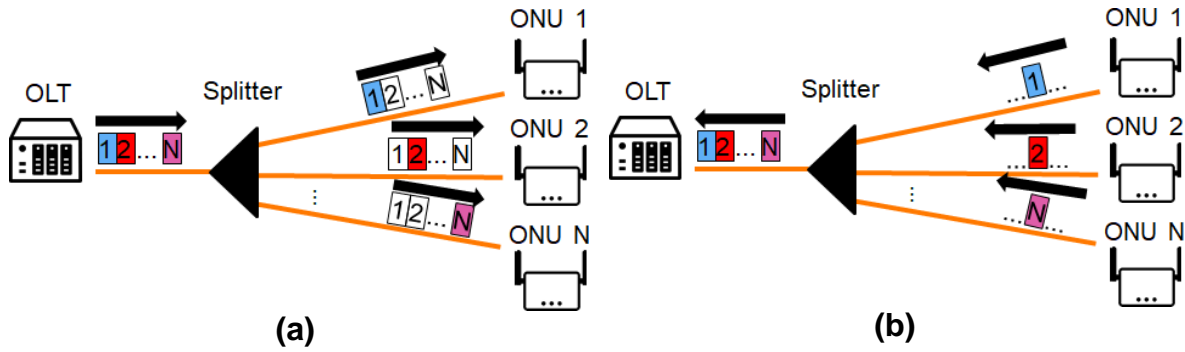


Figure 1.3: Simplified TDM-PON architecture in (a) downstream and (b) upstream configurations.

In WDM-PON, each ONU is assigned a wavelength, for downstream and upstream transmissions, through an Array Waveguide Grating (AWG) to multiplex and demultiplex wavelengths coming from the ONU or OLT. Here the division of ONU is based on the number of wavelengths, and the WDM-PON forms a Point-to-Point (PTP) system [11].

1.4 Overview of ITU-T and IEEE PON systems and standards

Different operators propose PON systems and solutions. Therefore, different equipment is developed to supply the PON market [12]. The PON systems were standardized to ensure interoperability between different devices and low cost of deployed infrastructure.

The main objective of the standards is to increase the data rate without a high power budget and allow a higher bandwidth to more subscribers [13]. In other words, the standards supply the required higher bit rates and increase in subscribers while addressing problems of latency, synchronization, power budget, etc.

Access networks Standards Development Organizations (SDOs) are guiding the research and development strategy of today and future generations of access networks [11]. Three major industrial organizations are leading the PON standardization: the Full Service Access Network (FSAN) group, the International Telecommunication Union (ITU), and more precisely, the ITU Telecommunication Standardization Sector (ITU-T) Question 2/ Study Group 15 (Q2/15), and the Institute of Electrical and Electronic Engineers (IEEE) 802.3 Ethernet Working Group [11].

The FSAN organization was established in 1995. It comprises 70 organizations with leading operators, internet service providers, and equipment provider groups [10], [14]. ITU-T and FSAN developed the APON/BPON, GPON, XG-PON, and NG-PON2 standards. The IEEE is also a certified standard development organization, primarily Local Area Network (LAN) service oriented. They developed the EPON and 10G EPON standards series [13]. Both standards seek low-cost devices and to have successive generations compatible with one another. For instance, each standard has a series of recommendations for the different system generations. For example, the ITU-T ensures Transmission Convergence (TC), Physical Media Dependent (PMD) specifications for PON.

Figure 1.4 shows the ITU-T and IEEE standards roadmap.

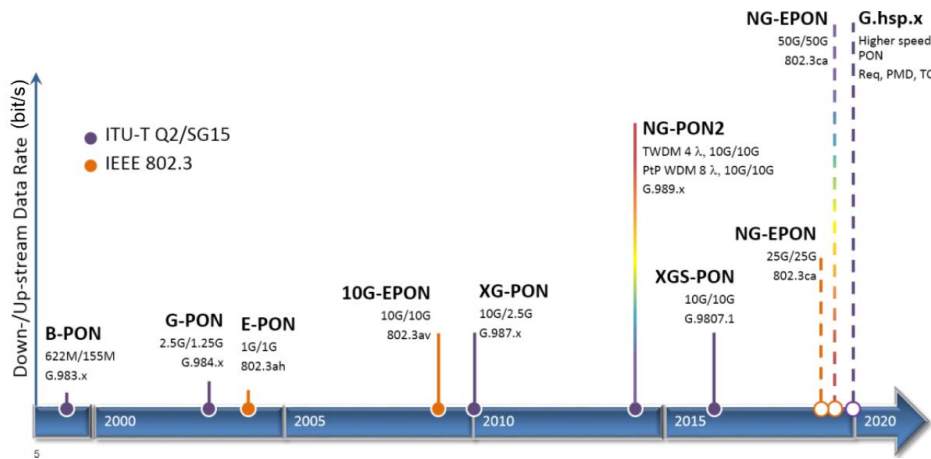


Figure 1.4: Roadmap of PON standardization by ITU-T in purple circles and by IEEE in orange circles [15].

In the 90s, both FSAN and ITU-T developed the first generation of A-PON, based on Asynchronous Transfer Mode (ATM) technology with a bit rate of 155 Mbit/s in DS and the US. When the bit rate of DS and US are equal, the system speed is entitled symmetric, otherwise is asymmetric. In 1995, the WDM technology was added to the A-PON, forming the B-PON, known by the recommendation G.983.x.[16] With an asymmetrical speed of 622Mbit/s in DS and 155Mbit/s in US.

In 2004, the Ethernet PON (E-PON) standard was developed by IEEE, recommendation 802.3ah, with a symmetric rate of 1.25 Gbit/s [17]. The EPON uses the Ethernet protocol instead of ATM, hence more suitable for data services, but it requires mapping all services in ethernet packets. However, it has poor bandwidth use and does not efficiently support real-time services [10]. In the same year, ITU-T and FSAN introduced the Gigabit PON (G-PON), using TDM in DS and US with variable rates up to 2.5 Gbit/s and 1.25 Gbit/s. The novelty of the G-PON was the high quality of delay-sensitive service, voice data, and video, also known as triple-play services.

Between 2009 and 2011, ITU-T and IEEE launched the standards capable of 10Gbit/s rates: First, IEEE introduced the 10G-EPON, followed by clause 802.03av [18] with symmetric and asymmetric rate, then ITU-T the asymmetric XG-PON, note that X represents 10, with 10Gbit/s in downstream and 2.5Gbit/s in upstream related in the recommendation G.987.x [19]. In 2016, ITU-T introduced the XG(S)-PON, where S means symmetric, with a rate of 10 Gbit/s upstream in recommendation G.9807.1 [19]. In parallel with the XG(S)-PON ITU-T proposed an system based on WDM, combined with the TDM, the Time and Wavelength Division Multiplexing (TWDM). The NG-PON2 solution allowed the transmission of 10Gbit/s per wavelength channel, achieving an aggregated rate of 40Gbit/s. Still, the costs due to complexity and tunable optical system obliged the vendors to reduce attention to this standard based on recommendation G.989 [20].

Then, the principal objective was to improve the bit rate in a single wavelength. The PON with bit rates of 25, 50, and 100 Gbit/s have been discussed in the IEEE 802.3ca 50G-EPON task force group. The task force aimed on the improvement of rates from 10Gbit/s to 25Gbit/s, extending next to 50Gbit/s and 100 Gbit/s, using multiplexing two and four wavelengths [21]. Finally, ITU-T started in 2018 the discussion for the 50Gbit/s per wavelength PON, known as 50G-PON or the Higher

Speed PON (HSP or HS-PON) considering the G.hsp.x series of recommendations approved in 2019 and consented in April 2021 [1]. Note that the rate transition from ITU-T is a leap from 10Gbit/s to 50Gbit/s using a single wavelength, commonly abbreviated 50Gbit/s/λ, which λ means wavelength.

The higher speed PON profits from the advances in key technologies such as optical transceiver bandwidth augmentation [22], Semiconductor Optical Amplifier (SOA) [23], and Forward Error Correction (FEC) based on Low-Density Parity Check (LDPC) [24]. We highlight that it is the first time ITU-T has recommended channel distortion through digital signal processing [1],[25]. This thesis follows the hypothesis proposed by ITU-T: a 50G-PON with a DSP-enabled ONU capable of equalization on the receiver side.

With the compromise of adjacent PON generations compatibility, the ITU-T proposes a legacy of PON with a dedicated wavelength plan for each generation, as depicted in figure 1.5.

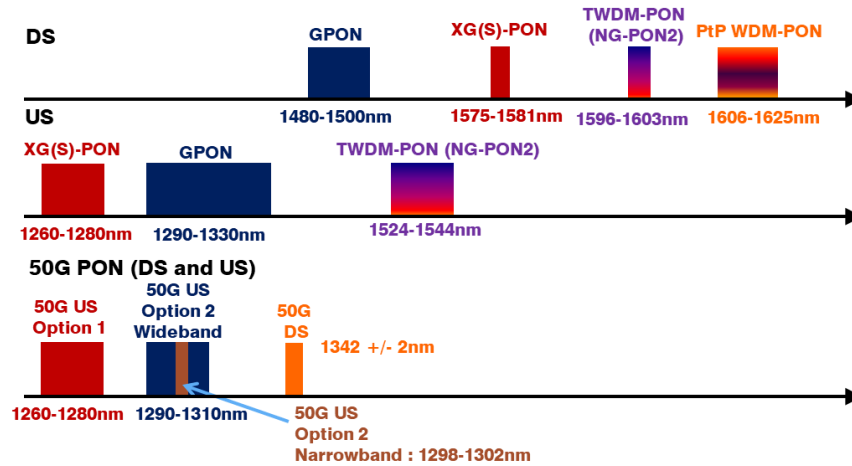


Figure 1.5: Wavelength plan for the actual and the 50G PON generation by ITU-T, adapted from [26].

For instance, we note that the GPON and the XGS-PON work on different wavelength intervals, imagining that multiple transceivers are used for the ONU-OLT links. For the 50G-PON, two options for upstream are considered considering an optical narrowband and wideband, and the wavelengths bandwidths vary from 1340 nm to 1344 nm. We also note that the coexistence of the HS-PON with either GPON or XGS PON systems with the compromise of legacy infrastructure is expected. A recent extension is studying possible triple coexistence between GPON, XG(S)-PON, and HS-PON. The wavelength window of 1284nm-1288nm has been proposed to enable a triple coexistence between GPON, XG(S)-PON, and HS-PON [27].

1.5 Major characteristics of PON devices

Each PON generation had compromises of cost, coexistence, and complexity. Here the essential features of the ITU-T PON are discussed.

1.5.1 Modulation and detection

The essential elements of the optical system are the semiconductor lasers, the fiber, and the photodiode. To ensure higher-speed transmissions, the optical transmitters and receivers are developed to be faster, consume less energy, and have higher bandwidth [13], [28], [29].

The two principal optical communication systems comprise Intensity Modulation and Direct Detection (IM/DD) or coherent detection. The main difference is that IM/DD only recovers the intensity of transmitted signals. In contrast, coherent detection recovers the amplitude and phase of signals with the help of a local oscillator.

In the 50G and previous PON scenarios, the IM/DD considers binary modulation format: Non-Return-to-Zero on-off keying (NRZ-OOK) [30]. Since the first generation, the IM/DD has been the choice for PON because it offers a good balance between optical performance and cost since minimizing the analog electronic aspects can be easily integrated into Application-Specific Integrated Circuits (ASICs) [31], [32]. The IM/DD system emitter comprises two main methods to modulate the electrical signal on an optical carrier: direct and external modulation, which is based on Electro-Optic Modulation (EOM) or Electro-Absorption Modulation (EAM).

The passive optical networks adopt Directly Modulation Laser (DML) and Externally Modulated Lasers (EML) because it relies on the existence of high-volume, low-cost optical-electronic components transceivers [13]. The optical transport networks use more expensive optical emitters such as the Mach-Zehnder Modulator (MZM) [33] and coherent detection.

The most widely used PON optical fiber is the Standard Single-Mode Fiber (SSMF) type G.652 [34]. It has a profile of attenuation and chromatic dispersion that is very interesting for the wavelengths used in the optical access networks range (from 1275 nm to 1675 nm) [5], as illustrated in figure 1.6.

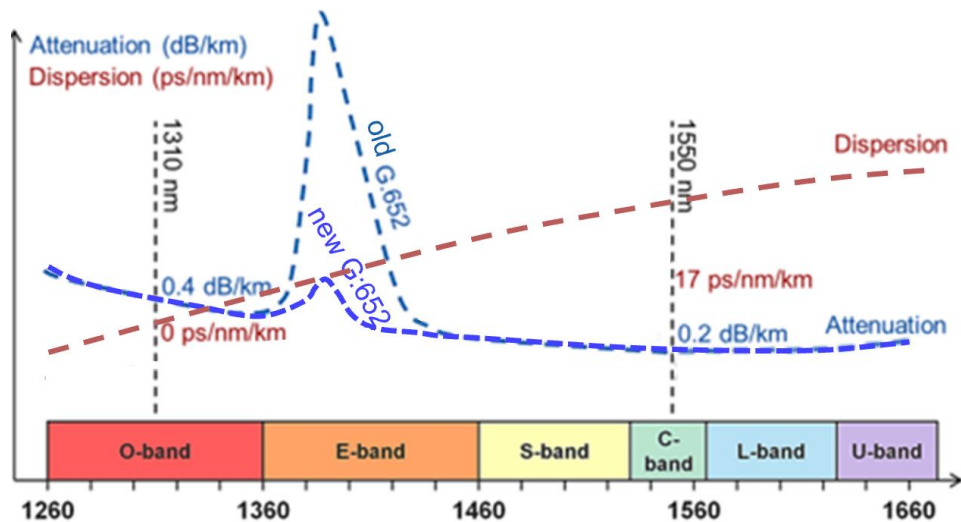


Figure 1.6: The attenuation and chromatic dispersion per wavelength in SMF, Adapted from [5], [35].

Note that the GPON, XGS-PON, and HS-PON use wavelengths of lower attenuation and dispersion (bands C and O). The downside of IM/DD is the frequency selectivity, hence Intersymbol Interference (ISI) due to 1) electro-optical device limitations, such as limited bandwidth, electro-optical conversion, and chirp, and 2) fiber constraint, principally Chromatic Dispersion (CD). The CD, chirp, and bandwidth limitations degrade the transmission quality, as we will see in more details in chapter 2.

At the front end of the IM/DD optical chain, there is a Photodetector (PD) capable of detecting the signal at the fiber output. In the PON, three options are considered, a PD without amplification (PIN photodiode), a PIN followed by an SOA, and last, an Avalanche Photodiode (APD) to ensure enough sensitivity to the receiver at the output of the ODN [23].

The above-mentioned PON impairments may be classified as linear or nonlinear. Table 1.1 summarizes the major impairments that affect the HS-PONs.

Table 1.1: The major impairments of the PON, adapted from [10].

	Impairments	Linearity
Transmitter	Chirp	Nonlinear
	Limited bandwidth	Linear
	Electro-optic conversion	Nonlinear
Fiber	Chromatic dispersion	Linear
	Power attenuation	Linear
Optical Receiver	Thermal noise	Gaussian
	Amplifier gain saturation	Nonlinear
	Limited bandwidth	Linear

We note that the NRZ-OOK format is used in PON because it can tolerate worse signal-to-noise ratios in the presence of CD [32]. The PON researchers seek solutions to reach higher bit rates despite the optical channel impairments by proposing new FEC techniques, modulation formats, and now DSP equalization to achieve reliable transmission in increasingly challenging environments.

1.5.2 Major PON requirements

We briefly introduced the main of PON evolution. Each PON generation had a proposed bit rate, wavelength (represented by λ) plan, and optical impacts caused by the IM/DD system. However, each PON generation has a requirement that should be respected to allow the desired performance by the operators.

The compromise of new PON systems is explained in [11]. The cost, the coexistence with legacy PON, and migration depend on the operator's network architecture and business model. Typically, the re-utilization of the already deployed optical distribution network reduces costs, mainly based on a maximum fiber reach and power budget. The optical design could severely influence the applications, especially considering the number of used wavelengths, the impacts, the used FEC technique, and the latency.

The typical TDM-PON standard ensures transmissions with a range of up to 20 km, a target sensitivity, and an Optical Budget (OB). The sensitivity is denoted by S and is the minimum average optical power required by the receiver to achieve a target Bit Error Ratio (BER) [35]. In the PON scenario, the OB is:

$$OB [dB] = P_{TX} [dBm] - S [dBm] \quad (1.1)$$

where P_{TX} is the average optical power at the output of the emitter, and S is the sensitivity of the receiver. The optical budget constitutes the principal limit in the realization of the architecture of the optical access network. For each PON generation, optical budget classes allow a minimal and maximal attenuation level.

Overall deployed and future PON targets common loss budget and fiber reach [12]. The $OB = 29$ dB is typically envisaged, and it is known as N1 in ITU-T. For instance, the HS-PON recommends the deployment of the N1 and C+ (32 dB) optical budget and the sensitivity of $S = -24$ dBm in downstream transmissions at 50Gbit/s.

The key enabling technologies for the HS-PON are the high-speed transceivers and FEC-LDPC. The optical transceiver options were discussed in [27]. Figure 1.7 shows the 50G-PON device options.

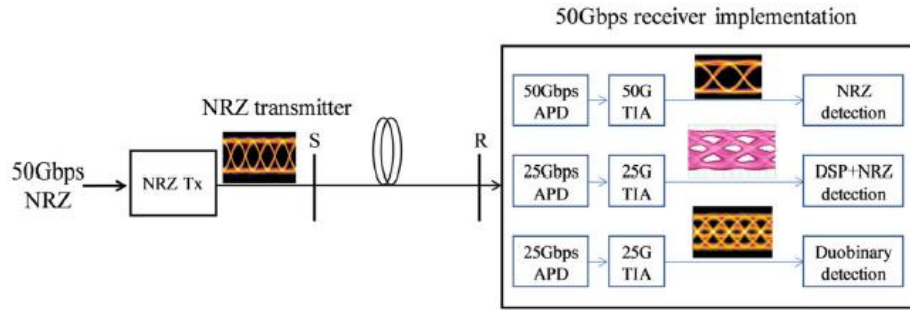


Figure 1.7: The implementation options for the HS-PON, obtained from [27]. Tx: Transmitter; TIA: transimpedance amplifier.

The optical emitter option enables transmissions at 50Gbit/s. Its 3dB bandwidth is conventionally 75% of the bit rate in this context. For example, the EML has a bandwidth $B = 37.5GHz$. On the frontend side, two APDs are considered: The 50Gbit/s capable, with $B = 37.5GHz$ which is more expensive, and the 25Gbit/s capable, with $B = 18.75 GHz$, which is less costly. A TIA follows the APD and a signal detector. See more details of the HS-PON options in [27].

During this thesis, we evaluate an IM/DD system with a 50G emitter and the 25G and 50G APDs options as illustrated in Figure 1.8.

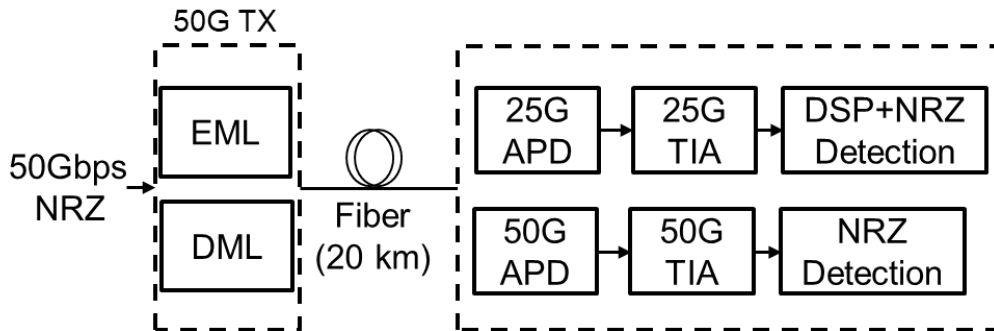


Figure 1.8: The explored solutions for the HS-PON during the thesis.

We suppose that the 25G receiver is the most practical choice because it is the less costly option. Furthermore, each new PON profits from devices already deployed in the previous generation. The main goal of this work is to evaluate the performance of 50G-PON in the presence of IM/DD impacts with ideal and more realistic devices, then to understand how much digital compensation techniques may contribute to the next passive optical network generation.

The forward error correction technique is essential to increase the optical budget and sensitivity. The FEC based on Reed-Solomon (RS) coding enabled the XGPON to operate with BER as low as 10^{-3} in downstream and was commonly used in previous PON generations. Furthermore, the HS-PON defines the pre-FEC-LDPC that allows a pre-FEC $BER = 10^{-2}$ threshold [12]. Table 1.2 summarizes the ITU-T PON standards.

Table 1.2: The major options of existing PON generations proposed by ITU-T, adapted from [10].

Standard	GPON	XG(S)-PON	NG-PON2	HS-PON
Recommendation	G.984.x	G.9807.x	G.989.x	G.hsp.x
Downstream rate (Gbit/s)	2.5	10	10	50
Upstream rate (Gbit/s)	1.25	2.5 or 10	10	25
Pre-FEC threshold and code (Downstream)	10^{-10} RS(255,239) (optional)	10^{-3} RS(248,216)	10^{-12} RS	10^{-2} (LDPC)
Optical budget (dB) and class	28 (B+)	29 (N1)	25 (L2)	29 (N1)
Receiver sensitivity in the downstream system with FEC (dBm)	-28	-28	?	-24

We highlight that, for the following of the thesis, the HS-PON recommended sensitivity $S = -24$ dBm based on the FEC-LDPC limit 10^{-2} , and the optical budget are used as performance metrics. Also, we suppose that the HS-PON has a 50Gbit/s capable optical emitter in the transmitter. We evaluate the PON's optimistic and realistic APD. In other words, we consider the 25G and 50G APD, followed by a device with distortion compensation capability, which will be introduced in the next chapter.

1.6 Concluding remarks

As the data consumption grows, access networks are organized to ensure quality transmission in upstream and downstream communication to the users in houses, offices, and other premises. We saw that bodies such as the ITU-T, the FSAN, and IEEE work on standards for each generation of passive optical networks.

This chapter introduced the motivation for PON, its applications, concepts, evolution, standards, impairments, and the technologies that preceded the 50G-PON. The motivation of this chapter was to show that each PON has requirements and key enabling technologies. It opens the discussion of the next PON generation, which targets a sensitivity $S = -24$ dBm and an optical budget of at least 29 dB. Which the HS-PON system is based on intensity modulation and direct detection with a binary communication format.

In the next chapter, the optical effects of the PON channel are detailed and evaluated. Also, a DSP-enabled receiver is proposed and evaluated in the context of 50G HS-PON, considering the above-mentioned performance requirements of sensitivity and optical budget presented in this chapter.

2 Intensity Modulation and Direct Detection based Optical Channel and Receiver Architecture

2.1 Introduction

The 50G TDM-PON is the step forward of the XG-PON. The PON operators will certainly use the 10Gbit/s PON infrastructure and key-enabling technologies to reach higher rates with low-cost compromise. The first chapter introduced the context of the next generation of passive optical networks and the structure and impairments of the PON. This chapter describes the 50G PON with DSP enabled, taking into account the limitations of the actual and the new PON devices under development.

The intensity modulation and direct detection is more detailed in this chapter. Two perspectives of the IM/DD system are studied. First, the optical vision of the IM/DD channel is detailed, and then the optical impairments are translated into the digital communication domain considering the equivalent discrete channel model. The receiver architecture assumes the DSP as a key enabling technology for the next generation of passive optical networks due to the limited performance of the optical receiver at 50Gbit/s.

This chapter is organized as follows: First, a general IM/DD model is presented in section 2.2. Then, the effects of chirp, chromatic dispersion, bandwidth limitation, and noise are introduced in section 2.3, especially considering the small signal regime. Section 2.4 presents the receiver architecture and the equivalent discrete model. Then, section 2.5 describes the implementation of the 50G simulation considered in the thesis. Then, section 2.6 shows the effects of the channel in the time and frequency domain based on the small signal regime parameters. Followed by discussions of the performance of the 50G PON channel. Section 2.7 highlights the key points of the chapter.

2.2 Intensity modulation and direct detection

Figure 2.1 represents the intensity modulated and direct detection optical communication system model [30], [36].

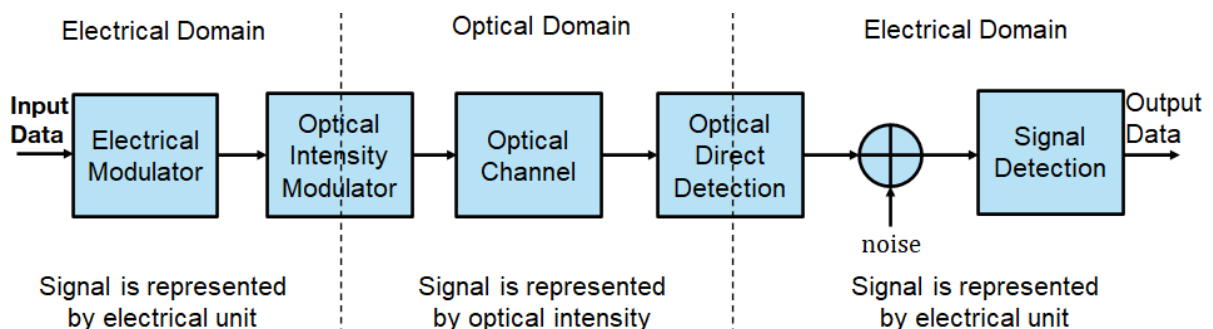


Figure 2.1: The IM/DD optical channel model.

In the IM/DD principle, digital data is converted into a real electrical signal that modulates the light intensity emitted by an optical source. The intensity-modulated

optical signal propagates through an optical channel. Then, the direct-detection-based receiver converts the optical intensity back to an electrical signal. The detector considers ideal square-law detection [35]. Consequently, the phase information of the received signal is lost. This model assumes Additive White Gaussian Noise (AWGN) over the received signal, and finally, the transmitted information is recovered through a symbol detector [37].

As mentioned in chapter 1, especially in the HS-PON context, the electrical modulator generates on-off-keying pulses at 50 Gbit/s with NRZ line coding. Three options represent the intensity modulator (IM): a Mach-Zehnder Modulator (MZM), which can be made close to an unchirped source, an Electro-Absorption Modulator (EAM), entitled here Externally Modulated Laser (EML), or a Directly Modulated Laser (DML). Single Mode Fiber (SMF) represents the optical channel, and the optical receiver consists of a PIN photodiode (PD) or an avalanche photodiode (APD).

The operational characteristics of the semiconductor laser, fiber, and photodiode are described well by rate equations [35]. Those equations are derived from Maxwell's equations, and they are used to represent the physics and the continuous time waveform [38]. When the amplitude of the optical signal is small, the system may operate in Small Signal Regime (SSR), hence the optical devices (IM, SMF and PD) are represented by transfer functions. Otherwise, if the amplitude of optical signal is large, the system operates in a large signal regime. In other words, both mentioned regimes represent the IM/DD model.

Here, the small signal regime is used to understand the linear impacts of the optical emitter, the fiber, and the photodiode, because it gives a good insight into the PON's physical phenomena with few parameters, also enlightens this model the contribution of linear equalizers to compensate optical impact. The following section introduces the small signal analysis and approximations.

2.3 Small signal regime transmission model

The laser is polarized with a bias current I_b . Lasing occurs when the bias is superior to the threshold current I_{th} . Then, the optical intensity is modulated through a current $I_m(t)$. The optical output pulses are based on the current levels of the electrical modulator, and the pulse format injected into the laser. As mentioned in chapter 1, in the 50G PON context, the pulse shaping is NRZ-OOK, with the frequency response $H_{NRZ}(f)$ [39]. Hence, the electrical modulation current is:

$$I_{in}(t) = I_b + I_m(t) \text{ [A]} \quad (2.1)$$

The electrical current $I_{in}(t)$ (intensity or volts unit) is converted into optical intensity $P_{in}(t)$ (watts unit), hence the output power is given by:

$$P_{in}(t) = \delta_{PI} \times I_{in}(t) \text{ [W]} \quad (2.2)$$

assuming the current above the threshold $I_{in}(t) \geq I_{th}$ and the current to the power scaling factor δ_{PI} . Naturally I_b defines the mean average optical power of the optical emitter P_{avg} . Figure 2.2 shows the electrical current-to-power conversion through a Laser Diode (LD).

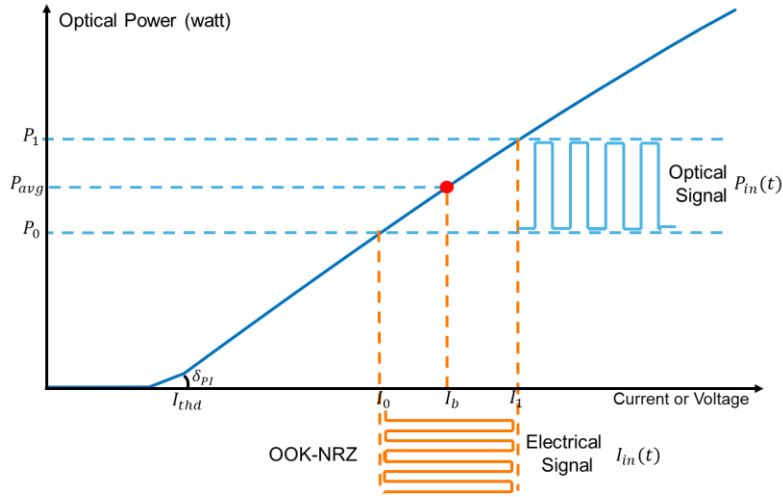


Figure 2.2: The electrical to optical conversion.

The magnitude of the modulating current $I_m(t)$ describes the optical field at the output of the laser

$$E_{in}(t) = \sqrt{P_{in}(t)} e^{j\phi(t)} e^{j\omega_0 t} \quad (2.3)$$

The channel model used here is based on [30] and [38]. The optical source is centered at $\omega_0 = 2\pi f_0$, and modulated by both intensity and phase components. $\phi(t)$ is the phase modulation term. It considers the modulation of the optical frequency of the light caused by $I_{in}(t)$, also known as chirp, and will be more detailed in the next section. Furthermore, the amplitude of the modulating current $I_m(t)$ is very important to understand in which regime the laser operates. When the amplitude of $I_m(t)$ is large, the laser rate equations define the optical model. However, when the amplitude of the modulating signal is small:

$$|I_m(t)| \ll |I_b - I_{thd}| \text{ [A]} \quad (2.4)$$

the laser rate equations can be linearized and solved analytically to obtain an approximate linear model of the laser in the form of a transfer function [35], [38]. This approach is used because the laser rate equations have nonlinear nature, and it is necessary to solve them numerically [35].

This section introduces the IM/DD based on the small signal perspective, where the small signal transfer function is composed of the laser amplitude modulation $H_{LAS}(f)$, the fiber transfer function $H_{SMF}(f)$, and the photodiode transfer function $H_{PD}(f)$, as depicted in figure 2.3.

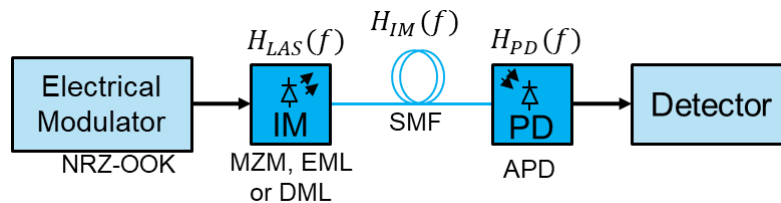


Figure 2.3: The simplified IM/DD PON system.

As mentioned in chapter 1, especially in the HS-PON context, the electrical modulator generates on-off-keying pulses at 50 Gbit/s with NRZ line coding. Here, we study the MZM, the EML, and the DML. Single Mode Fiber (SMF) represents the optical channel, and the optical receiver consists of a PIN photodiode or an avalanche photodiode (APD).

2.3.1 Laser transfer function

Since the optical signal is intensity modulated, it presents a double-sided band in the optical domain. The optical source suffers from effects that cause oscillations and impact the emitted signal. In small signal regime, the modulation transfer function of the semiconductor laser is given by [35]:

$$H_{LAS}(\omega) = \frac{1}{1 - \left(\frac{\omega}{\omega_r}\right)^2 + j2\gamma\left(\frac{\omega}{\omega_r}\right)} [\text{W/A}] \quad (2.5)$$

Here, the angular electrical modulation frequency is $\omega = 2\pi f$, the angular relaxation oscillation frequency is $\omega_r = 2\pi f_r$, and the damping parameter is γ . We look forward to a transfer function that describes the intensity modulation without taking into account the chirp and the electro-to-optical conversion. Furthermore, the optical channel is a single-mode fiber. Hence the signal is constrained by frequency chirp and chromatic dispersion [40].

The laser rate equation describes the interaction between phase and intensity modulation in a laser. Consequently, the changes in carrier density impact the optical field inside the laser cavity. The relation between the instantaneous frequency $\nu(t)$ and the optical modulation power $P_{in}(t)$ is reported by [35]:

$$\nu(t) = \nu_0 + \Delta\nu(t) = \frac{\alpha}{4\pi} \left(\frac{1}{P_{in}(t)} \frac{dP_{in}(t)}{dt} + \kappa P_{in}(t) \right) \quad (2.6)$$

With

$$\Delta\nu(t) = \mu(t) - \mu_0 = \frac{1}{2\pi} \frac{\partial\phi(t)}{dt} \quad (2.7)$$

μ_0 is the emission frequency at threshold, α is the chirp parameter, κ is the laser adiabatic chirp constant related to the intensity modulation and gain compression. All these parameters depend on the laser's physical characteristics, for example, the confinement factor and carrier lifetime. In equation 2.6, the term $\frac{\alpha}{4\pi} \left(\frac{1}{P_{in}(t)} \frac{dP_{in}(t)}{dt} \right)$ represents the transient chirp, it only exists when the emitted power varies with time. The term $\frac{\alpha}{4\pi} (\kappa P_{in}(t))$ is entitled adiabatic chirp.

2.3.2 Intensity modulation transfer function

The term $\phi(t)$ designs the light chirp due to the intensity modulation of the electrical signal. During intensity modulation $I_{in}(t)$ varies, hence the optical modulation power of the source $P_{in}(t)$ changes causing the frequency chirp, in other words $P_{in}(t)$ cause the variation of the carriers' density, and the source refractive index is directly impacted [30],[41].

Based only on chromatic dispersion, the propagated slowly-varying envelope is expressed by [35]:

$$E_{rec}(\omega) = E_{in}(\omega)e^{-j\beta(\omega)L_F} \quad (2.8)$$

The optical field at the output of fiber in the frequency domain is calculated through the Fourier transform, where $E_{in}(\omega)$ is the frequency-domain electrical field obtained after the Fourier transform of $E_{in}(t)$. $\beta(\omega)$ is the propagation constant that may be expanded through Taylor expansions into [42]:

$$\beta(\omega) = \beta_0 + (\omega - \omega_0)\beta_1 + \frac{1}{2}(\omega - \omega_0)^2\beta_2 + \frac{1}{6}(\omega - \omega_0)^3 + \dots \quad (2.9)$$

with

$$\beta_n = \left. \frac{\partial^n \beta(\omega)}{\partial \omega^n} \right|_{\omega=\omega_0} \quad (2.10)$$

the optical source is centered at $\omega_0 = 2\pi f_0$, each of the terms β_0 and β_1 are related to the phase and group velocities of the modulated electromagnetic field. β_2 and β_3 are associated with the fiber's chromatic and third-order dispersion parameters and the residual terms to higher-order dispersion [30], [42]. Assuming optical emission far from the zero-dispersion wavelength, $\beta(\omega)$ may be truncated to the third term [42]. Here, β_0 can be neglected because the rapidly varying part of the optical field does not influence the amplitude of the channel frequency response, also β_1 may be ignored by switching from a static to a moving referential with velocity $v_g \equiv 1/\beta_1$ [30]. Hence, the only term considered is β_2 [42]:

$$\beta_2 = -\frac{\lambda_0^2 D}{2\pi c} \quad (2.11)$$

where D is the fiber dispersion coefficient, and c is the speed of light in the vacuum. Assuming that $\frac{1}{P(t)} = \frac{1}{P_{avg}}$, the intensity modulation transfer function is developed in [46] and investigated in [32], [47]:

$$H_{SMF}(\omega) = \left| \cos(\theta) - \alpha \sin(\theta) \left(1 - j \frac{\omega_c}{\omega} \right) \right| \quad (2.12)$$

where $\omega_c = 2\pi f_c$ is related to the adiabatic chirp, responsible for the different emission frequencies observed under steady state when bits "1" or "0" are transmitted.

$$\theta = \frac{L_F D \lambda_0^2 \omega^2}{4\pi c} \quad (2.13)$$

The chromatic dispersion coefficient is D , and the emission wavelength is λ_0 . Note that the impact of chromatic dispersion is also present in θ . The small signal transfer function (equation 2.12) may be decomposed based the optical emitter, as depicted in table 2.1 [41]:

Table 2.1: The fiber small signal transfer functions and parameters [30].

Emitter	$H_{IM}(\omega)$	Chirp factor	Adiabatic chirp frequency
Unchirped	$ \cos(\theta) $	$\alpha = 0$	$f_c = 0 \text{ GHz}$
EML (EAM)	$ \cos(\theta) - \alpha \sin(\theta) $	$0 \leq \alpha \leq 1$	$f_c \geq 0.1 \text{ GHz}$
DML	$ \cos(\theta) - \alpha \sin(\theta) \left(1 - j \frac{\omega_c}{\omega}\right) $	$1 \leq \alpha \leq 3$	$f_c \geq 1 \text{ GHz}$

2.3.3 Photodetector model

The PD converts the signal from the optical domain to the electrical at the receiver front end by capturing the intensity of the complex envelope $E_{rec}(t)$. Due to the chromatic dispersion there is a frequency shift of the optical sidebands, hence there is a mixing of the sidebands during the square-law detection process, consequently the channel presents deep frequency attenuation.

The PD responds to optical intensity only, and all the phase information is lost. Considering the square-law rule and neglecting noise, the photocurrent generated at the output of the receiver photodiode [45] is

$$I_{rec}(t) = R|E_{rec}(t)|^2 = RP_{out}(t) \quad (2.14)$$

strictly positive, proportional to the electrical field's intensity at the fiber's output and the PD responsivity. The PIN photodiode is described by equation 2.14. Here, the Received Optical Power (ROP) is conventionally used to report the optical signal intensity at the fiber output. Note that the ROP is the mean optical power of the received signal, and it is related to $|E_{rec}(t)|^2$. But, in PON, APDs are typically used because they improve the sensitivity due to the avalanche multiplication factor. Hence the APD output is:

$$I_{rec}(t) = M_{PD}RP_{out}(t) \quad (2.15)$$

For the 50G-PON APDs, a typical avalanche multiplication factor value is $M_{PD} = 8$ and the responsivity is $R = 0.9 \text{ A/W}$ [46].

The conversion considered in equation 2.15 is noise free. However, this is not the case in a real receiver. In this direct detection model, two fundamental noise mechanisms are considered, the shot noise and thermal noise [35], [47]–[49]. Shot noise occurs because an electric current is made of a stream of electrons generated at random times. Hence the photocurrent becomes:

$$I_{rec}(t) = RP_{out}(t) + i_s(t) \quad (2.16)$$

Mathematically, $i_s(t)$ is a stationary random process with Poisson statistics, however, for high enough density of photons, it is well approximated to white Gaussian noise. The variance of the shot noise is obtained assuming a photodiode with equivalent noise bandwidth B_{PD} , and constant received optical power $I_p = RP_{out}(t)$ [35]:

$$\sigma_s^2 = 2q_e(I_p + I_d)B_{PD} \quad (2.17)$$

where I_d is the noise due to dark current and q_e is the electron charge [35]. The power of quantum noise is proportional to the received power. The thermal noise arrives into

the generated current $I_{out}(t)$ due to the random thermal motion of electrons. This motion manifests as a fluctuating current added to the PD current. Hence the photodiode current becomes [35]

$$I_{out}(t) = RP_{out}(t) + i_s(t) + i_T(t) \quad (2.18)$$

Where the thermal noise component $i_T(t)$ behaves as white Gaussian noise with variance:

$$\sigma_T^2 = \left(\frac{4k_B T_p}{R_L} \right) F_n B_{PD} \quad (2.19)$$

k_B is the Boltzmann constant, T_p is the absolute temperature, R_L is the load resistance, and F_n is the noise figure [35].

The thermal noise does not depend on the received optical power, unlike the shot noise. However, the APD enhances the shot noise. Therefore, the gain of SNR of the APD is not directly proportional to M_{PD} . The electrical equivalent SNR at the output of the APD is represented by:

$$SNR = \frac{I_p^2}{\sigma_s^2 + \sigma_T^2} \approx \frac{I_p^2}{\sigma_w^2} \quad (2.20)$$

Here, we consider an equivalent thermal noise represented by σ_w^2 . The noise due to amplification and quantum noise is neglected.

Finally, the PD electrical bandwidth limitation is mathematically modeled by low-pass filters, such as the Bessel filter and the Butterworth filter [45]. Hence, the end-to-end frequency response of the IM/DD channel is:

$$H_{IM/DD}(f) = H_{NRZ}(f)H_{LAS}(f)H_{IM}(f)H_{PD}(f) \text{ [dB]} \quad (2.21)$$

This section introduced the laser, intensity modulation and photodiode expressions based on the small signal regime, which is a linear approximation of the laser rate equations [35]. Table 2.2 indicates the models used to represent the optical emitter, the SMF, and the photodiode.

Table 2.2: The devices and models of the IM/DD channel model, based on [50].

Device	Model	
	Small signal regime	Large signal regime
Laser	Modulation transfer function $H_{LAS}(f)$	Complete rate equations
Fiber	Modulation transfer function $H_{IM}(f)$	Slowly-varying envelope
Photodiode	Square-law device cascaded to a low-pass filter $H_{PD}(f)$	square-law device cascaded to a low-pass filter

2.4 The receiver architecture

This thesis considers 50G PON with digital signal processing at the receiver side, assuming the consented ITU-T Physical Media Dependent (PMD) specifications [1]. To reach the PMD recommendations of ITU-T for the next generation of IM/DD passive

networks, the classical optical receiver is modified, as shown in figure 2.4., to introduce DSP functions in the digital demodulation process. Here, the equalization is assumed in the ONU, at the end-user side, as mentioned in chapter 1. More details about the developed equalizers are detailed in chapters 3,4 and 5. The Automatic Gain Control (AGC) scales the signal at the output of the APD into the dynamic range of the receiver to scale the signal into the receiver dynamic range (Appendix B details the AGC) since the PON requires a large optical budget and that the signals are in a large attenuation range.

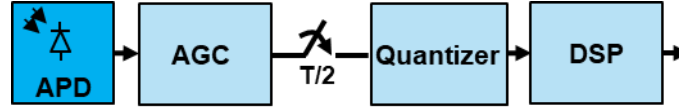


Figure 2.4: The DSP-enabled receiver architecture.

Then, the waveform is sampled at rate $T/2$, with $T = \frac{1}{50 \times 10^9} = 20 \text{ ps}$. The samples output is quantized through a mid-riser quantizer (more details in Appendix C). Here, the ADC is represented by the AGC, the sampler, and the quantizer. Finally, the ADC output is processed by a digital signal processor with equalization capability (the options of distortion compensators are detailed in chapters 3, 4, and 5, respectively) to compensate for the channel distortions.

2.4.1 Discrete-time equivalent channel model

The ADC-based receiver relates to a discrete-time digital communication channel model. The digital receiver is confronted with two main impairments: Intersymbol Interference (ISI) and noise [39]. ISI is a distortion that causes the pulses with transmitted information to be smeared in time and consequently superimposed so that the receiver can not correctly identify the transmitted symbols.

Here, the continuous-time effects of CD, chirp, limited bandwidth, and noise of the IM/DD system introduced in section 2.3 are captured into a fundamental discrete-time baseband equivalent model in the presence of intersymbol interference. Assuming x_n the transmitted data symbols, the noise samples as w_n , and the samples at the output of the electrical receiver are y_n . The fundamental discrete baseband equivalent model [51] is illustrated in figure 2.5.

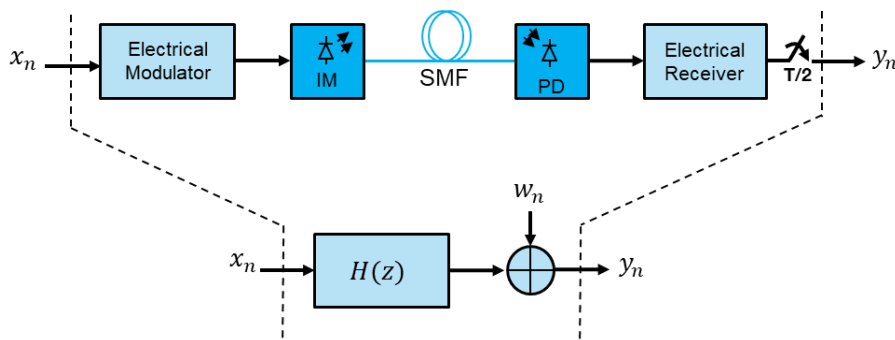


Figure 2.5: The discrete-time equivalent channel model.

The channel is represented by $H(z) = \sum_{l=0}^{L-1} h_l z^{-l}$, h are the channel taps and L the number of taps of the channel. The transmitted data symbols are independent sequences with a energy $E_x = 0.5$ and variance σ_x^2 , with a binary alphabet $\{a_0, a_1\} \in A$ based on the Extinction Ratio (ER) of the intensity modulator and the energy (more details in Appendix A). We remind that the transmission rate is $R_b = 50 \text{ Gbit/s}$, hence the period of a symbol is $T = 20 \text{ ps}$. The samples w_n are modeled as real additive white Gaussian noise with zero mean $w_n \sim N(0, \sigma_w^2)$. This work assumes a Fractionally Spaced Receiver (FSR) with $T/2$ sample interval, corresponding to an ONU with an analog-to-digital converter with a sampling rate $F_s = 100 \text{ Gsa/s}$.

Assuming a discrete-time equivalent channel model $\{\mathbf{h}_0, \dots, \mathbf{h}_{L-1}\}$ covering L successive symbol periods T , in a discrete-time interval $[nT, (n+1)T[$, the ADC output is [51]:

$$\mathbf{y}_n = \sum_{i=0}^{L-1} \mathbf{h}_i x_{n-i} + \mathbf{w}_n \quad (2.22)$$

With:

$$\mathbf{h}_i = \begin{pmatrix} h_{i,\ell-1} \\ \vdots \\ h_{i,0} \end{pmatrix} \quad (2.23)$$

$$\mathbf{w}_i = \begin{pmatrix} w_{i,\ell-1} \\ \vdots \\ w_{i,0} \end{pmatrix} \quad (2.24)$$

$$\mathbf{y}_n = \begin{pmatrix} y_{n,\ell-1} \\ \vdots \\ y_{n,0} \end{pmatrix} \quad (2.25)$$

here, the fractionally spaced receiver comprises $\ell = 2$ samples per symbol period T . In the case of N successive observations, the channel output in vector form is represented succinctly by :

$$\mathbf{y}_n = \mathbf{H}\mathbf{x}_n + \mathbf{w}_n \quad (2.26)$$

Where \mathbf{H} is the $N\ell \times (N + L - 1)$ channel convolution matrix that presents Toeplitz propriety [55]. \mathbf{y}_n and \mathbf{w}_n are $N\ell \times 1$ vectors. Hence the matrix form is:

$$\begin{pmatrix} y_n \\ \vdots \\ y_{n-N+1} \end{pmatrix} = \begin{pmatrix} h_0 & \cdots & h_{L-1} & 0 & \cdots & 0 \\ 0 & \ddots & & \ddots & & \vdots \\ \vdots & & \ddots & & \ddots & 0 \\ 0 & \cdots & 0 & h_0 & \cdots & h_{L-1} \end{pmatrix} \begin{pmatrix} x_n \\ \vdots \\ x_{n-N-L+2} \end{pmatrix} + \begin{pmatrix} w_n \\ \vdots \\ w_{n-N+1} \end{pmatrix} \quad (2.27)$$

2.5 50G HS-PON implementation

The 50G PON downstream scenario has been simulated in MATLAB (Mathworks®) and VPIphotonics (VPI Transmission Maker™). Figure 2.6 illustrates the PON and the simulated devices.

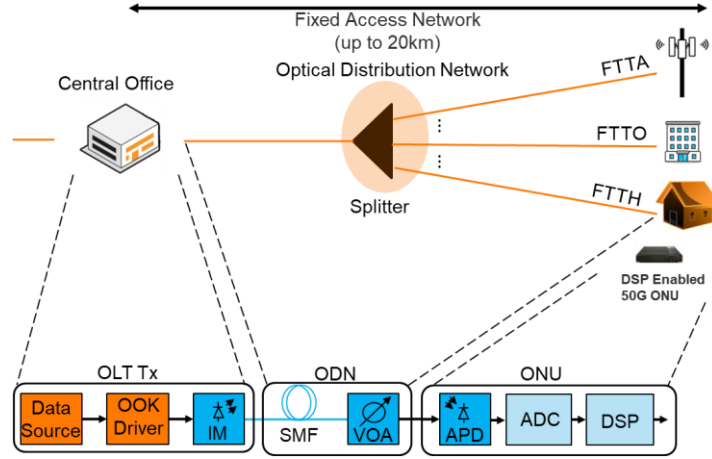


Figure 2.6: The emulated 50G-PON with a DSP-enabled ONU.

The OLT in the central office is emulated as a data source that sends OOK pulses through an intensity modulator (MZM, EML, or DML). The optical distribution network impairments of attenuation and distortion are obtained through the single-mode fiber and a variable optical attenuator. Finally, the frontend receiver comprises an APD, an ADC, and a digital signal processor.

As mentioned in chapter 1, the frequently used devices in the PON transceivers are the externally modulated laser, the directly modulated laser, and the avalanche photodiode in a fiber link with distances up to 20km. The set of simulation parameters was chosen to approximate these devices, based on the literature [30], [40], [43], [50], [53], [54], where the downstream case at $\lambda = 1344nm$ and dispersion coefficient $D = 3.85 ps/nm.km$ was fixed, and the parameters of the intensity modulator, VOA and APD varied in each simulation scenario.

2.6 Simulated performance of the 50G-PON

In practice, the end-to-end real PON channel operates in large signal regime conditions. However, the small signal model is useful for estimating the 50G-PON channel distortions. Also, its applicability was already verified with EML and DML at 50Gbit/s simulations with an extinction ratio lower than 2 dB and fiber with distances up to 20 km [50], [53].

This section evaluates the IM/DD effects regarding the channel frequency response based on the small signal model. This is followed by the performance in terms of bit error ratio through the large signal model-based simulations because the large signal model has closer end-to-end conditions to the PON in practice.

2.6.1 Small signal regime simulation parameters

The impact of chromatic dispersion, chirp, and bandwidth limitation is evaluated here in frequency and time domain through small signal regime simulations realized entirely in MATLAB. The main objective is to understand the linear distortions of the IM/DD channel, especially the EML and DML emitters.

The simulation of the channel was as follows: A pulse was generated by the electrical modulator with NRZ pulse format $H_{NRZ}(f)$, then the electrical signal was injected into the intensity modulator (EML or DML) whose threshold current is $I_{th} = 20 \text{ mA}$ and bias $I_b = 80 \text{ mA}$. Next, the current $I_{in}(t)$ is converted to power $P_{in}(t)$ by applying the factor $\delta_{PI} = 0.2$ to $I_{in}(t)$. The signal amplitude was $\Delta I = 0.1 \text{ mA}$, considering the small signal constraint.

Afterward, the spectrum of signal is obtained through the Fast Fourier Transform (FFT), then $H_{LAS}(f)$ is applied to the spectrum. Next, the electrical field of the signal is propagated through the fiber considering the slowly-varying envelope model, the frequency response of fiber and chirp were also applied in the frequency domain. Finally, the square-law photodiode detects the electrical field of the signal $|E_{rec}(\omega)|^2$ and the 4th order Bessel filter $H_{PD}(\omega)$ is applied to the signal, then the channel's impulse response is obtained.

As mentioned in section 2.5, the parameters used in the simulations correspond to values found in the literature [28], [30], [38], [41], [50], and are based on real experiments. The measurement experience is detailed in [43]. The channel frequency response (S21 parameter) is obtained using an experimental setup composed of an optical emitter, fiber, and a network analyzer.

In this work, the optical emitter with $\alpha = 0$ is entitled unchirped, or MZM. The EAM-based emitter, which $\alpha = 0.5$ and $f_c = 0$ is entitled EML. And when the IM presents adiabatic chirp $f_c \sim 2 \text{ GHz}$ and $\alpha = 3$, the optical emitter is called DML.

Table 2.3 summarizes the small signal simulation parameters.

Table 2.3: Main parameters of the 50G-PON simulation in small signal regime.

Frequency Response	Parameter	MZM	EML	DML
$H_{AM}(f)$ (equation 2.5)	f_r (GHz)	25	25	25
	γ	0.75	0.75	0.75
$H_{IM}(f)$ (equation 2.12)	α	0	0.5	3
	f_c (GHz)	0	0	2 GHz
	L_F (km)	20	20	20
$H_{PD}(f)$	B_{PD} (GHz)	18.75	18.75	18.75

The small-signal parameters of the IM/DD system simulation are based on the expected values for real transceivers of the next realistic 50G-PON. For example, the receiver's bandwidth $B_{PD} = 18.75 \text{ GHz}$ enables 25Gbit/s transmissions, as mentioned in section 1.5.

2.6.2 Analysis of the unchirped, EML, and DML sources in small signal regime

Figure 2.7 shows the frequency response of the simulated optical 50G IM/DD channel emitter.

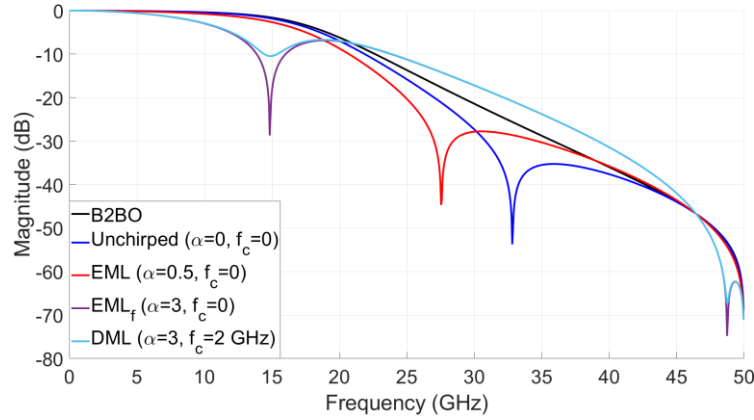


Figure 2.7: Frequency responses of the channel in the configuration of B2BO, EML, DML, and MZM with 20km of single-mode fiber at $\lambda = 1344$ nm.

Here, the behavior of small-signal frequency responses of the channel of interest are studied, especially the EML in red and DML in light blue. In black the back-to-back configuration (B2BO) is shown, the channel does not present severe frequency selectivity because there is only a transmitter with 3dB bandwidth of 37.5GHz and an APD with bandwidth of 18.75GHz. The APD filtering dominates the channel distortion as expected. We observe that the channel behaves as a low-pass filter. The unchirped based channel, presents a spectral null at 34 GHz due to the fiber and quadratic detection. Hence the propagation at 20km presents notches in the bandwidth of the $R_b = 50\text{Gbit/s}$ signal, even with an expensive modulator.

When the chirp factor is increased to $\alpha = 0.5$ the spectral null manifests in 27 GHz in the EML case due to the increase of transient chirp. Assuming a fictitious EML, entitled EML with higher chirp factor $\alpha = 3$, we notice that the frequency null is at the main lobe of the signal. Hence the ISI further degrades the received data quality. Also, a new notch is present at 48 GHz. The DML case is considered when the adiabatic chirp is $f_c = 2$ GHz and $\alpha = 3$. Compared to the EML_f, the spectral attenuation of the DML is lower, and the DML notches are in the same frequency presented with the EML_f, but the adiabatic chirp reduces the dips levels.

One may ask why not use DML over EML in PON. In practice, the DML is more impaired. As mentioned in section 1.5, typically, it is used in distances up to 10km due to the emission power limitation. Furthermore, the adiabatic chirp adds nonlinearities to the channel. Consequently, advanced DSP techniques, such as the Maximum Likelihood Sequence Estimation (MLSE), are necessary to reach the PON recommended performance [55].

Figure 2.8 shows the simulated impulse response of B2BO, unchirped, EML, DML based channels through slowly varying envelope propagation.

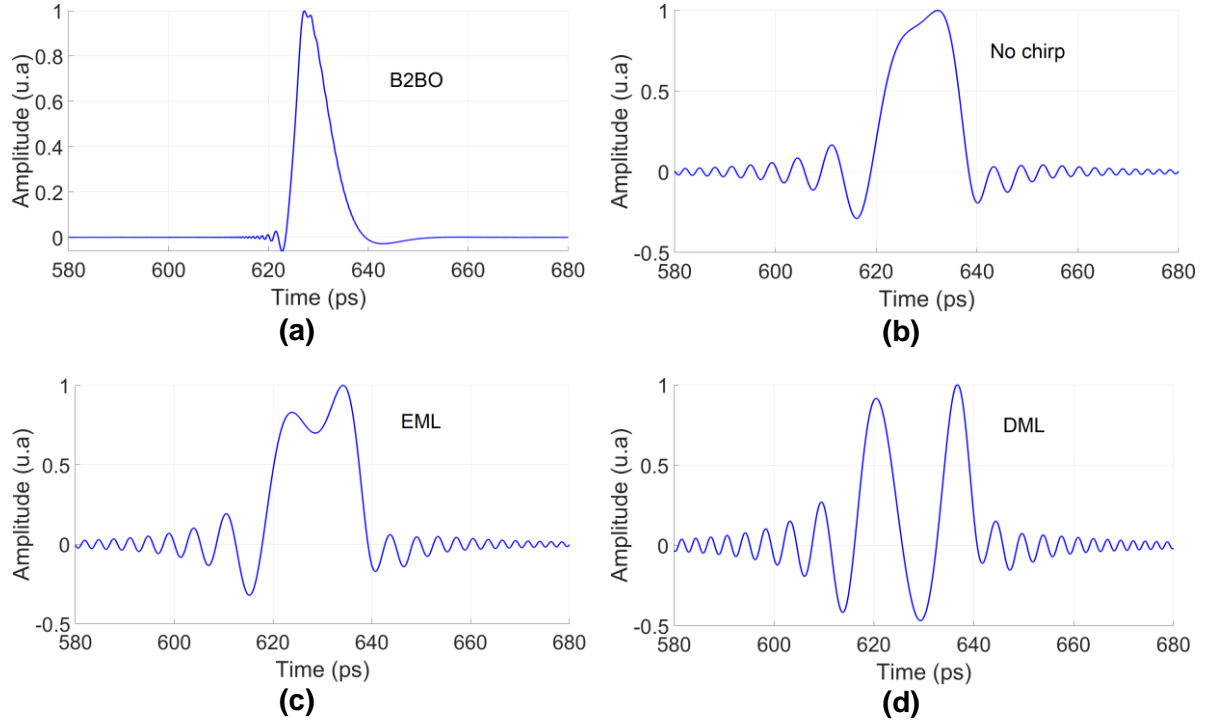


Figure 2.8: Impulse response of the simulated channels after slowly-varying envelope propagation through 20km of fiber and a 25G APD (i.e. $B_{PD} = 18.75 \text{ GHz}$), which emitter was (a) back-to-back, (b) unchirped source, (c) EML, and (d) DML.

The energy impulse response in setup B2BO has most of the energy during the period of a symbol interval $T = 20 \text{ ps}$. Hence the channel distortions in B2BO are not severe, as verified in the frequency analysis. However, after 20km of fiber with the MZM, the pulse is increased to $T_{out} = 30 \text{ ps}$ hence the distortion due to ISI becomes important. When the EML replaces the MZM, the pulse duration is around $T_{out} = 40 \text{ ps}$. Finally, with the DML, the adiabatic chirp causes the division of a single pulse into two single pulses, as verified in [56].

2.6.3 Parameters of the 50G PON channel large signal simulations

Now that the impact of the EML and DML in linear regime has been evaluated, the conditions of the channel have been changed to consider a more realistic 50G PON downstream transmission scenario. Here, the performance in terms of bit error ratio is evaluated in the large signal regime. Still, the small signal simulated frequency response is used to understand the linear impacts of the IM/DD channel.

The performance of the digital communication IM/DD channel has been evaluated through VPI and MATLAB co-simulations. The modulation, propagation, and photodetection were realized through VPI environment. The optical emitter is based on VPI's semi analytical laser rate equation model. The process of automatic gain control, sampling, quantization, DSP, and bit error ratio calculation by error counting was performed using MATLAB.

Figure 2.9 shows the simulated channel in a large signal regime.

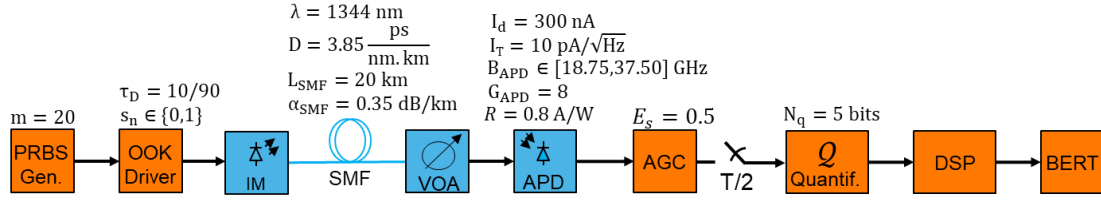


Figure 2.9: The evaluated 50G PON IM/DD setup during the thesis considering EML and DML as intensity modulators in large signal conditions.

The VPI sampling frequency was set to 200GSa/s in order to ensure enough bandwidth for the optical, and physical phenomena in simulation, hence the received waveform at the output of the APD was resampled to have 100GSa/s. PRBS20 sequences were generated and formatted into electrical NRZ-OOK pulses with the rise time $0.1 \times T$ and fall time $0.9 \times T$, entitled here $\tau_D = 10/90$, for driving the intensity modulator, the EML and DML were simulated based on the semi-analytical VPI models ModulatorEA and LaserPulsed, respectively [57]–[59]. Both had 3dB bandwidth $B_{IM} = 32$ GHz. The resonance frequency was $f_r = 18$ GHz with emission wavelength $\lambda = 1344$ nm. The IM parameters are based on estimated real components at 50Gbit/s, they were discussed in the ITU-T 50G-PON research group.

In the semi-analytical EML-based simulation, the chirp factor was $\alpha = 0.5$, and the average output power is $P_{avg} = 10$ dBm and extinction ratio $ER = 6$ dB. The DML-based simulation had $\alpha = 3$, adiabatic chirp $f_c = 2$ GHz, mean output power $P_0 = 9$ dBm and extinction ratio $ER = 5$ dB. Due to the DML power limitation and nonlinearities, we assumed a 1 dB extinction ratio penalty with respect to the EML.

Then, the optical signals were propagated into $L_{SMF} = 20$ km of SMF with dispersion coefficient $D = 3.85 \frac{\text{ps}}{\text{nm.km}}$, and attenuation factor $\alpha_{SMF} = 0.35$ dB/km, hence the fiber attenuation is 7dB, and the worse scenario cumulated dispersion $D \times L_F = 78$ ps/nm of the downstream ITU-T transmission with respect to the 50G-PON standard is assumed.

A VOA controlled the ROP. Afterward, the APD detects the signal. We simulated the two ITU-T APD options envisaged for the HS-PON. The receivers options were mentioned in section 1.5. Here, the 50G APD has a bandwidth $B_{APD} = 37.5$ GHz and the 25G APD has the bandwidth $B_{APD} = 18.75$ GHz. The APD responsivity was $R = 0.8$ A/W, and multiplication gain $G_{APD} = 8$. The thermal noise current was $I_{th} = 10$ pA/ $\sqrt{\text{Hz}}$ and dark current $I_{dc} = 300$ nA.

In MATLAB, the waveform is loaded, processed by the automatic gain control device to ensure that the received signal has energy $E_s = 0.5$ and is within the dynamic range of the quantizer with resolution $N_q = 5$ bits. We remark that 5 bits is the expected effective number of bits of the 50G PON ADC [25]. However, in this chapter, the DSP receiver is very basic and reduces to a simple threshold detector, followed by a bit error ratio counter. Finally, table 2.4 shows the main parameters of the large signal simulation.

Table 2.4: Main parameters of the 50G-PON simulation in large signal regime.

Parameter	Device	
-	EML	DML
α	0.5	3
f_c (GHz)	0	2
Extinction ratio (dB)	6	5

2.6.4 Performance of 50G PON channel

As mentioned in section 2.4, the receiver architecture comprises equalization. This will be the subject of the forthcoming chapters. Also, this receiver does not comprise the LDPC forward error correction.

Figure 2.10 displays the performance of the EML and DML based system through 20km of fiber and with the two APD options. The impacts of chromatic dispersion and chirp with the EML are very critical. Both EML-based transmissions' BER performance (with the 25G and 50G APD) are superimposed. Hence, the degradation due to limited bandwidth is not perceived.

The EML-based channels with the APDs with bandwidths of 18.75GHz and 37.5GHz do not even reach the required ITU-T sensitivity $S = -24$ dBm based on the soft decision LDPC FEC limit $FEC_{LDPC} = 1 \times 10^{-2}$ [60].

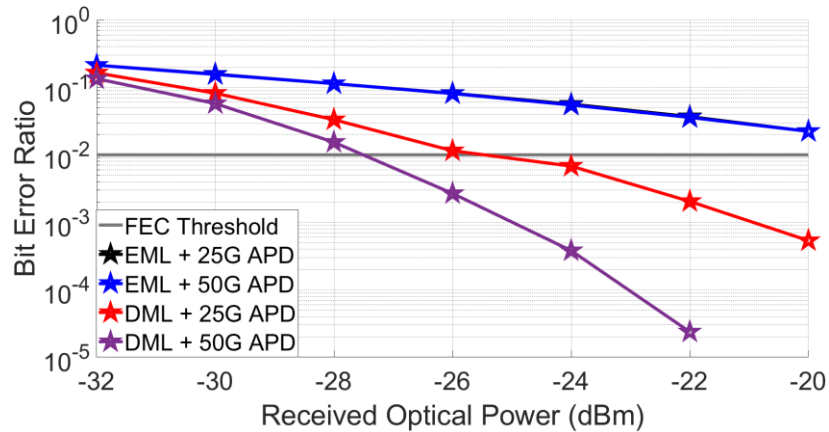


Figure 2.10: simulated BER vs ROP in large signal regime assuming two optical emitter options (EML and DML) followed by 20km of fiber and two APD (25G and 50G).

When using a DML as an optical emitter, the performance of the system is better than EML-based channels thanks to the adiabatic chirp since the severe frequency attenuation is reduced when using DML, as observed in the small-signal model. The DML + 25G APD Rx and the DML + 50G APD achieve the required ITU-T sensitivity and optical budget (N2). In these scenarios, the degradation due to CD and chirp is not high because the adiabatic chirp is beneficial to mitigate the spectral nulls, accordingly to the small signal frequency response analysis. Furthermore, the 25G APD-based receiver (Rx) has a sensitivity penalty of at least 4dB compared to the 50G APD-based Rx.

Comparing the EML and DML-based channels is remarkable that the channel with EML suffers from severe ISI due to the frequency attenuation related to SMF propagation. However, we note that the DML-based system with 25G APD has a 2dB

margin to the ITU-T sensitivity; since it suffers from less critical frequency attenuation than the EML.

Finally, to contrast the small signal and large signal behavior, we compared the frequency responses of the EML and DML-based channels based on the estimated impulse response of the channels, as indicated in figure 2.11.

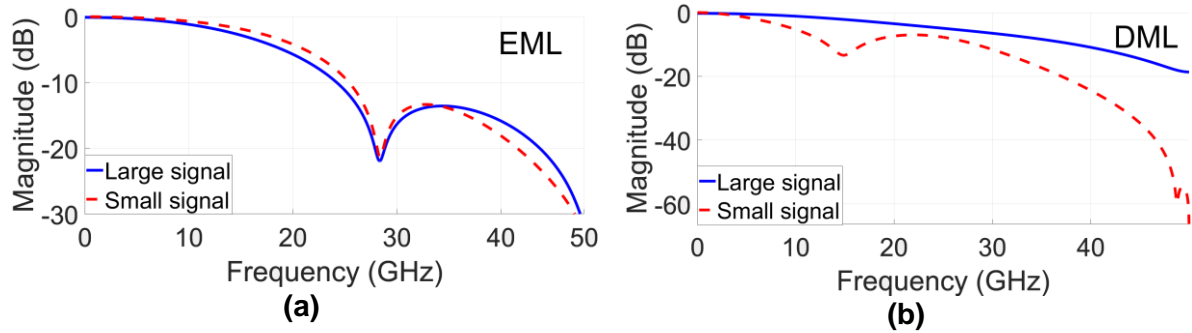


Figure 2.11: small signal (analytical) and large signal (numerical) transfer function comparison over (a) EML and (b) DML.

The large-signal frequency response was estimated through a least mean square estimator (more details on Appendix D), otherwise the small-signal transfer function was obtained analytically.

Both large signal transfer functions were estimated through the least mean squared estimation. We see that the small signal regime and large signal have excellent correspondence when the EML is used. However, in the DML case due to adiabatic chirp the estimated and theoretical does not agree. It is even possible to observe spectral null in the DML small signal frequency response at 50GHz that is not observed in the estimated frequency response.

2.7 Concluding remarks

A performance gap exists between the recommended 50G-PON requirements and the simulated PON, especially in a link with 20 km, where the chromatic dispersion and chirp effects are present. Nevertheless, ISI compensation was not used and may be the solution to ensure the target performance recommended by ITU-T.

This chapter introduced the IM/DD optical channel, the discrete equivalent channel model, and the architecture of the DSP receiver that will be used in the following of thesis. Here, two models were used to simulate the 50G PON in downstream mode. The small signal regime was important to understand how the IM/DD channel behaves in terms of frequency response and intersymbol interference. The large signal regime simulations were used to evaluate the channel performance with the envisaged receivers for the 50G-PON.

The small signal results showed the origin of ISI in the IM/DD, furthermore the EML-based channel presents severe ISI at 20km due to chirp and chromatic dispersion. With a bit rate of 50Gbit/s it presents spectral nulls in the bandwidth of the signal, and, based on the small signal simulation evaluation, we could understand the impacts in large signal transmissions simulations. Hence, the EML-based system could not achieve the target sensitivity proposed by ITU-T. Otherwise, the DML presented

more linear distortion due to adiabatic chirp and could perform well beyond the FEC limit in large signal simulation, in other words the adiabatic chirp is beneficial to reduce the linear impact of 50G-PON channel. Comparing the simulated frequency response of the EML and DML in large signal regime with the theoretical small signal model, we could see that the EML has a good correspondence. Consequently, a linear analysis is still pertinent, but with the DML, the small signal regime analysis does not agree very well with the large signal model, in terms of simulated and theoretical frequency response.

The next chapters will discuss the theory and the implementation of digital equalizers. We start with the most equalizer, to more advanced distortion compensators during the thesis. The next chapter introduces the linear equalizer to deal with the IM/DD impairments described in this chapter.

3 Digital Filter Based Linear Equalization Techniques to Compensate the 50G-PON Channel Distortions

3.1 Introduction

Digital systems in the presence of ISI use filter-based equalization [61], [62]. Because equalization mitigates channel distortion, hence improving the performance of the system. Linear Equalization (LE) is one of the simplest forms of distortion compensation, requiring only a feedforward equalizer (FFE).

The previous chapter described the nature of the HS-PON distortions, its modeling, and a DSP-enabled receiver architecture. The combined effects of CD, chirp, limited bandwidth and noise severely degrade transmission performance in downstream transmissions at 50Gbit/s. Consequently, the sensitivity and optical budget required by the ITU-T for the next PON generation are not met [63].

Here, the communication system is based on the equivalent discrete channel model presented in section 2.4. In this chapter, we describe the linear equalizer structure and implementation to the downstream HS-PON at 50Gbit/s, considering the EML, DML laser sources at the transmitter and a receiver based on APD with limited bandwidth in VPI Photonics and MATLAB co-simulations.

The chapter is organized as follows: In section 3.2 the zero-forcing (ZF) and minimum mean square error (MMSE) criteria are explained. In section 3.3 we describe the MMSE linear equalizer (MMSE-LE), then closed form equations calculations in 3.4. In section 3.5, the structure of the least-mean square (LMS) algorithm-based linear equalizer is presented, then the procedure to optimize the number of taps and delay of the MMSE-LE is introduced in section 3.6. Then, sections 3.7 and 3.8 show the results with the MMSE-LE-based receiver over the 50G-PON setup in closed form and adaptive manner, respectively. Finally, section 3.9 highlights the MMSE-LE results, and section 3.10 summarizes the chapter key points.

3.2 Equalization-based digital filters

The primary purpose of filter-based equalization is to mitigate ISI of frequency selective channels. The filter-based equalization is achieved through the convolution of the finite impulse response (FIR) filter coefficients, known as taps, with the received sampled waveform y_n , so that, the output of the cascade of equalizer and channel z_n approaches a frequency-flat Nyquist folded spectrum [51]. Then, a Symbol-by-Symbol (SBS) detector is inserted at the output of the equalizer z_n as described in figure 3.1.

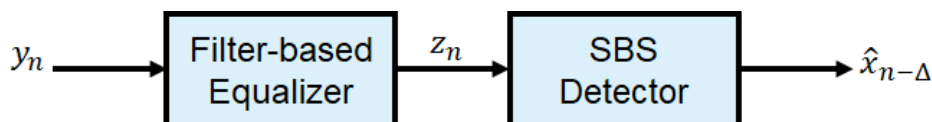


Figure 3.1: Filter-Based Equalization Block Diagram, based on [51].

However, the equalization process has the collateral effect of noise enhancement. i.e., when the equalizer compensates for the channel distortion, it may enhance the noise, especially when the channel presents deep frequency fading.

There are three different classes of filtering-based equalizers: Linear Equalization (LE), decision-feedback equalization (DFE), and interference cancellation. To adjust the equalizer taps, three performance criteria have been considered [51]. The most obvious criterion is the reduction of the error probability P_e , however, to find the equalizer parameters is a mathematical challenge that leads to non-linear equations with exponential computational complexity [64]–[67]. Therefore other sub-optimum criteria have been proposed to compensate ISI with reduced distortion, such as the zero-forcing (ZF) and the minimum mean-square error [68]–[70]. The zero-forcing equalizer (ZFE) condition is to completely eliminate ISI at the sampling instant by inverting the channel frequency response [71]

$$H_{ZF}(f) = \frac{1}{H_{ch}(f)} \quad (3.1)$$

where $H_{ch}(f)$ and $H_{ZF}(f)$ are the frequency response of the channel and of the ZFE, respectively. However, the noise is neglected. Consequently, it may lead to severe noise enhancement over channels with spectral nulls or near-nulls, such as the PON optical channels [30], [72], and the 50G-PON channel presented in section 2.5.

On the other hand, the MMSE criterion balances the compensation of ISI and noise enhancement at the symbol by symbol detector, also known as slicer, input by reducing the ISI distortion and the variance of the noise σ_w^2 [73]. It enables the MMSE equalizers to achieve better performances than the ZF equalizers. Hence we choose to flow solely on MMSE linear equalization in this thesis.

3.3 The MMSE linear equalizer

The classic structure of the linear equalizer is shown in figure 3.2.

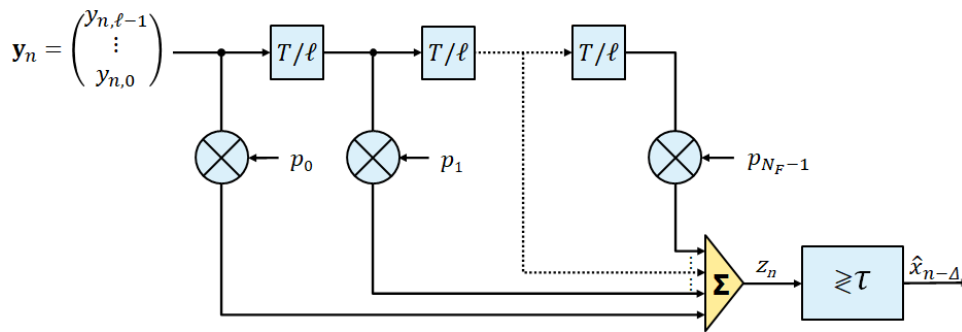


Figure 3.2: The linear equalizer structure.

At each symbol interval T , the LE multiplies N_F taps $\mathbf{p}^H = [p_0, p_1, \dots, p_{N_F-1}]$ to the received sequence $\mathbf{y}_n = [y_{n,\ell-1}, \dots, y_{n,0}]$ and outputs the equalized sample

$$z_n = \mathbf{p}^H \mathbf{y}_n = \mathbf{p}^H (\mathbf{H} \mathbf{x}_n + \mathbf{w}_n) \quad (3.2)$$

Thus the output is the sum of a linear combination of several transmitted symbols plus a noise term. Afterward z_n is processed by the SBS detector with decision threshold τ .

Conventionally, the taps of the linear equalizer are spaced reciprocally to T , known as a symbol-spaced equalizer (SSE). In the thesis, we consider Fractionally Spaced Equalization (FSE). Hence the time interval between each tap becomes $T/\ell = T/2$. Compared to the SSE, the advantages of the FSE are 1) The FSE adaptively realizes the optimum linear receiver [74] that consists of an analog matched filter, a symbol rate sampler, and a T-spaced SSE. 2) The T-spaced LE cannot digitally synthesize the analog-matched filtering, and 3) The FSE can jointly perform both matched filtering and equalization in the digital domain.

3.3.1 The criterion of the MMSE-LE

The minimum mean square error linear equalizer is a linear FIR filter with taps \mathbf{p}^H optimized to minimize the mean-square error between the transmitted symbols and the outputs of the LE $J = \mathbb{E}\{|z_n - x_{n-\Delta}|^2\}$

$$\mathbf{p}^* = \arg \min_{\mathbf{p}} \mathbb{E}\{|z_n - x_{n-\Delta}|^2\} \quad \text{with } z_n = \mathbf{p}^H \mathbf{y}_n \quad (3.3)$$

at the input of the slicer. However, the minimization of the MSE does not translate into the error probability $P_E = p[\hat{x} \neq x]$ reduction since it leads to a non-trivial performance analysis [51].

An alternative metric has been proposed to evaluate the performance of MMSE equalizers. The most common procedure involving the definition of the equivalent signal-to-noise ratio SNR_{EQ} at the output of the equalizer

$$\text{SNR}_{EQ} \triangleq \frac{\sigma_x^2}{\mathbb{E}\{|z_n - x_{n-\Delta}|^2\}} \quad (3.4)$$

since it facilitates evaluating the performance of transmission systems that uses compensation techniques such as digital equalization [51], [73]. Assuming that the equalizer output will be affected by Gaussian additive noise, higher SNR_{EQ} implies a lower error probability. This is not always true, but it enables a better comprehension of receiver performance notions. However, the issue is worse because MMSE-optimized equalizers are intrinsically biased. The output of the equalizer could be interpreted as an attempt to reduce the combination of ISI and noise

$$z_n = \beta(x_n + \psi_n) \quad (3.5)$$

Where β is the bias introduced by the equalizer, and ψ_n is an uncorrelated distortion [73].

The presence of the bias essentially shifts the channel output (may be seen as a gain) and artificially enhances the output SNR of signals. To address the problem in the thesis, we adjusted the decision threshold of the symbol detector to account for the bias, either calculated through closed form equations or adaptively.

Two methods are proposed to calculate the LE taps \mathbf{p}^* . When the channel taps $\mathbf{h} = \{h_{0,0}, h_{0,1}, \dots, h_{L-1,\ell-1}\}$ and signal-to-noise ratio $\text{SNR} = \frac{2E_s}{N_0}$ are known, the FIR-based equalizer taps may be obtained through closed form expressions [51], [64], [75], [76]. However, in practical implementations, the channel statistics are unknown, so adaptive approaches based on the steepest-descent methods are used to calculate

the taps [64], [69], [77]. For instance, we use the least mean square method, entitled here least mean square linear equalizer (LMS-LE), which tacitly accounts for the true correlation statistics of OOK symbols.

The LMS-LE converges towards the performance of the closed form MMSE-LE. During the thesis, the former and latter optimization methods were used to calculate the taps. The closed form equations were used for the theoretical prediction of the performance of the LE, and the channel taps and SNR were estimated through the least square estimation (see details in Appendix D). The LMS-LE was implemented through MATLAB simulations in offline mode, using the transmitted and received data.

3.4 The closed form MMSE-LE

The calculations that follow require prior estimation of the discrete-time channel impulse response \mathbf{h}_n , and the signal-to-noise ratio $SNR = \frac{\mathbb{E}\{|s_n|^2\}}{\mathbb{E}\{|w_n|^2\}} = 2E_s/N_0$. The optimal filter taps \mathbf{p}^H are calculated to minimize the MSE $\min_{\mathbf{p}^*} \mathbb{E}\{|s_{n-\Delta} - z_n|^2\}$, where $0 \leq \Delta \leq N + L - 2$ is the restitution delay, introduced to approximate the anti-causality of the equalizer. In other words, the MMSE-LE taps are applied on the channel output, modeled in section 2.4 as $\mathbf{y}_n = \mathbf{H}\mathbf{x}_n + \mathbf{w}_n$, to provide the output sequence z_n , which is the best estimate of the transmitted sequence x_n in mean square error sense.

The standard MMSE-LE, closed form solution for zero-mean constellations is well known to be

$$\mathbf{p}^H = \mathbf{R}_{yy}^{-1} \mathbf{R}_{yx} \quad (3.6)$$

where,

$$\mathbf{R}_{yy} \triangleq \mathbb{E}(\mathbf{y}_n \mathbf{y}_n^H) = \sigma_x^2 \mathbf{H} \mathbf{H}^H + \sigma_w^2 \mathbf{I} \quad (N_F \times N_F \text{ matrix})$$

$$\mathbf{R}_{yx} \triangleq \mathbb{E}(\mathbf{y}_n s_{n-\Delta}^H) = \sigma_x^2 \mathbf{h}_\Delta \quad (N_F \times 1 \text{ vector})$$

\mathbf{R}_{yy} is defined as a strictly positive, definite autocorrelation matrix. σ_x^2 is the variance of the transmitted symbols. We remind that \mathbf{H} is the channel convolution matrix, explained in section 2.3, and the superscript H represents the Hermitian transposition operator. σ_w^2 is the white Gaussian noise variance. When $\sigma_w^2 > 0$, \mathbf{R}_{yy} becomes a strictly positive Toeplitz matrix that can be exploited to reduce computation complexity [78]. \mathbf{I} is the identity matrix, and \mathbf{h}_Δ is denoted as the product of the matrix \mathbf{H} with the unit vector \mathbf{e}_Δ , having a 1 in position Δ , hence it represents the column Δ of \mathbf{H} , $\mathbf{h}_\Delta \triangleq \mathbf{H}(:, \Delta)$. The minimum mean square error is given by

$$J_{min} = E_s(1 - \beta) \quad (3.7)$$

The standard MMSE-LE assumes tacitly zero-mean transmitted symbols $\mathbb{E}\{\mathbf{x}_n\} = 0$. However, the NRZ-OOK modulation format has a non-zero mean. Hence the MMSE-LE closed form has to be modified to account for the statistics of OOK symbols. This new closed form solution was carried out in [76]. Considering the actual statistics

of OOK symbols: $\mathbb{E}\{x_n\} = 0.5$, $E_s = \mathbb{E}\{|x_n|^2\} = 0.5$ and $\sigma_x^2 = \mathbb{E}\{|x_n|^2\} - \mathbb{E}\{x_n\}^2 = 0.25$, the MMSE-LE taps values in the thesis are given by [76]

$$\mathbf{p}^H = \mathbf{r}_{s,\Delta+1}^H \mathbf{H}^H (\mathbf{H} \mathbf{R}_x \mathbf{H}^H + \sigma_w^2 \mathbf{I})^{-1} \quad (3.8)$$

with

$$\mathbf{R}_x = \mathbb{E}(\mathbf{x}_n \mathbf{x}_n^H) = \sigma_x^2 \mathbf{I} + \mathbb{E}^2(x_n) \mathbf{1} \mathbf{1}^H = \begin{pmatrix} 1/2 & 1/4 & \cdots & 1/4 \\ 1/4 & 1/2 & \ddots & \vdots \\ \vdots & \ddots & \ddots & 1/4 \\ 1/4 & \cdots & 1/4 & 1/2 \end{pmatrix} \quad (3.9)$$

$$\mathbf{r}_{x,\Delta+1} = \mathbb{E}(\mathbf{s}_x \mathbf{s}_{x-\Delta}^*) = \sigma_x^2 \mathbf{e}_{\Delta+1} + \mathbb{E}^2(x_n) \mathbf{1} = \left(\frac{1}{4}, \dots, \frac{1}{4}, \frac{1}{2}, \frac{1}{4}, \dots, \frac{1}{4} \right)^t \quad (3.10)$$

where \mathbf{R}_x and $\mathbf{r}_{x,\Delta+1}$ takes into consideration the OOK correlation statistics [76]. The equalizer bias β is given by:

$$\beta = \mathbf{p}^H \mathbf{h}_{\Delta+1} \quad (3.11)$$

J_{min} is also corrected, considering the additional penalty for OOK.

$$J_{min} = E_s(1 - \beta) + \mathbb{E}^2(s_n)(\beta - \mathbf{p}^H \boldsymbol{\Sigma}_H) \quad (3.12)$$

The MSE, and consequently the output SNR is affected by the restitution delay Δ . This parameter gives a degree of freedom to the equalizer design and may be adjusted to increase performance, particularly when the equalizer has a short length N_F . The optimum restitution delay Δ_{opt} can be calculated in closed form by first computing a matrix \mathbf{Q} considering the N_F taps

$$\mathbf{Q} = \mathbf{H}^H (\sigma_x^2 \mathbf{H} \mathbf{H}^H + \sigma_w^2 \mathbf{I})^{-1} \mathbf{H} \quad (3.13)$$

Then, select the optimal Δ obtained through \mathbf{Q} :

$$\Delta_{opt} = \arg \max_{0 \leq i \leq N+L-2} Q(i, i) \quad (3.14)$$

The SNR at the output of the equalizer is given by:

$$SNR_{EQ} = \frac{\mathbb{E}\{|\beta x_{n-\Delta}|^2\}}{\mathbb{E}\{|v_n|\}} \quad (3.15)$$

Where, v_n is the residual ISI and the filtered white Gaussian noise. The corresponding bit-error probability P_b at the equalizer output may be approximated by:

$$P_b = \frac{1}{2} \operatorname{erfc} \left(d \sqrt{\frac{SNR_{EQ}}{2}} \right) \quad (3.16)$$

Assuming that v_n is well-modeled as AWGN independent from the signal and $d = x_1 - x_0$ is the minimal distance of the transmitted OOK constellation.

3.5 The adaptive LMS-LE

The last section assumed a perfect estimation of the channel in reception. In practice, the noise will affect channel estimation, thus the calculation of the closed form equalizer vector. Also, channel estimation requires calculations that may be too complex concerning the constraints of HS-PON. In this section, we develop the adaptive equalizer implemented in the HS-PON 50G setup. As the closed form version, LMS-LE aims to find the optimal set of taps that minimizes MSE iteratively.

The LMS-LE operates in two phases: The first phase is data-aided, known as training, and the second phase is decision-directed, known as tracking [69], [79]. During the training phase, a known sequence \mathbf{x}_n is transmitted and a synchronized version of this sequence is generated at the receiver to acquire information about the channel characteristics. At each symbol interval T the taps are gradually optimized, in a steepest-descent manner, towards the optimal value that minimizes the MSE $\mathbb{E}\{|e_n|^2\}$. After reaching the steady state at the training phase, the taps of the LMS-LE are continually adjusted based on the decisions of the symbol detector $\hat{x}_{n-\Delta}$ that may not be necessarily correct [64].

$$e_n = \begin{cases} z_n - x_{n-\Delta}, & \text{(Training)} \\ z_n - \hat{x}_{n-\Delta}, & \text{(Tracking)} \end{cases} \quad (3.17)$$

If properly implemented, the SBS detector decisions are usually correct most of the time. The tracking phase allows the equalizer to track slow variations in the channel characteristics and maintain precise equalization [61], [69].

Figure 3.3 show the LMS-LE block diagram.

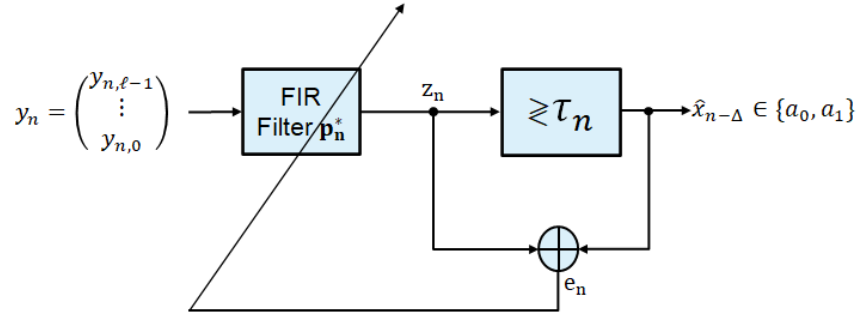


Figure 3.3: Block diagram of the adaptive linear equalizer.

The standard LMS update algorithm with a set of taps \mathbf{p}_n^H is given by equation 3.18.

$$\mathbf{p}_{n+1}^H = \mathbf{p}_n^H - \mu e_n \mathbf{y}_n^H \quad (3.18)$$

The convergence to the optimum set of taps depends on the channel characteristics, such as the channel delay, channel distortion, and variation in time. Here, at the beginning of the training phase the start values of the taps are zero, except the first tap, it starts with value one. μ is the step size that dictates the convergence speed and accuracy of the LMS-LE taps. $\mathbf{y}_n = [y_n, y_{n-1}, \dots, y_{n-N+1}]$ represents the state of the equalizer at the instant n , and the adaptive decision threshold τ_n , assuming $\mathbb{E}\{v_n\} = 0$ is calculated iteratively by:

$$\tau_n = \gamma\tau_{n-1} + (1 - \gamma)z_n \quad (3.19)$$

where γ is a convergence parameter, the mean square at the equalizer output can be:

$$MSE_n = \gamma MSE_{n-1} + (1 - \gamma)|e_n|^2 \quad (3.20)$$

The MSE trajectory is an important metric. The MSE transient analysis enables monitoring the convergence of the equalizer taps. Here it is used in the LMS versions of the LE and DFE.

3.6 MMSE-LE optimization methodology

The number of taps N_F and the restitution delay of the linear equalizer was optimized to ensure the implementation of a LE-based receiver with reduced complexity. Figure 3.4 demonstrate the optimization flow-chart of the MMSE-LE.

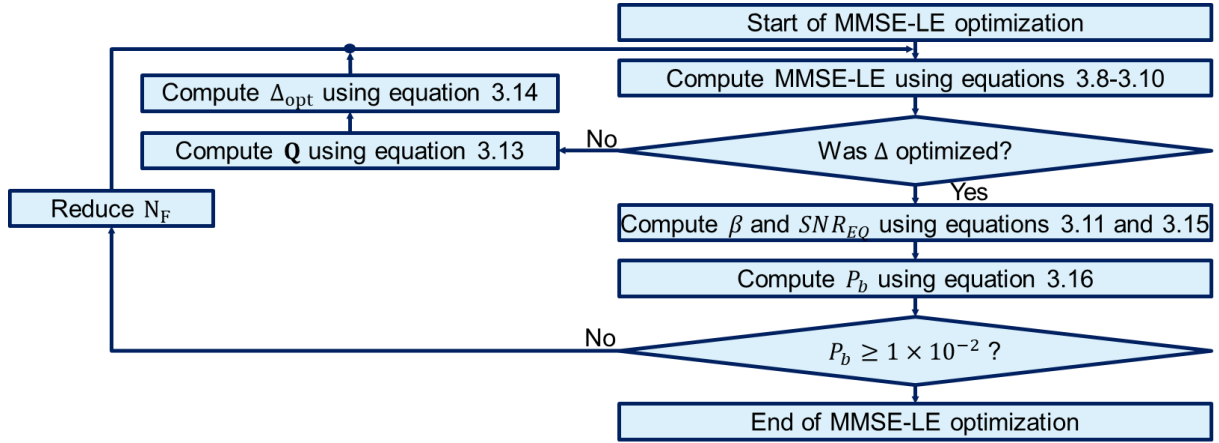


Figure 3.4: The MMSE-LE closed form optimization flow-chart.

This approach considers a point of measurement with $ROP = -24$ dBm because it is the ITU-T HS-PON sensitivity [1] supposing FEC LDPC hard-decision decoding, which pre-FEC BER is $BER = 1 \times 10^{-2}$, as discussed in section 1.4. The number of $T/2$ spaced taps N_F , the optimum delay Δ_{opt} and the predicted error probability after equalization P_b were used for the evaluation of the MMSE-LE. We chose the LMS-LE implementation over the EML and DML-based channels since 1) the LMS-LE is the adaptive implementation of the MMSE-LE and in practice it is most likely to be used since the channel impulse response is unknown and 2) it does not require matrix inversion computations hence is simpler in complexity sense.

3.7 Theoretical performance of the MMSE-LE over the 50G-PON

In this section, the performance of the MMSE-LE over the HS-PON 50G channels, based on EML and DML, will be reported. The relevance of predicting the theoretical performance of the equalizer from the closed form equations will be demonstrated through a comparison with the simulated performance of the adaptive LMS-LE.

The main goal is to evaluate how much gain the MMSE-LE can provide to the HS-PON in terms of sensitivity and optical budget, where the number of taps N_F , and restitution delay Δ are optimized, as presented in the previous section.

The minimum and maximum performance gain through MMSE-LE are studied. Some performance reference equalization use cases are proposed: When N_F is the lowest value to enable the target sensitivity $S = -24 \text{ dBm}$, the low-complexity performance is obtained. The good-balance use case increases the performance margin. It balances equalization complexity and equalization performance. When aiming for maximum equalization performance, i.e., the overall performance of the receiver does not improve further when more N_F taps are used, the performance use-case is entitled best-effort.

Table 3.1 shows the evaluated channels and the transmission chain nomenclature.

Table 3.1: Configuration of the simulated channels presented in chapter 2 and abbreviation.

Channel Configuration	Channel title
EML + SMF (20km) + APD (18.75 GHz)	EML + 25G Rx
EML + SMF (20km) + APD (37.5 GHz)	EML + 50G Rx
DML + SMF (20km) + APD (18.5 GHz)	DML + 25G Rx
DML + SMF (20km) + APD (37.5 GHz)	DML + 50G Rx

We remind that the channel performances are in a context with maximal cumulated chromatic dispersion for the 50G-PON, hence 20km of SMF. It was abbreviated to SMF, also the $0.75 \times B_{APD}$ was associated with the bit rate of operation of the receiver.

3.7.1 Closed form performance prediction

The prediction of the performance of the fractionally spaced T/2 MMSE-LE was based on the SNR and channel taps estimated by the least square estimator (more details of least square estimation in Appendix D). Figure 3.5 shows the evolution of SNR_{EQ} vs N_F with the configuration EML + 25G and EML + 50G Rx, through different operation points $ROP = \{-20, -24, -32\} \text{ dBm}$, as insets.

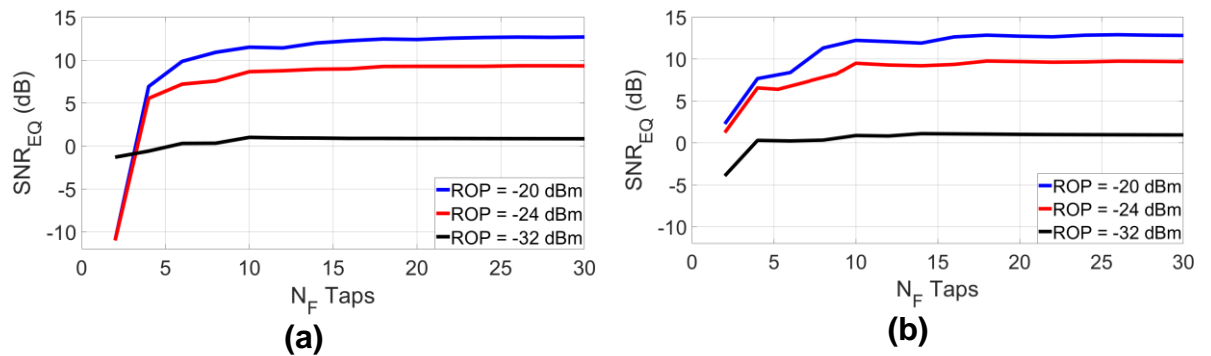


Figure 3.5: closed form SNR_{EQ} vs N_F performance over channels EML + (a) 25G Rx and (b) 50G Rx.

The computed curves have a similar increase of SNR_{EQ} when N_F increases. Naturally, the higher ROP dictates the level of SNR_{EQ} , since the ROP is directly proportional to the power of the received signal. When the MMSE-LE has $N_F = 2$ taps, the SNR_{EQ} is relatively low for both receivers. However, a remarkable SNR_{EQ} gain is obtained when $N_F = 4$, hence, indicating low-complexity equalization performance. Once the number of taps is between $N_F = 6$ to $N_F = 10$ a case of a good balance between complexity and performance is verified. Finally, with $N_F = 16$ taps the performance of best effort is reached. The SNR_{EQ} has similar values for a fixed value of N_F taps and ROP considering the two channels, therefore, the improvement of the performance of MMSE-LE is not severely impacted when the bandwidth is limited to 18.75 GHz or 37.5 GHz.

In figure 3.6 the SNR_{EQ} vs N_F for the setup DML + 25G Rx and DML + 50G Rx receivers are shown.

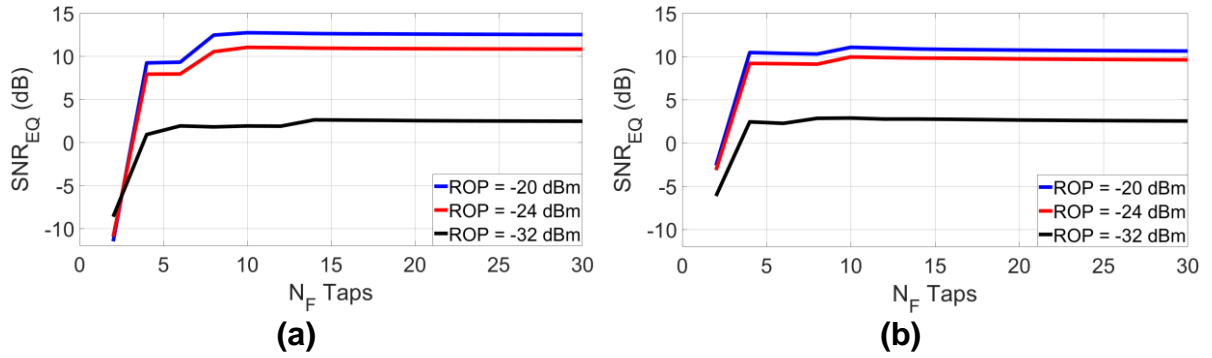


Figure 3.6: closed form SNR_{EQ} vs N_F performance over channels DML + (a) 25G Rx and (b) 50G Rx.

We observed that in both DML-based configurations, a low SNR_{EQ} is calculated when $N_F = 2$ taps, such as the EML case. When $N_F = 4$ taps, both setups achieve an important SNR_{EQ} gain, almost as high as the infinity length. This indicates that the performance improvement of the linear equalizer may not be expressive when the number of taps is increased, as observed in the EML case. When $N_F = 6$ taps good-balance performance results. Finally, we reach the best-effort performance with $N_F = 12$ taps.

Comparing the SNR_{EQ} , both DML-based channels with LE and the channel with the 25G receiver achieve better performances because the noise predominates the ISI in the 50G channel, a natural behavior since the photodiode filtering increases ISI and limits noise, thus improving the SNR. Since the LE compensates ISI balancing noise enhancement when the noise at the output of the channel has increased, the performance of the equalizer deteriorates. In other words, we saw in section 2.6 that the bandwidth limitation is the predominant linear ISI effect of the DML-based channel. In this case, filtering is more beneficial to reduce noise in the signal bandwidth than to increase ISI.

Evaluating the performance of the EML + 25G Rx and the DML + 25G Rx channels + MMSE-LE, the DML-based channel achieved better SNR_{EQ} with fewer

taps, hence less complexity. In the case of the DML-based channels with 50G receivers, the same trend is observed. Therefore, the DML channel has better performance than the EML channels considering linear equalization. It is a logical result because, as observed in the performance without equalization in section 2.6, the channels in the presence of adiabatic chirp are not impacted by severe ISI, hence the assumed linear distortion from the DML is slighter than the EML.

Afterward, the evolution of optimum delay Δ vs N_F taps to different points of operation $ROP = \{-20, -24, -32\}$ dBm for the EML and DML setups are illustrated in figures 3.7 and 3.8, respectively.

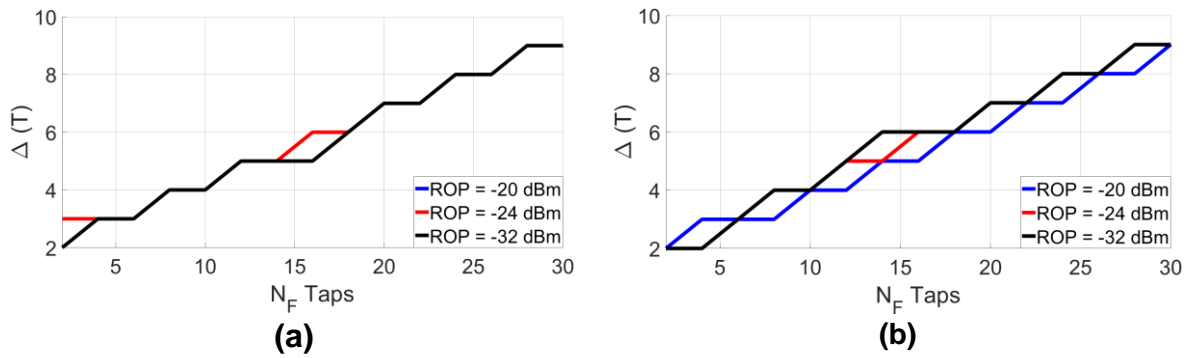


Figure 3.7: Optimum delay Δ vs N_F over channels EML + (a) 25G Rx and (b) 50G Rx.

For the EML + 25G Rx, the optimal delay is the same regardless of the ROP. The same trend is noted for the EML + 50G Rx. The optimal delay for $ROP = -24$ and $ROP = -32$ dBm is practically the same, but there is a difference of one symbol period T when the ROP is increased to $ROP = -20$ dBm. For the EML + 50G Rx, the optimum delay is practically the same for $ROP = -24$ and $ROP = -32$ dBm. However, when the ROP is increased to -20 dBm, there is a delay discrepancy of T . A rule of thumb would be to set the delay as half the number of N_F taps +1 to not obtain severely degraded equalization performances, but it depends on the ROP and the channel.

For the channel DML + 25G Rx, the optimum delay for $ROP = -20$ dBm is practically the same as at $ROP = -32$ dBm. When the ROP is increased from $ROP = -32$ dBm to $ROP = -24$ dBm, there is a variation of the optimum delay. Finally, considering the channel DML + 50G Rx, the optimum delay for $ROP = -20$ dBm, and $ROP = -24$ dBm are similar and may change when the ROP is decreased to $ROP = -32$ dBm.

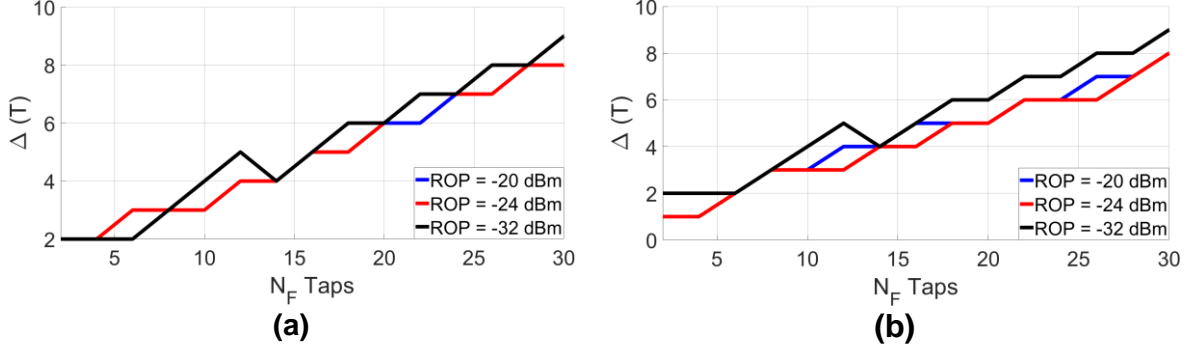


Figure 3.8: Optimum delay Δ vs N_F over channels DML + SMF (a) 25G Rx (b) 50G Rx.

Considering that the restitution delay of the equalizer in HS-PON is $\tau_D = T \times \Delta$, and $T = \frac{1}{50 \times 10^9} = 20 \text{ ps}$. The increase of latency to the MMSE-LE varies from $\tau_D = 20 \text{ ps} \times 2 = 40 \text{ ps}$ in low-complexity case to $\tau_D = 20 \text{ ps} \times 9 = 180 \text{ ps}$ for the best performance scenario, which is negligible considering the latency requirements for HS-PON applications, which are on the order of μs [27].

Figures 3.9 and 3.10 show the predicted BER vs N_F , for several feedforward-optimized tap sets $N_F = \{2, 4, \dots, 16\}$ with EML and DML. The closed form-based prediction indicates that with the EML-based setup, at least $N_F = 6$ taps are necessary to reach the target sensitivity $S = -24 \text{ dBm}$ at the FEC threshold $BER_{FEC} = 10^{-2}$. $N_F = 8$ and $N_F = 10$ enables good-balance performance for the EML+25G and EML+50G receivers, respectively. $N_F = 16$ taps are enough for best-effort performance.

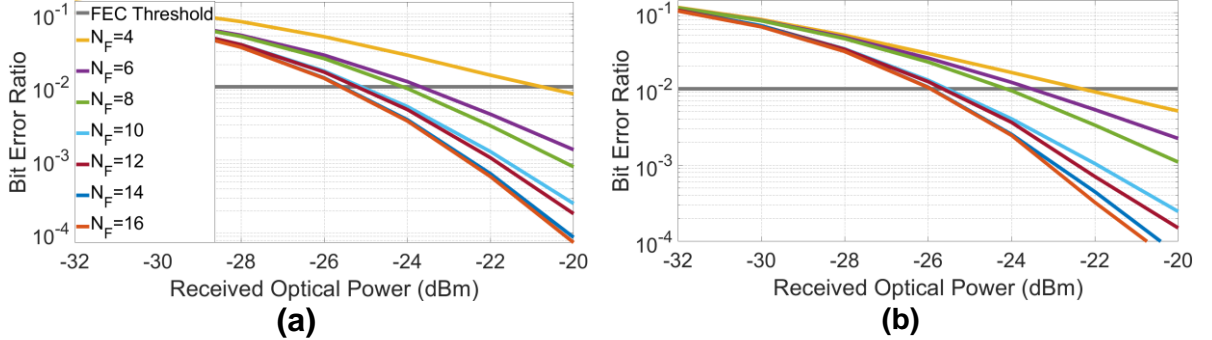


Figure 3.9: closed form BER vs N_F performance over channels EML + SMF + (a) 25G Rx (b) 50G Rx.

For the DML channel, the BER vs N_F estimations indicate that low-complexity performances can be achieved with $N_F = 4$ taps, a sensitivity $S = -26 \text{ dBm}$ for the DML + 25G Rx, and $S = -28 \text{ dBm}$ for the DML + 50G Rx. $N_F = 8$ taps appear sufficient to read the maximum sensitivity gain possible with the MMSE-LE in this scenario.

For the DML + 50G Rx setup, we see no significant improvement in sensitivity with the MMSE-LE. Indicating that the channel ISI penalty can be compensated with $N_F = 10$ taps.

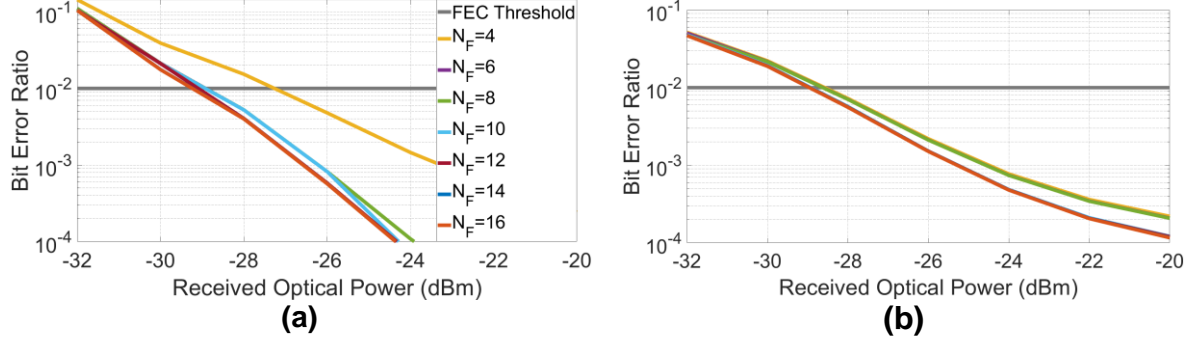


Figure 3.10: closed form BER vs N_F over channels DML + SMF + (a) 25G Rx and (b) 50G Rx.

Figure 3.11 shows the $T/2$ spaced MMSE-LE taps with ROP = -24 dBm, for $N_F = 16$ and $\Delta = 4$. we observed that for both the EML + 25G Rx and EML+50G Rx scenarios, the 16 taps have non-negligible energy. Therefore the FFE here spans $T_{span} = N_F \times \frac{T}{\ell} = 16 \times \frac{T}{2} = 8$ symbol periods.

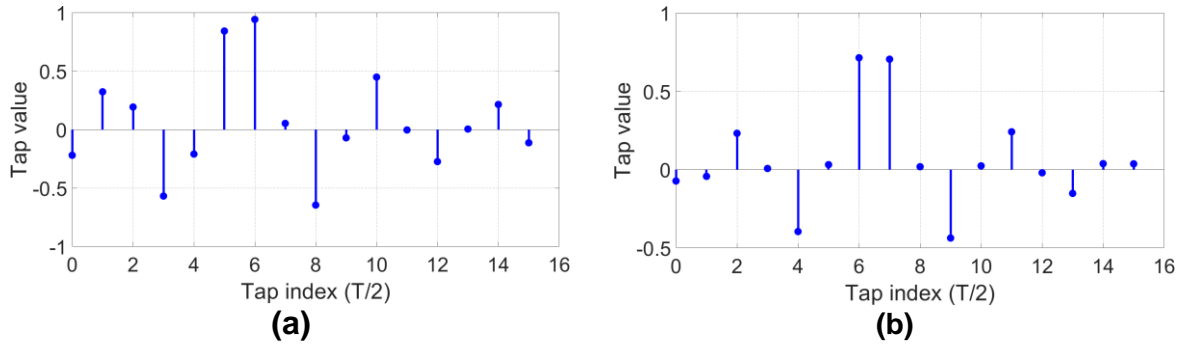


Figure 3.11: MMSE-LE impulse response over channels EML + SMF + (a) 25G Rx (b) 50G Rx.

It is also important to point out that the taps with higher energy (taps 5 and 6) are close to each other. It implies that delay optimization for equalizers having a low number of taps N_F is critical.

Figure 3.12 show the MMSE-LE impulse response of the DML-based setup. For the DML + 25G receiver setup, we see that the energy is concentrated in the $N_F = 4$ taps (from tap 6 to tap 9) around the tap with the highest energy (tap 7), hence the feedforward filter spans $T_{span} = 4 \times \frac{T}{2} = 2T$ symbol periods. Here the number of taps can be reduced to decrease the equalization complexity and keep the same performance.

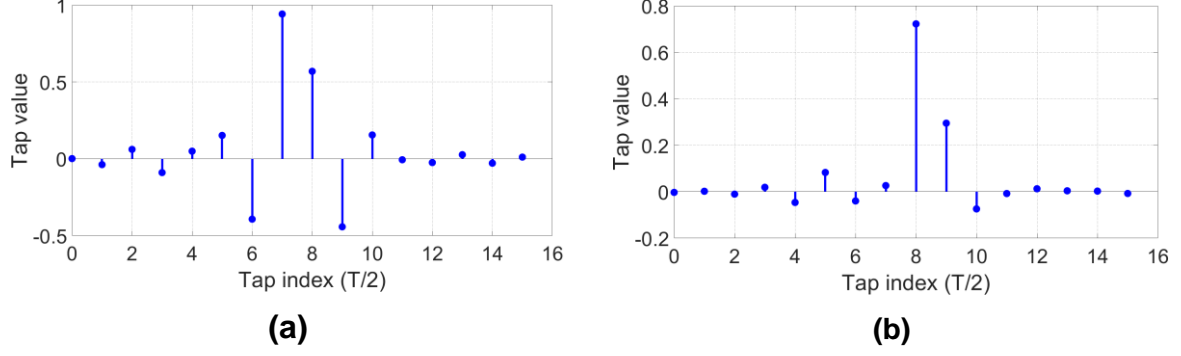


Figure 3.12: MMSE-LE impulse response over channels EML + SMF + (a) 25G Rx (b) 50G Rx.

In the DML + 50G receiver case, we see that the energy is concentrated in two taps (taps 8 and 9), a quasi-free ISI channel in which the FFE span only a symbol period $T_{span} = T$.

Table 3.2 summarizes the predicted performances with the MMSE-LE.

Table 3.2: Closed form predictions of the MMSE-LE over EML and DML 50G channels

Setup	MMSE-LE	SNR _{EQ} (dB)	Predicted sensitivity (dBm)
EML + 25G Rx	$N_F = 4, \Delta = 3$	5.5	-20.0
	$N_F = 6, \Delta = 3$	7.2	-24.0
	$N_F = 16, \Delta = 6$	8.6	-25.0
EML + 50G Rx	$N_F = 6, \Delta = 3$	6.3	-23.0
	$N_F = 8, \Delta = 3$	7.3	-24.0
	$N_F = 16, \Delta = 6$	9.3	-25.0
DML + 25G Rx	$N_F = 4, \Delta = 1$	7.9	-27.0
	$N_F = 8, \Delta = 4$	11.0	-28.0
DML + 50G Rx	$N_F = 4, \Delta = 3$	9.2	-28.0
	$N_F = 8, \Delta = 3$	9.1	-28.0

3.8 Simulated performance of the LMS-LE over the 50G-PON

After the theoretical prediction of equalizer performance in closed form, the LMS-LE was optimized and implemented at the output of the EML and DML-based channels. The MMSE-LE optimum parameters were used in the LMS-LE configuration. The step size was fixed to $\mu = 0.001$, $N_{DA} = 200\,000$ symbols were used during the training phase. $N_{DD} = 800\,000$ symbols were used during the tracking phase and, subsequently, for the bit error ratio performance evaluation. To estimate the learning curve of MSE, a step size value $\gamma = 0.999$ was chosen.

3.8.1 The EML + 25G Rx

The measured BER vs ROP curve without equalization and at the output of LMS-LE with the EML + 25G channel is illustrated in figure 3.13.

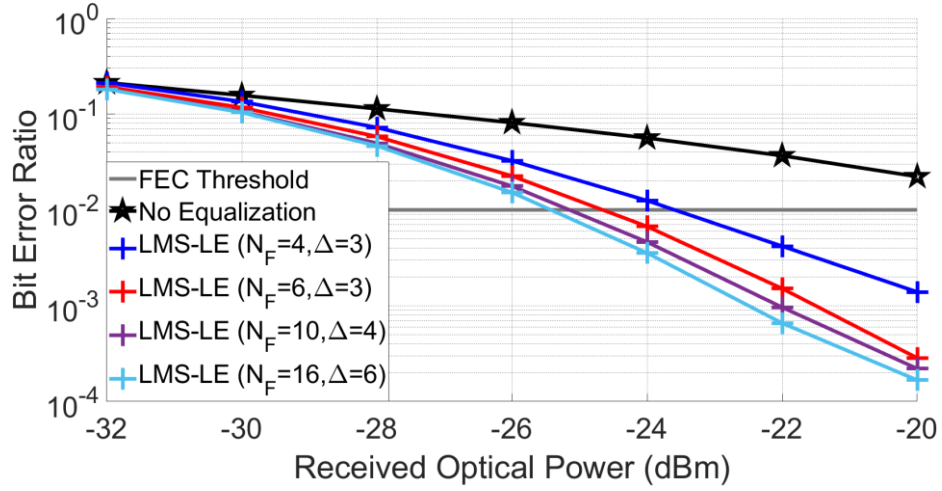


Figure 3.13: BER vs ROP measured with setup EML + 25G Rx at the output of the LMS-LE.

The LMS-LE handles well the linear impact of CD, chirp, and bandwidth limitation, differently than the receiver without equalization. When the LMS-LE is used with parameter $N_{FFE} = (N_F = 4, \Delta = 3)$, a sensitivity $S_{LMS-LE} = -23$ dBm is reached, so a simple linear equalizer provides a gain of at least $G = 4$ dB to the HS-PON receiver. With $N_F = 6$ taps, the ITU-T sensitivity is achieved: $S_{LMS-LE} \leq -24$ dBm. When $N_F = 10$ taps and $N_F = 16$ taps, the sensitivity calculated at the LMS-LE-based receiver reaches $S = -25$ dBm. Note that the IM/DD impact is sufficiently compensated with 10 taps, more taps improve the performance slightly, even at high ROP.

3.8.2 The EML + 50G Rx

The performance of the EML + 50G Rx system is shown in figure 3.14.

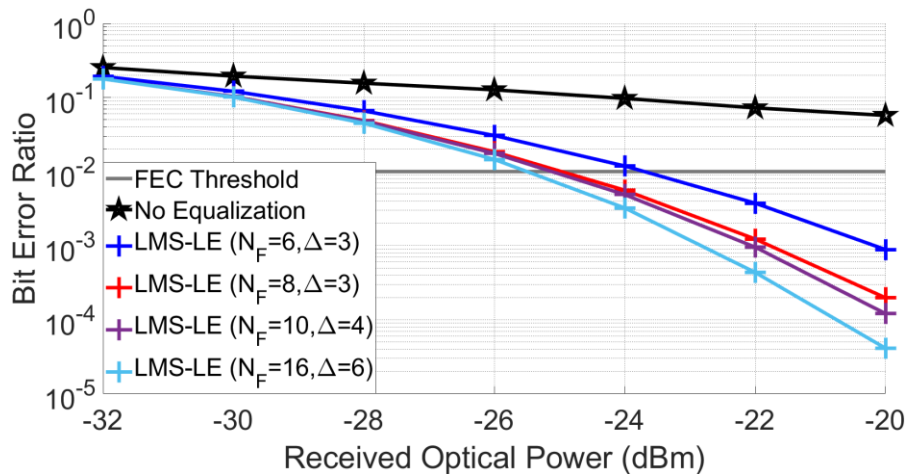


Figure 3.14: measured BER vs ROP with setup EML + 50G Rx at the output of the LMS-LE.

The LMS-LE deal well with the IM/DD impact, despite this channel presenting less ISI and more noise than the previous one. With $N_{FFE} = (N_F = 6, \Delta = 3)$ the sensitivity $S = -23$ dBm is achieved. This simulation result confirms that the noise predominates the ISI and consequently decrease the LMS-LE performance, as verified in the MMSE-LE predictions. This receiver requires $N_F = 8$ taps to achieve $S = -24$ dBm, which is the good balance performance and with $N_F = 16$ taps reach $S = -25$ dBm.

We can infer the noise impact and bandwidth limitation by comparing the performance with $N_F = \{10, 16\}$ taps with the 25G Rx and 50G Rx. Note the performance gap for $ROP > -24$ dBm, it is clear that for higher SNR $N_F = 16$ taps improves more the 50G receiver.

The LMS-LE with the 37.5 GHz APD (50G Rx) has worse performance than the LMS-LE with the 18.75 GHz APD (25G Rx). We verified that the impact of noise is more severe than the ISI in terms of symbol decisions, which is why the EML+SMF+50G Rx configuration required more taps to achieve the same sensitivity as the EML + 25G Rx simulated setup.

3.8.3 The DML + 25G Rx

Figure 3.15 shows the BER vs ROP for the DML + 25G Rx configuration. As we evaluated in section 2.6, the performance is good with the DML considering the ITU-T requirement, mainly because the adiabatic chirp of the DML adds non-linearities to the received waveform but dampens the spectral notches caused by chromatic dispersion and chirp interplay. Still, there is a considerable bandwidth limitation of the 18.75GHz APD, compared to the bit rate of 50 Gbit/s.

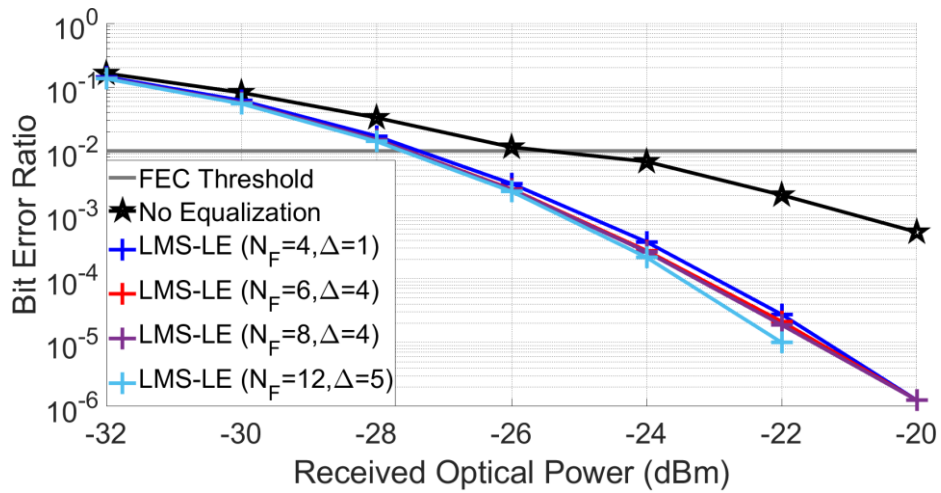


Figure 3.15: measured BER vs ROP with setup DML + 25G Rx at the output of the LMS-LE.

The LMS-LE compensates well for the IM/DD DML linear impacts, especially the bandwidth limitation, which is the most important here. The number of required taps is small because this channel distortion is not critical. The LMS-LE compensate well the bandwidth limitation with only four taps and the receiver improves the receiver sensitivity by 2dB, hence achieves $S_{LMS-LE} = -27$ dBm. When the number of taps is increased, there is no significant improvement, consequently, the linear distortion of

the channel is easy to compensate for, as we expected in the MMSE-LE predictions. The best overall performance is obtained with $N_F = 12$ taps. We cannot evaluate here how much nonlinear distortion the DML adds, but it is not a critical effect.

3.8.4 The DML + 50G Rx

Figure 3.16 illustrates BER vs N_F performance over the DML + SMF 50G Rx configuration. This is an almost ISI-free channel, there is no linear impact to justify using the LMS-LE. It was foreseen in the MMSE-LE prediction. Furthermore, comparing this and the previous channel performance, we confirm that the bandwidth limitation is the only impairment of the DML + APD simulated setup.

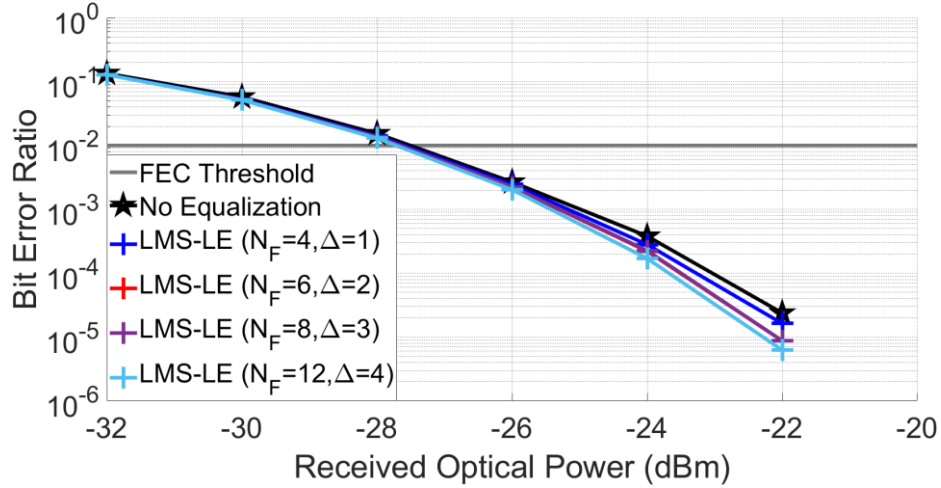


Figure 3.16: measured BER vs ROP with setup DML + 50G Rx at the output of the LMS-LE.

All the studied channels achieved the recommended sensitivity through the T/2 spaced LMS-LE, the best-effort performances required 16 taps with the EML-based channel and 12 taps with the DML + 25G Rx channel. The maximum restitution delay $\Delta = 6 = 120$ ps introduced by the LMS-LE is negligible to the HS-PON requirements of latency which is in order of μ s.

3.8.5 Transient analysis of the LMS-LE

The estimated MSE vs Iteration of the LMS-LE was monitored for each equalization parameters $N_{FFE} = (N_F, \Delta)$ with all simulated IM/DD PON channels. We show in figure 3.17 the LMS-LE transient evolution with the channels EML + 25G and EML + 50G Rx with $ROP = \{-20, -24, -32\}$ dBm and $N_F = 16$ taps.

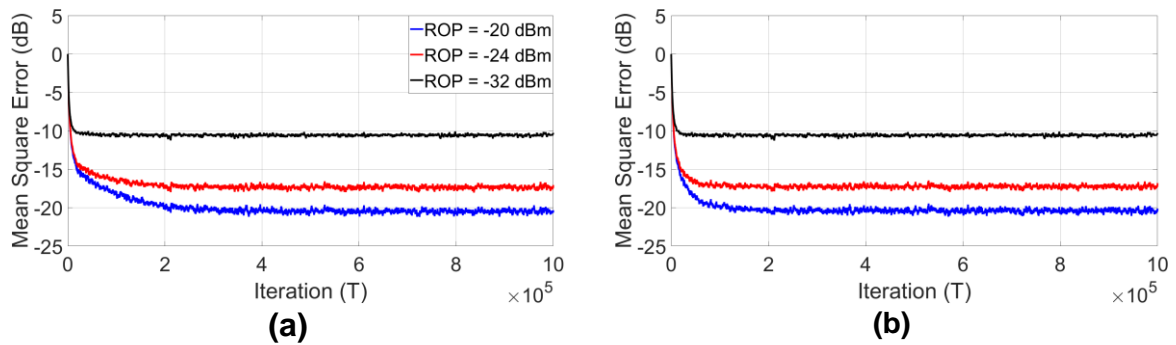


Figure 3.17: MSE vs iteration over channels EML + SMF + (a) 25G Rx and (b) 50G Rx.

The EML + 25G Rx channel requires $N_{sy} = 100 \times 10^3$ symbols to train the equalizer regardless of the ROP, hence the training period to achieve the steady-state is $T_{SS} = N_{sy} \times T = 100 \times 10^3 \times 20 \text{ ps} = 2.0 \mu\text{s}$. During the tracking phase, it reaches a final $MSE = -17 \text{ dB}$ with respect to $ROP = -24 \text{ dBm}$. The EML + 50G Rx channel requires $N_{sy} = 90 \times 10^3$ symbols for the training phase, hence the LMS-LE converge after $T_{SS} = 90 \times 10^3 \times 20 \text{ ps} = 1.8 \mu\text{s}$, it achieves $MSE = -17 \text{ dB}$ in tracking phase for a $ROP = -24 \text{ dBm}$.

The LMS-LE converges to close values with both receivers thus the calculated BER of the EML+SMF+25G Rx and the EML+SMF+50G Rx after equalization has a good agreement. For instance, when the received power is $ROP = -24 \text{ dBm}$ the obtained BER is $BER = 3 \times 10^{-3}$.

Figure 3.18 represents the MSE learning curve over the DML + 25G Rx and DML + 50G Rx channels.

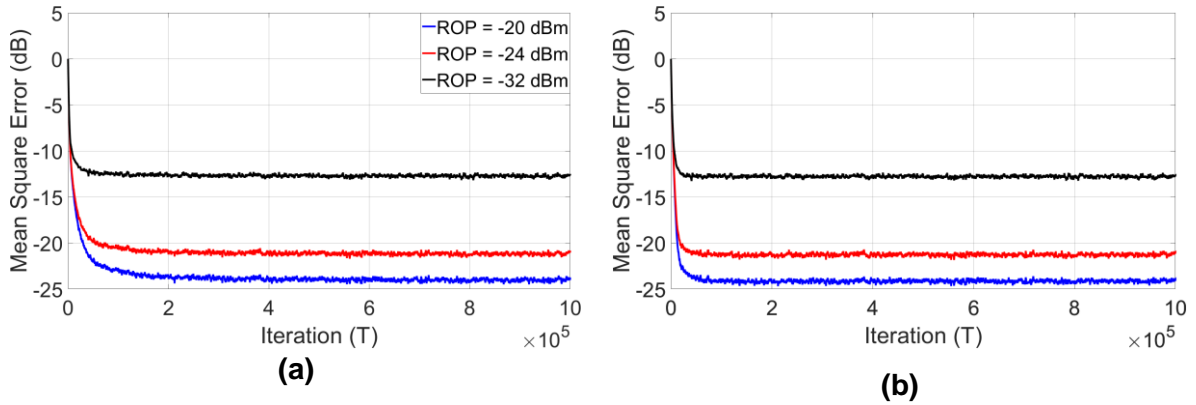


Figure 3.18: MSE vs iteration over channels DML + SMF + (a) 25G Rx and (b) 50G Rx.

As in the previous simulations, the number of symbols to train the equalizer in practice is the same regardless of the ROP. The DML + 25G Rx requires $N_{sy} = 160 \times 10^3$ symbols during the training phase, consequently it takes $T_{SS} = 3.2 \mu\text{s}$ to converge. The 50G-based Rx channel requires $N_{sy} = 80 \times 10^3$ training symbols, thus $T_{SS} = 1.6 \mu\text{s}$ to achieve steady-state. At the end of the tracking phase, both receivers achieve the same MSE value of -20 dB when $ROP = -24 \text{ dBm}$. The obtained BER is $BER = 2 \times 10^{-4}$ with both receivers.

3.9 Main results of the linear equalizer

Comparing the EML and DML-based channels, we see that the latter achieves better MSE than the former, given an ROP and the APD 3dB bandwidth. As described in the small-signal analysis of section 2.6, it is normal because the EML channel suffers from severe ISI due to frequency-nulls present on the 50 GHz bandwidth, differently to the DML whose adiabatic chirp smooths the channel spectral attenuation. The training period required to train the LMS-LE of all channels is acceptable, considering the ITU-T HS-PON requirements for downstream transmissions [1].

Finally, Table 3.3 show the comparison of the measured and predicted sensitivities in the EML and DML simulations and optical budget $OB = P_{TX} - S$ introduced in chapter 1. The optical launch power of the EML was $P_{TX} = 10$ dBm and the optical launch power of the DML was $P_{TX} = 11$ dBm, assuming the DML has less launch power than the EML.

Table 3.3: Main results obtained with the MMSE-LE

Setup	MMSE-LE configuration	Predicted sensitivity (dBm)	Simulated sensitivity (dBm)	Optical budget (dB)
EML+25G Rx	$N_F = 4, \Delta = 3$	-20	-23	33
	$N_F = 6, \Delta = 3$	-24	-24	34
	$N_F = 16, \Delta = 6$	-25	-25	35
EML+50G Rx	$N_F = 6, \Delta = 3$	-23	-23	33
	$N_F = 8, \Delta = 3$	-24	-24	34
	$N_F = 16, \Delta = 6$	-25	-25	35
DML+25G Rx	$N_F = 4, \Delta = 1$	-27	-26	35
	$N_F = 8, \Delta = 4$	-28	-27	36
DML+50G Rx	$N_F = 4, \Delta = 3$	-28	-26	35
	$N_F = 8, \Delta = 3$	-28	-27	36

For the EML + 25G and EML + 50G receivers case, the measured and predicted sensitivity have a good agreement, except when $N_F = 4$ taps because the channel ISI in this case is not well modeled by the MMSE-LE since the channel ISI spans more symbols than assumed by the prediction. The good agreement between predictions and measurements indicates that the effects caused by the EML-based channel are sufficiently linear. Consequently, the linear equalizers may be designed through 50G closed form equations without simulating equalization performance.

For the DML + 25G and DML + 50G receivers, there is a 1 dB difference between the predicted and measured sensitivities. So, the linear discrete equivalent channel model for DML emitters is not precisely accurate for the channel estimation due to the adiabatic chirp effect. This result corroborates the evaluation of the channel based on DML made by O. Duill et al. It was found that the linear channel model at 50Gbit/s for DML, based on a small-signal regime, is severely degraded at 50Gbit/s due to adiabatic chirp [50].

The MMSE-LE-based receivers for EML and DML meet the optical path loss recommendations. After the implementation of the linear equalizers, the maximum optical path loss of class C+ (32 dB) is reached.

3.10 Concluding remarks

Linear equalization is a key technology that may be used to ensure the required performance for 50G-PON. In the simulations, the LE demonstrates a huge potential for the HS-PON since it handles very well the linear impacts of bandwidth limitation in the presence of noise.

The MMSE-LE enables 50Gbit/s NRZ-OOK transmissions to meet the sensitivity and optical budget requirements defined by the ITU-T. We verified that the LMS-LE simulated performance are close to the MMSE-LE closed form performance

estimations in simulations of optical transmissions over 20km of fiber with EML and DML and receivers based on APD with limited bandwidth. This means that the design of equalizers may be done without numerical simulations.

All the proposed setups met the required sensitivity and optical budget with linear equalization. The limits of linear equalization were evaluated. It was verified that the delay added by the MMSE-LE is negligible for the DSP-enabled HS-PON applications. For the EML + 25G Rx taps setup, a -24dBm sensitivity low-complexity equalization performance was reached with $N_F = 6$ taps and up to $S = -25$ dBm with $N_F = 16$ taps, in best-effort performance. With the DML + 25G Rx channel, we see that the linear equalizer can reach the sensitivity of -27 dBm with $N_F = 4$ taps, but the linear equalizer cannot offer high sensitivity gain, considering that the adiabatic chirp of the DML is elevated hence the channel does not introduce severe ISI.

When the receiver bandwidth is increased, there is not an effective increase in receiver performance. Instead, the residual noise at the equalizer input becomes dominant. Consequently, more taps are needed by the MMSE-LE to maintain the same sensitivity as the 25G receiver, either with EML or with DML at the transmitter.

Finally, considering the transient analysis of the LMS-LE, we observe that the restitution delay value is in the order of 100ps, which conforms with the low-latency requirement by ITU-T. The number of symbols to train the equalizer is in the order of 100 000 symbols. Therefore, one μ s is enough for the training period of the linear equalizer considering the 50 Gbit/s bit rate acceptable in the downstream transmissions, considering the 125 μ s ONU time slot.

4 Decision Feedback Equalization to improve the 50G-PON Receiver

4.1 Introduction

The decision feedback equalization is a powerful tool to compensate for severe ISI. As we saw in the previous chapter, the linear equalizer compensates well for the channel distortions, but since the ISI is severe, the DSP receiver may use a more advanced equalizer to compensate for the linear distortion completely.

The IM/DD channel suffers from severe ISI due to frequency fading, as discussed in Chapter 2. Then, chapter 3 introduced linear MMSE-based equalization, balancing noise enhancement, and distortion. It was interesting for the 50G-PON channel because it presents frequency nulls. We saw the closed-form MMSE-LE equations and adaptive LMS-LE evaluation in EML and DML simulations. Considering the sensitivity and optical budget recommended by ITU-T, the LMS-LE achieved the required performance. However, the MMSE-LE does not entirely compensate for the frequency selectivity of the 50G IM/DD channel. There is still residual ISI in the LE output. To deal with the severe ISI of the HS-PON channel, the Decision Feedback Equalizer (DFE) is introduced and assessed in this chapter.

We organized this chapter as follows. Section 4.2 introduces the structure and the principle of work of the MMSE-DFE. Afterward, the closed-form equations used to compute the equalizer taps in standard form, and the corrected form, specialized to the NRZ-OOK alphabet are introduced in section 4.3. Section 4.4 presents the Least Mean Square Decision Feedback Equalizer (LMS-DFE). Next, the optimization procedure used to minimize the number of taps of the feedforward filter (N_F) and the feedback filter (N_B) are introduced in section 4.5. Afterward, the closed-form prediction and measured LMS-DFE performance with the EML and DML-based channels are shown in section 4.6. and 4.7, respectively. Finally, section 4.8 highlights the achievements of the MMSE-DFE, and section 4.9 discusses the chapter content.

4.2 The MMSE decision feedback equalizer

The MMSE-LE described in chapter 2 may suffer from noise enhancement, which reduces its effectiveness, especially in the channel with low SNR and spectral null. Furthermore, it cannot completely eliminate severe ISI [68]. The non-linear equalization has been extensively analyzed to improve the linear receiver [80]–[82]. Among the main contributions, the idea of compensating distortion using previous decisions was proposed by Austin [83]. Then, the first minimum mean square error-based DFE was presented by Mosen in 1971 [84].

The DFE structure is illustrated in figure 4.1 [64]. The MMSE-DFE is the non-linear alternative to the MMSE-LE. It attempts to compensate for the severe ISI without penalty of performance due to the noise enhancement present in the MMSE-LE. The MMSE-DFE performance is not necessarily better than the linear equalizer in terms of MSE. The DFE consists of two FIR filters and a decision device. The feedforward filter turns the discrete-time channel into a causal transfer function. Hence it is an anticausal filter and contains N_F fractionally spaced taps at time interval T/ℓ [51]. The feedback section comprises a strictly causal feedback filter with N_B T -spaced taps. The input of the feedforward filter is the received signal y_n . The feedback filter has at its input the

sequence of decisions on previously detected symbols $\hat{x}_{n-\Delta}$, assumed to be correct [84]. The main goal of the feedback filter is to remove the trailing ISI from the present symbol z_n caused by previously detected symbols $\hat{x}_{n-\Delta}$ [61], [68]. The equalized symbol z_n is the sum of the feedforward and feedback sections. Finally, z_n is processed by a memoryless symbol-by-symbol detector with threshold τ [51]. The DFE is nonlinear because of the presence of the hard-decision device in the feedback loop [68].

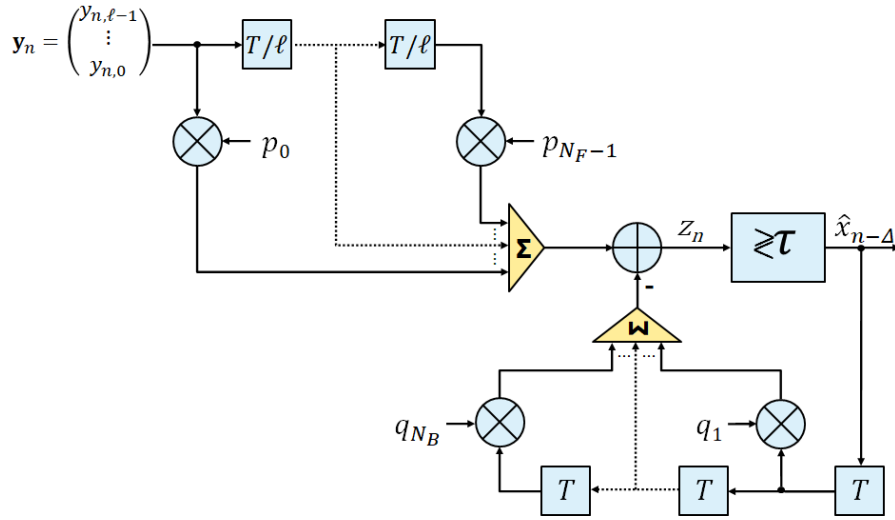


Figure 4.1: The decision feedback equalizer structure.

The DFE assumes that previous decisions are correct. However, feedback decisions might be erroneous in real implementations, which can drastically diminish the performance of the equalizer and be disastrous. Some authors propose the amplitude scaling of the feedback symbols to reduce the error probability of feedback decisions [85]. Otherwise, the practical method to evaluate the impact of wrong decisions is empirical since the analytical evaluation is computationally complex [73], [86], [87].

The main goal of this chapter is to propose a study of MMSE-DFE considering the constraints present in the next generation of PON with DSP enabled at the receiver [25], [88].

4.3 The closed-form MMSE-DFE

The calculations of the MMSE-DFE taps in closed-form require knowledge of the channel impulse response \mathbf{h} and the SNR, just like the MMSE-LE presented in section 3.4. First, the standard closed-form MMSE-DFE equations derived from the work of Al-Dhahir and Cioffi are presented [75], [76], [89]. Then, novel closed-form equations to calculate the MMSE-DFE for the NRZ-OOK alphabet are introduced, derived in [76] were introduced.

Figure 4.2 illustrates the structure of the DFE in terms of feedforward (FF) and feedback (FB) FIR filters sections.

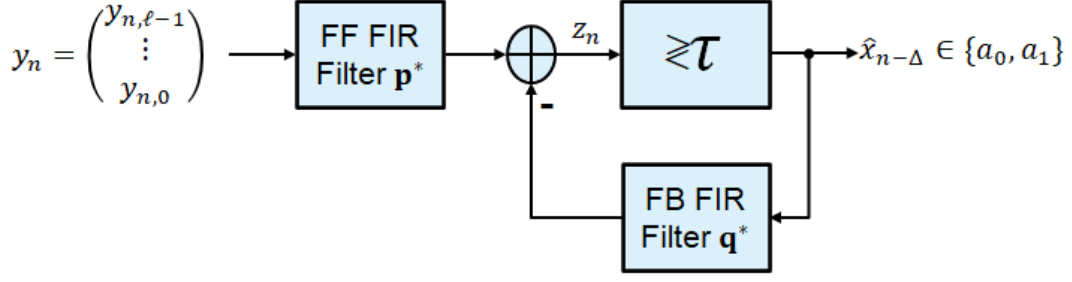


Figure 4.2: The decision feedback equalizer structure in terms of FF and FB sections.

The finite-length MMSE-DFE contains two FIR filters. It comprises the fractionally spaced FF filter taps $\mathbf{p} = [p_{0,0}, \dots, p_{N_F-1, \ell-1}]^T$ with $N_F = N_{sp} \times \ell$ taps, where N_{sp} is the number of considered successive symbol periods and T/ℓ the interval between each tap. The symbol-spaced FB filter taps $\mathbf{q} = [q_1, \dots, q_{N_B}]^T$ with $1 \leq N_B \leq L-1$, considering L as the T-spaced length of the channel impulse response. The DFE taps are obtained according to the MMSE criterion $J(\mathbf{p}^*, \mathbf{q}^*) = \mathbb{E}\{|z_n - x_{n-\Delta}|^2\}$, where the restitution delay of the feedforward filter is $0 \leq \Delta \leq N_F + L - 2$. Considering the past estimated symbols are correct, $x_n = \hat{x}_n$, the equalized sample z_n at the input of the symbol-by-symbol detector at instant n is [76]

$$z_n = \mathbf{p}^T \mathbf{y}_n - \mathbf{q}^T \mathbf{x}_{n-\Delta-1} \quad (4.1)$$

As also observed in section 3.5, $\mathbf{y}_n = [y_n, \dots, y_{n-N_F+1}]^T$ is the $N_F \times 1$ received samples vector at the output of the discrete channel. $\mathbf{p} = [p_0, \dots, p_{N_F-1}]^T$ is the $N_F \times 1$ FF taps vector. $\mathbf{q} = [q_1, \dots, q_{N_B}]^T$ is the $N_B \times 1$ FB taps vector, and $\mathbf{x}_{n-\Delta-1} \stackrel{\text{def}}{=} \begin{pmatrix} x_{n-\Delta-1} \\ \vdots \\ x_{n-\Delta-N_B} \end{pmatrix}$ is the feedback symbols vector at the output of the symbol-by-symbol detector, also with dimensions $N_B \times 1$. The optimal standard MMSE-DFE FF filter be computed as [76]

$$\mathbf{p}^H = E_x \mathbf{h}_{\Delta+1}^H (E_x \mathbf{H} (\mathbf{I} - \mathbf{J}_\Delta \mathbf{J}_\Delta^H) \mathbf{H}^H + \sigma_w^2 \mathbf{I})^{-1} \quad (4.2)$$

with

$$\mathbf{h}_{\Delta+1} \stackrel{\text{def}}{=} \mathbf{H}(:, \Delta+1) \quad (4.3)$$

and \mathbf{J}_Δ is an $N_F + L - 1 \times N_B$ matrix of zeros and ones defined by

$$\mathbf{J}_\Delta \stackrel{\text{def}}{=} \begin{pmatrix} \mathbf{0}_{(\Delta+1) \times N_B} \\ \mathbf{I}_{N_B} \\ \mathbf{0}_{s \times N_B} \end{pmatrix} \quad (4.4)$$

where $\mathbf{0}_{(\Delta+1) \times N_B}$ is a zero matrix of dimensions $\Delta+1 \times N_B$, \mathbf{I}_{N_B} is an identity matrix with $N_B \times N_B$ dimension. $\mathbf{0}_{s \times N_B}$ is also a zero matrix. The parameter s is defined as

$$s \stackrel{\text{def}}{=} N_u + L - 2 - \Delta - N_B \quad (4.5)$$

with $N_u = N_F/\ell$. It is not recommended to let residual ISI at the output of the DFE, therefore $s = 0$ [76]. The optimal MMSE-DFE FB filter is given by

$$\mathbf{q}^H = \mathbf{p}^H \mathbf{H} \mathbf{J}_\Delta \quad (4.6)$$

thus, theoretical minimum mean square error of the standard MMSE-DFE is given by

$$J_{min} = E_x(1 - \beta) \quad (4.7)$$

the bias of the MMSE-DFE is

$$\beta = \mathbf{p}^H \mathbf{h}_{\Delta+1} \quad (4.8)$$

hence, the SNR_{EQ} at the output of MMSE-DFE is

$$SNR_{EQ} = \frac{\beta}{1 - \beta} \quad (4.9)$$

One noticed that the standard MMSE-DFE considers zero-mean symbols in the filter computation, which is not the case for the OOK constellation in HS-PON emitters. The correct MMSE-DFE closed form computation formulas account for the non-zero mean of transmitted OOK symbols $\mathbb{E}\{x_n\} = 0.5$ and $\sigma_x^2 = 0.25$, the modified MMSE-DFE optimal taps have been calculated in [76], yielding the following new closed-form solution:

$$\mathbf{p}^H = \mathbf{r}_{s,\Delta}^H (\mathbf{I} - \mathbf{J}_\Delta \mathbf{J}_\Delta^H) \mathbf{H}^H (\mathbf{H} (\mathbf{I} - \mathbf{J}_\Delta \mathbf{J}_\Delta^H) \mathbf{R}_s (\mathbf{I} - \mathbf{J}_\Delta \mathbf{J}_\Delta^H) \mathbf{H}^H + \sigma_w^2 \mathbf{I})^{-1} \quad (4.10)$$

where the terms $\mathbf{r}_{s,\Delta}^H (\mathbf{I} - \mathbf{J}_\Delta \mathbf{J}_\Delta^H) \mathbf{H}^H$ and $(\mathbf{H} (\mathbf{I} - \mathbf{J}_\Delta \mathbf{J}_\Delta^H) \mathbf{R}_s (\mathbf{I} - \mathbf{J}_\Delta \mathbf{J}_\Delta^H) \mathbf{H}^H)$ take into consideration the true OOK correlation statistics.

The equalizer bias remains

$$\beta = \mathbf{p}^H \mathbf{h}_{\Delta+1} \quad (4.11)$$

however, the minimum mean square error at the output of the MMSE-DFE J_{min} should consider the OOK penalty

$$J_{min} = E_s(1 - \beta) + \mathbb{E}^2(s_n)(\beta - \mathbf{p}^H \boldsymbol{\Sigma}_H + \boldsymbol{\Sigma}_{q_i}^*) \quad (4.12)$$

with

$$\boldsymbol{\Sigma}_{q_i}^* \stackrel{\text{def}}{=} \sum_{i=1}^{N_B} q_i \quad (4.13)$$

For a given pair $N_{DFE} = (N_F, N_B)$ the optimum delay for the closed-form MMSE-DFE may be computed as follows [76]. First a matrix \mathbf{M}_Δ is computed

$$\mathbf{M}_\Delta = \mathbf{H}^H (\sigma_x^2 \mathbf{H} (\mathbf{I} - \mathbf{J}_\Delta \mathbf{J}_\Delta^H) \mathbf{H}^H + \sigma_w^2 \mathbf{I})^{-1} \mathbf{H} \quad (4.14)$$

For each admissible $0 \leq \Delta \leq N + L - 2$, then the matrix \mathbf{Q}_Δ is computed

$$\mathbf{Q}_\Delta = \mathbf{M}_\Delta(\Delta + 1, \Delta + 1) \quad (4.15)$$

Then the optimal delay is obtained

$$\Delta_{\text{opt}} = \arg \max_{0 \leq \Delta \leq N+L-2} \mathbf{Q}_\Delta \quad (4.16)$$

This matrix computation considers the parameter $s \geq 0$. If $s < 0$ the number of feedback taps is increased to the calculation of \mathbf{Q}_Δ , i.e., $N_B = N_B + s$ if $s < 0$. The delay optimization is crucial in the MMSE-DFE optimization described in 4.5.

4.4 The adaptive LMS-DFE

The LMS has training and tracking phases, as mentioned in section 3.5. The feedforward and feedback coefficients are simultaneously adjusted to minimize the MSE [64], [69]. figure 4.3 illustrates the diagram of the LMS-DFE.

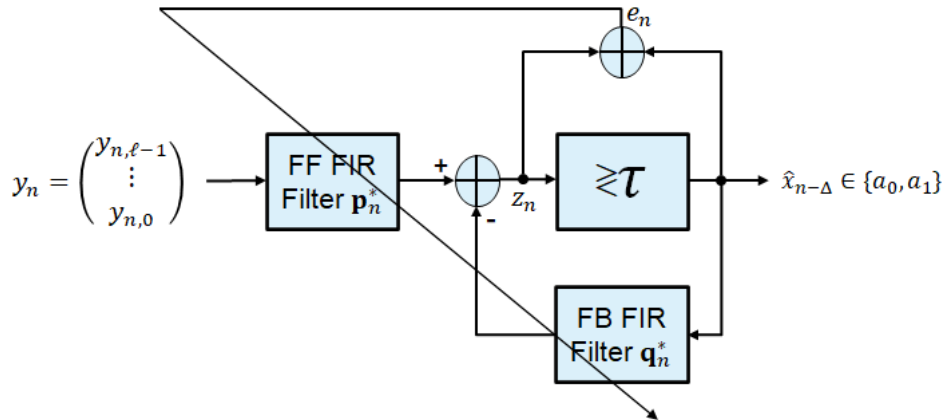


Figure 4.3: The adaptive decision feedback equalizer structure.

The LMS update equation of the feedforward filter taps, considering the steepest-descent approximation, is given by

$$\mathbf{p}_{n+1}^H = \mathbf{p}_n^H - \mu e_n \mathbf{y}_n^H \quad (4.17)$$

thus, it is the same equation as introduced for the LMS-LE. The update equation of the feedback filter taps is

$$\mathbf{q}_{n+1}^H = \mathbf{q}_n^H + \mu e_n \hat{\mathbf{x}}_n^H \quad (4.18)$$

where $\hat{\mathbf{x}}_n \stackrel{\text{def}}{=} [\hat{x}_{n-\Delta-1}, \dots, \hat{x}_{n-\Delta-N_B}]^T$ is a $N_B \times 1$ vector with the symbol-by-symbol detector decisions. Here, at the beginning of the training phase the start values of the FF taps are zero, except the first tap, it starts with value one, as in the LMS-LE. The FB initial taps values are zero.

4.5 MMSE-DFE optimization methodology

To propose a method for determining the minimum number of taps in the feedforward and feedback filters of the MMSE-DFE to meet the recommended receiver sensitivity for the HS-PON $S \leq 24$ dBm, a DFE parameters optimization approach using closed-form equations is shown in figure 4.4.

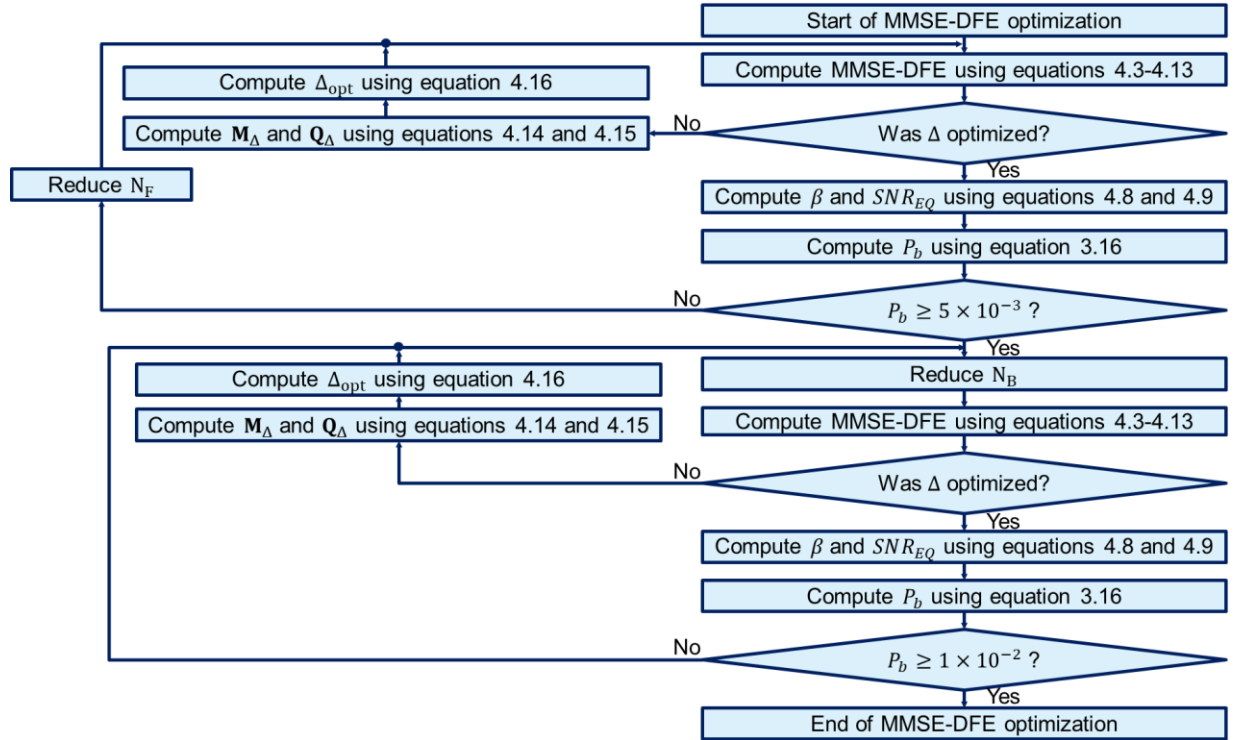


Figure 4.4: The MMSE-DFE closed-form optimization flow-chart.

This strategy was employed in closed-form prediction to simplify the LMS-DFE implementation without simulation. It is analogous to the procedure that was provided in section 3.6, which considers the LE. Here, the main objective is to achieve the BER after equalization below the LDPC FEC threshold based on hard decision $BER = 10^{-2}$, therefore to ensure error probability $P_b \leq 10^{-2}$ in the MMSE-DFE.

First N_F is minimized with the number of feedback filter taps fixed to $N_B = L - 1$. L is the estimated impulse response length obtained through least square estimation

(see Appendix D). When the target performance $BER = 5 \geq 10^{-5}$ during the optimization of N_F is obtained, then N_B is reduced. For each set of N_F and N_B taps, the restitution delay Δ is set to its optimal value Δ_{opt} , considering the closed-form optimization approach proposed in section 4.3. Finally, the theoretical approximate performance curves $BER = f(ROP, N_F, N_B, \Delta)$ is evaluated and will be presented in the next section.

4.6 Performance of MMSE-DFE over 50G-PON channels

This section describes the results obtained with the MMSE-DFE-based receiver and 25G and 50G Rx over the channels with EML and DML as emitters. Like presented in the section 3.7, the MMSE-DFE performance is predicted through closed-form equations with the procedure of section 4.5. The feedforward and feedback filters were respectively optimized. The closed-form performances are used as a reference throughout the section and compared to the performance measured with the implemented LMS-DFE, using the sensitivity of the receiver $S = f(N_F, N_B, \Delta)$ as a performance metric. Finally, the best performance of the LMS-LE and LMS-DFE are compared.

4.6.1 Closed-form prediction

First, the fractionally spaced (at $T/2$) feedforward filter equalization performance is predicted through the closed-form equations, where the number of taps of the feedback filter is fixed to $N_B = 3$ because the estimated channel impulse response had $L = 4$ T -spaced taps. Afterward, the feedback filter is optimized, considering the optimal number of taps at the feedforward section N_F and the target sensitivity $S = -24$ dBm.

Figure 4.5 illustrates the evolution of SNR_{EQ} vs N_F , obtained using equation 4.9, over the channels based on the EML + 25G Rx and EML + 50G Rx with $N_B = 3$ taps in the feedback section, at different ROP values $ROP = \{-20, -24, -32\}$ dBm, are shown.

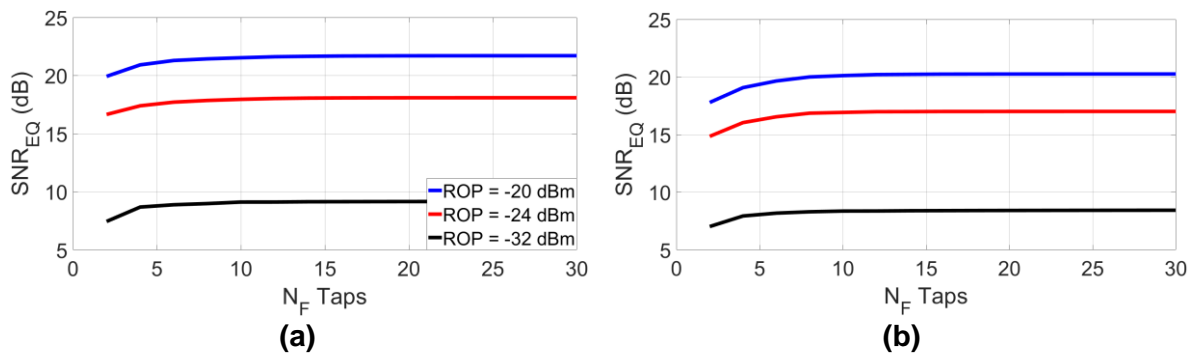


Figure 4.5: closed-form SNR_{EQ} vs N_F with $N_B = 3$ performance over channels EML + SMF + (a) 25G Rx and (b) 50G Rx.

When comparing the $SNR_{EQ} = f(ROP, N_F, N_B = 3, \Delta)$ of the two scenarios, the 25G receiver has a higher SNR_{EQ} . Hence, the residual noise impacts the MMSE-DFE performance when the 3dB bandwidth of the APD is higher. This trend was already

observed with the MMSE-LE in section 3.5. A reduced complexity MMSE-DFE could use 2 FF taps. When $N_F = 4$ the SNR_{EQ} increases by 1 dB in both cases. Only four taps in the feedforward filter appear to be sufficient for good-balance equalization with the 25G and 50G receivers. The best performance is reached for both receivers when $N_F = 8$.

Figure 4.6 illustrates the predicted SNR_{EQ} vs N_F taps evolution for the DML-based channel with $N_B = 3$ taps.

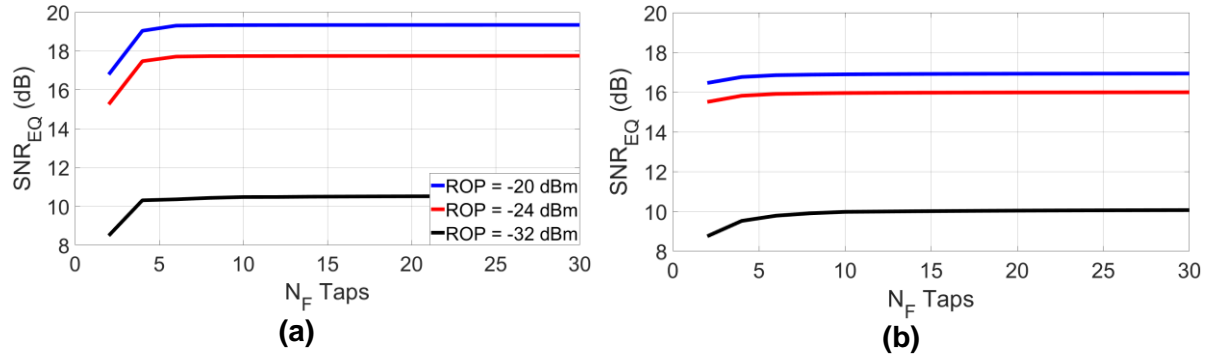


Figure 4.6: closed-form SNR_{EQ} vs N_F performance over channels DML + SMF + (a) 25G Rx and (b) 50G Rx.

The 25G Rx + MMSE-DFE has higher SNR_{EQ} than the 50G Rx, similar to the previously studied EML-based channels, consequently, when FIR-based equalization is used, the 25G Rx has better equalization performance than the 50G Rx, once again, due to the fact that the large Rx bandwidth increases the total noise power collected. $N_F = 2$ taps at the feedforward section may lead to low complexity performance for both receivers. When the number of feedforward taps is increased to $N_F = 4$, the SNR_{EQ} improved by 2dB with the 25G Rx + MMSE-DFE regardless of the ROP, the 50G Rx is slightly enhanced. Hence four taps may be enough for good-balance performance. When $N_F \geq 6$, the SNR_{EQ} does not increase significantly, so the performance infinite length equalization is achieved with six FF taps.

Figures 4.7 and 4.8 illustrate the predicted BER vs ROP evolution over channels with EML and DML emitters, respectively, using $N_B = 3$ feedback taps and a varying number of FF taps $N_F = \{2, 4, \dots, 16\}$.

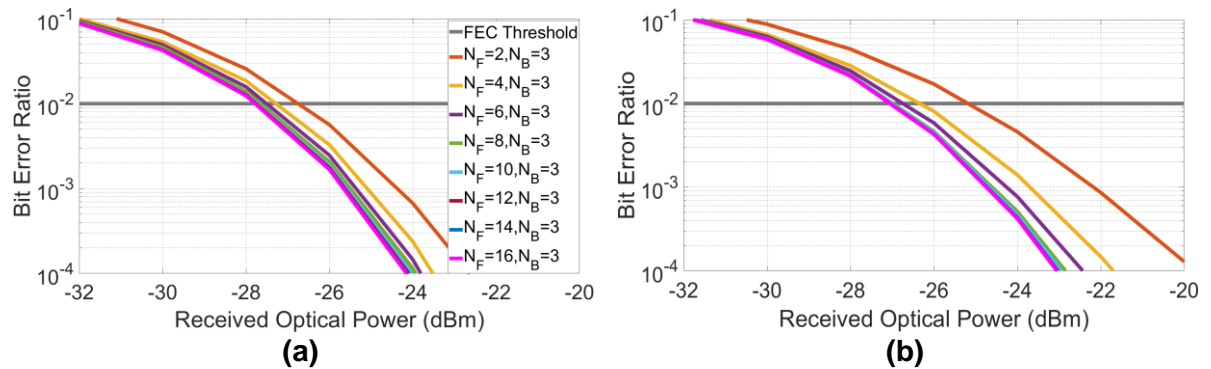


Figure 4.7: closed-form BER vs ROP performance over channels EML + SMF + (a) 25G Rx and (b) 50G Rx.

An Rx sensitivity $S \leq -25$ dBm is predicted with both receivers when $N_{DFE} = (N_F = 2, N_B = 3)$ taps are used. The 25G receiver has $S = -26$ dBm, and the 50G receiver has $S = -25$ dBm predicted sensitivity. The estimated sensitivity when $N_{DFE} = (N_F = 4, N_B = 3)$ taps is $S = -27$ dBm with the 25G receiver and $S = -26$ dBm with the 50G receiver. No improvement is expected when $N_F \geq 6$. The MMSE-LE needed at least $N_F = 6$ taps to ensure the ITU-T recommended performance $S \leq -24$ dBm, thus the LMS-DFE may achieve higher performance with similar or inferior computational complexity than the LMS-LE.

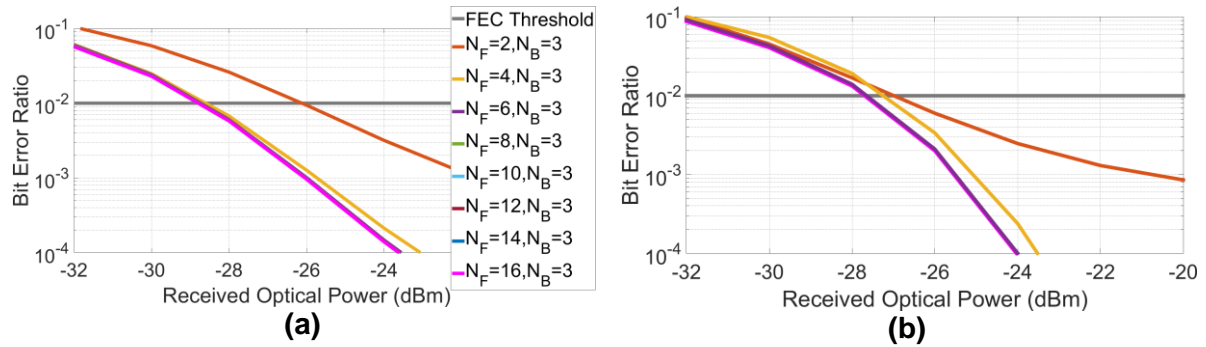


Figure 4.8: closed-form BER vs ROP performances over channels DML + SMF + (a) 25G Rx and (b) 50G Rx.

The predicted performance for the channel with the DML emitter and 25G and 50G receivers improves significantly when the number of feedforward taps is doubled, from $N_F = 2$ to $N_F = 4$, where the improvement is more pronounced with the former receiver. When $N_{DFE} = (N_F = 2, N_B = 3)$ taps, a sensitivity $S = -26$ dBm is predicted for both receivers, but the prediction with the 50G receiver is not well precise. Using $N_{DFE} = (N_F = 4, N_B = 3)$ the predicted sensitivity is $S = -28$ dBm for the 25G receiver and $S = -27$ dBm for the 50G receiver. When $N_F \geq 6$, the sensitivity of the two receivers does not improve further. With the DML + SMF + 50G Rx the MMSE-DFE prediction is constrained with two FF taps, as we already constated this arrives due to the limited number of taps prediction. Otherwise, when $N_F \geq 4$ it converges to the same BER.

The number of FF filter taps to ensure low complexity performance and best-effort performance is $2 \leq N_F \leq 6$, considering the four simulated channels with EML and DML as emitters. Let us now optimize the size of the feedback filter in each scenario. We will limit the number of feedback taps to 3 to keep low complexity.

Figures 4.9 and 4.10 illustrate the BER vs ROP curves obtained with the EML emitter with the 25G Rx and 50G Rx receivers, respectively. The number of feedforward taps was fixed to $N_F = \{2, 4, 6, 8\}$ and the evolution of the sensitivity as a function of the feedback taps was studied for $N_B = \{1, 2, 3\}$.

A single feedback tap significantly increases the expected overall DFE performance. Observing the performance evolution when the set of taps is increased

from $N_{DFE} = (N_F = 2, N_B = 1)$ to $N_{DFE} = (N_F = 2, N_B = 2)$ the residual ISI at the output of the FF filter is expected to be well compensated. Another form to have less ISI at the output of the feedforward section is to increase the number of N_F taps. The low-complexity set of taps here is $N_{DFE} = (N_F = 2, N_B = 1)$ with $S = -26$ dBm.

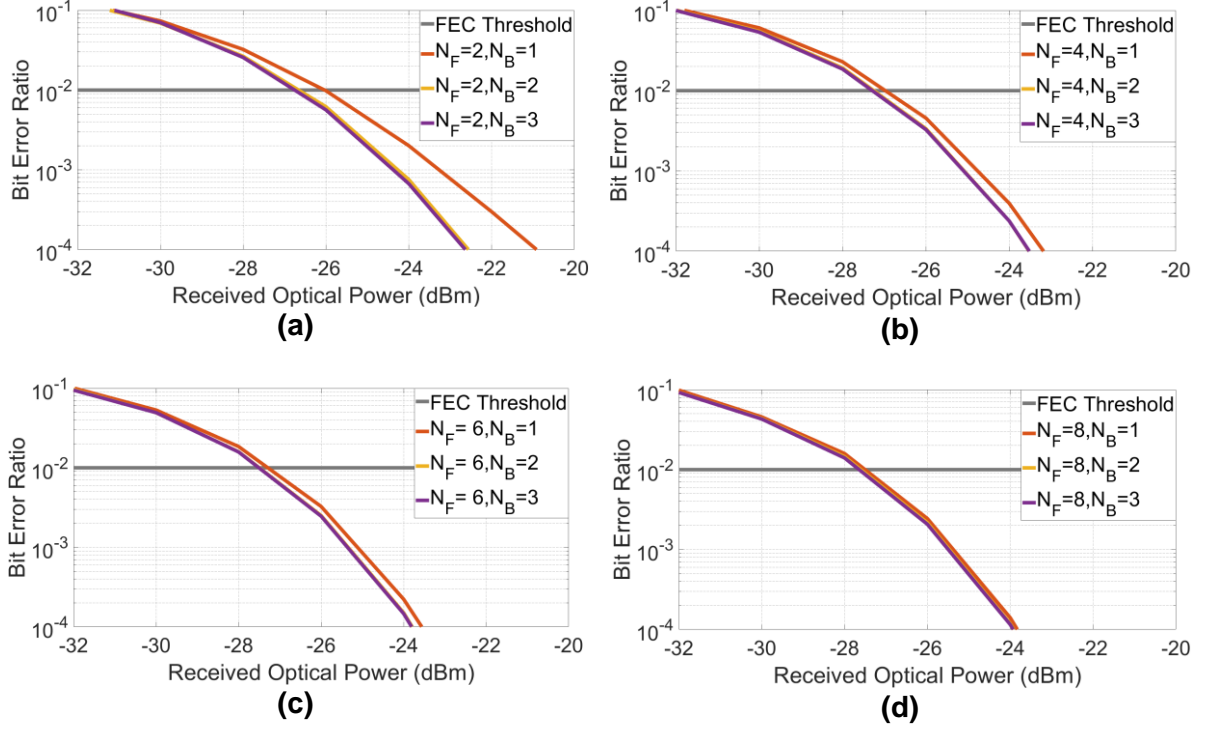
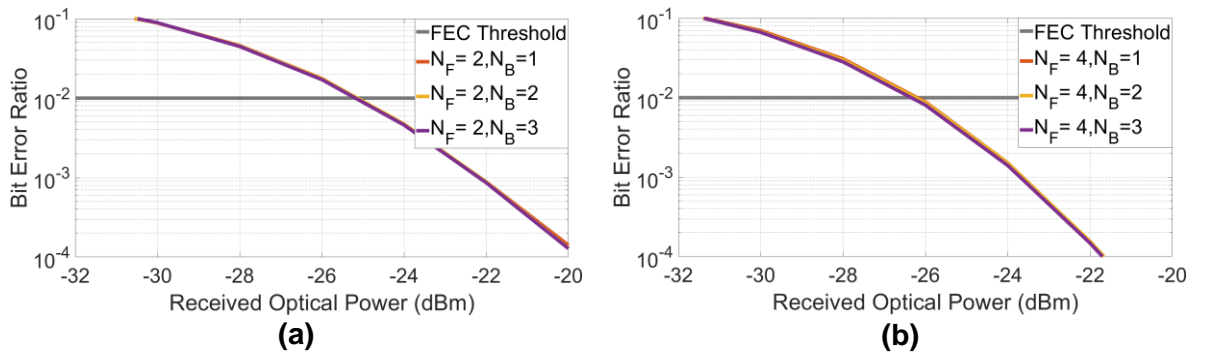


Figure 4.9: closed-form BER vs ROP performance over channel EML + 25G Rx with (a) $N_F = 2$, (b) $N_F = 4$, (c) $N_F = 6$ and (d) $N_F = 12$ taps.

The good-balance use case is obtained with $N_{DFE} = (N_F = 4, N_B = 2)$ and sensitivity $S = -27$ dBm, the same sensitivity is expected with the best-effort set is $N_{DFE} = (N_F = 6, N_B = 1)$.



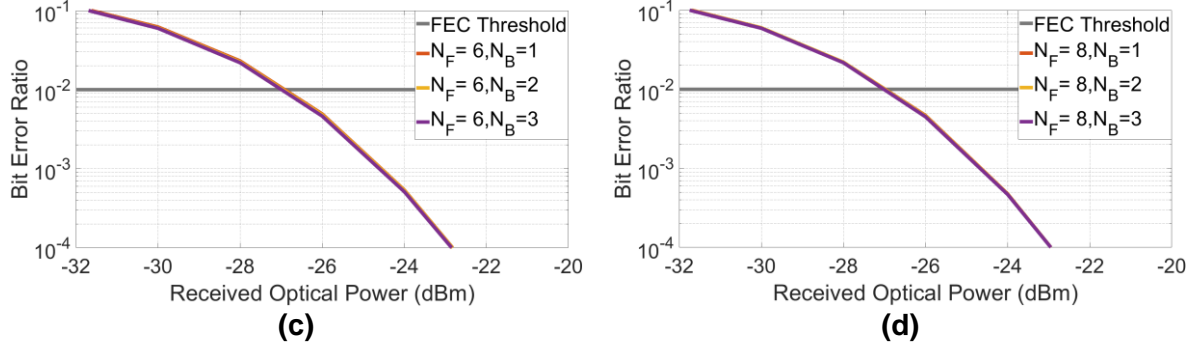


Figure 4.10: closed-form BER vs N_B performance over channel EML + 50G Rx with (a) $N_F = 2$, (b) $N_F = 4$, (c) $N_F = 8$ and (d) $N_F = 8$ taps.

With the setup the EML + 50G Rx, increasing the number of taps in the feedback section does not improve the sensitivity of the receiver, regardless of the number of taps N_F , so the trailing ISI at the output of the feedforward section is theoretically compensated by a single feedback tap $N_B = 1$, likely the former scenario. The low-complexity set of taps $N_{DFE} = (N_F = 2, N_B = 1)$ may achieve $S = -25$ dBm. The good-balance predicted performance is obtained with $N_{DFE} = (N_F = 4, N_B = 1)$ reaching $S = -26$ dBm. Finally, the sensitivity $S = -27$ dBm is reached with $N_{DFE} = (N_F = 8, N_B = 1)$ taps.

Figures 4.11 and 4.12 illustrate the BER vs ROP curves obtained with the DML emitter and 25G Rx and 50G Rx receivers, respectively. The number of feedforward taps was fixed at $N_F = \{2, 4, 6, 8\}$, and we studied the evolution of the sensitivity using $N_B = \{1, 2, 3\}$ feedback taps.

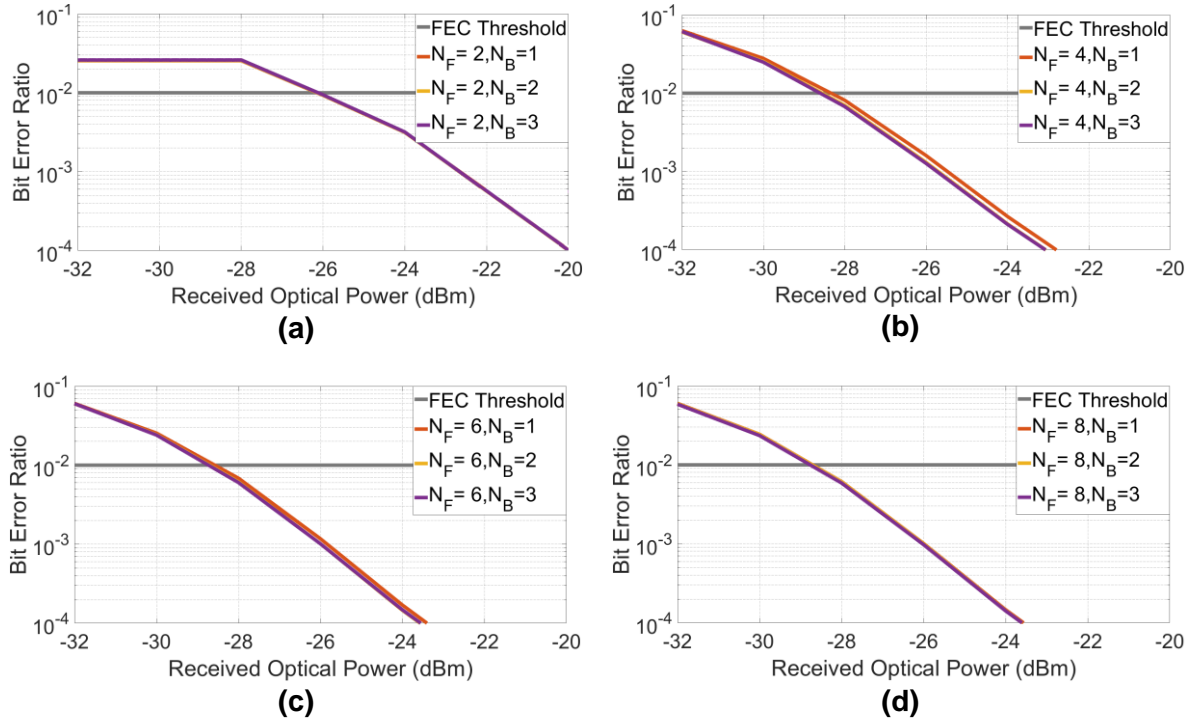


Figure 4.11: closed-form BER vs N_B performance over channel DML + 25G Rx with (a) $N_F = 2$, (b) $N_F = 4$, (c) $N_F = 6$ and (d) $N_F = 8$ taps.

When $N_{DFE} = (N_F = 2, N_B = 1)$ the sensitivity $S = -26$ dBm is achieved, hence the low-complexity performance is achieved. Also, when the ROP is lower than -28 dBm, the performance prediction is limited with this small set of taps. It is verified that increasing the number of feedback taps does not significantly improve the receiver performance. Therefore the trailing ISI at the feedforward filter output is properly compensated with $N_B = 1$ tap. This trend is noted for $N_{DFE} = (N_F = 4, N_B = 1)$, where good-balance performance is obtained for a predicted $S = -28$ dBm performance. In both cases, $N_{DFE} = (N_F = 6, N_B = 1)$ and $N_{DFE} = (N_F = 8, N_B = 1)$ the sensitivity $S = -28$ dBm persists, thus, $N_{DFE} = (N_F = 6, N_B = 1)$ can be viewed as a best-effort configuration.

Through the 50G receiver, when $N_{DFE} = (N_F = 2, N_B = 1)$ the low-complexity performance is achieved with sensitivity $S = -27$ dBm. The receiver improvement is negligible when the number of feedback taps N_B is increased. Likewise, when the number of taps is increased $N_{DFE} = (4 \leq N_F \leq 8, 1 \leq N_B \leq 3)$ there is no improvement of the receiver sensitivity, a natural behavior since the channel DML + 50G has an ISI-free behavior, as observed with the MMSE-LE in section 3.7.

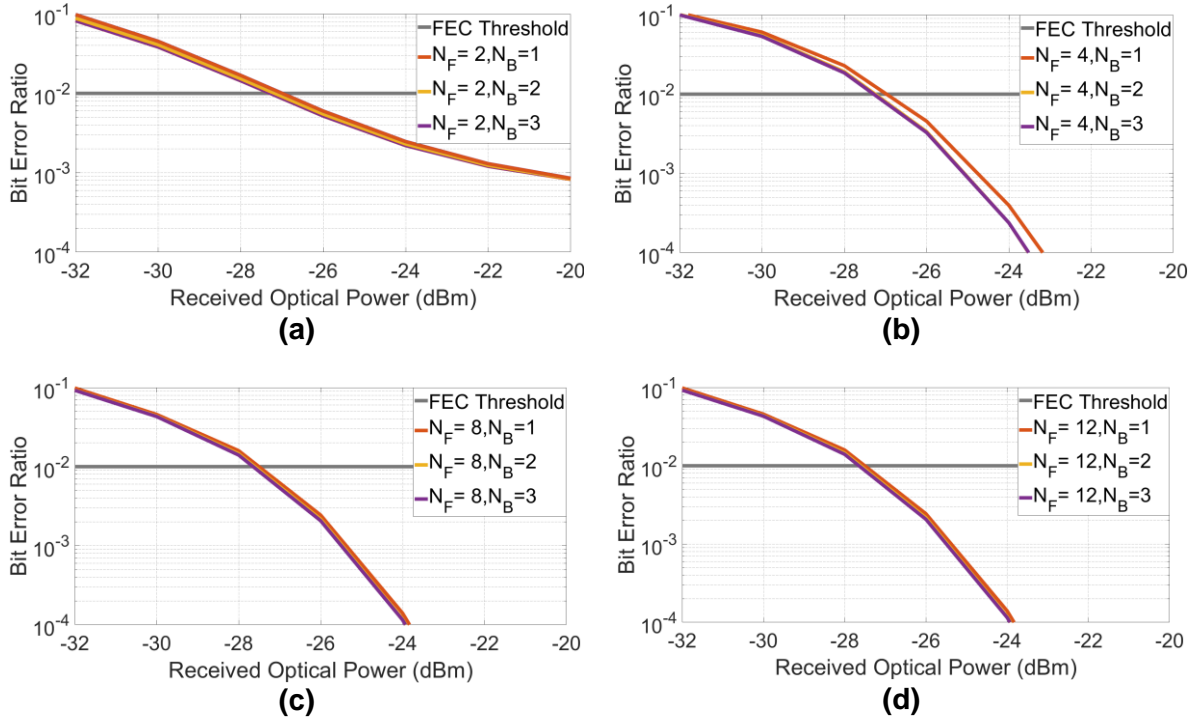


Figure 4.12: closed-form BER vs N_B performance over channel DML + 50G Rx with (a) $N_F = 2$, (b) $N_F = 4$, (c) $N_F = 8$ and (d) $N_F = 12$ taps.

The optimal delay of MMSE-DFE Δ is a function of ROP, number of taps in the feedforward, and number of taps in the feedback section, $\Delta = f(ROP, N_F, N_B)$. To evaluate the optimal delay in only two dimensions, the ROP was fixed to $ROP = -24$ dBm here. The optimal delay evolution Δ vs N_F of the EML + 25G and EML + 50G receivers is respectively illustrated in figure 4.13 with varying FB taps $N_B = \{1, 2, 3\}$.

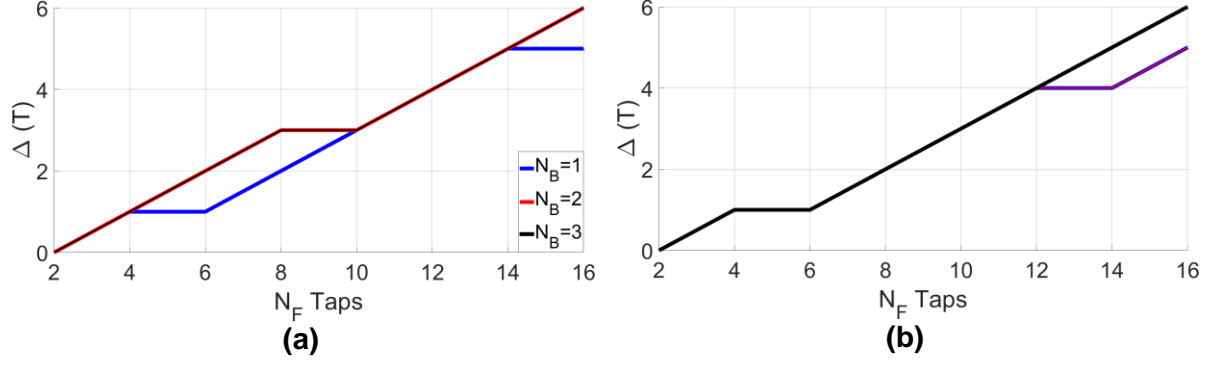


Figure 4.13: Optimum delay Δ vs N_F over channels EML + SMF + (a) 25G Rx and (b) 50G Rx.

In both scenarios N_B does not remarkably change the optimal delay value. When the channel has more bandwidth limitation (25G Rx), the delay varies more when the number of FB taps N_B changes. In a practical implementation without the knowledge of the optimal delay, setting Δ to half of FF taps, i.e., $\Delta = N_F/2$ is a recommendation since it is close to the optimal values.

Figure 4.14 illustrates the predicted delay evolution Δ vs N_F through the DML-based channel.

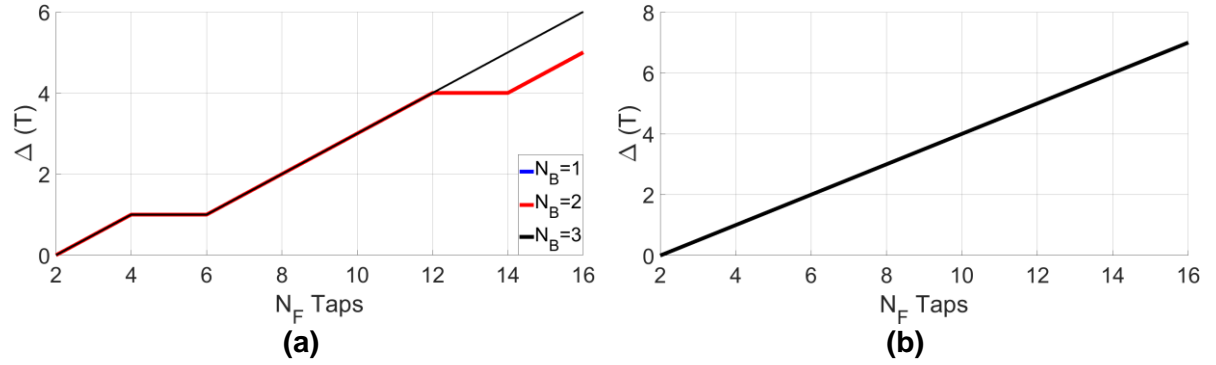


Figure 4.14: Optimum delay Δ vs N_F over channels DML + SMF + (a) 25G Rx and (b) 50G Rx.

We observed the same trend with the EML-based channels. The number of FB taps N_B does not significantly impact the optimal delay. When the 50G Rx is used, the optimal delay increases only with N_F . Setting the delay to half of the feedforward taps is also a good choice in practice.

The MMSE-DFE delay is in the interval $0 \leq \tau_D \leq 120$ ps, when $N_{DFE} = (0 \leq N_F \leq 16, 1 \leq N_B \leq 3)$ and thus negligible considering the required latency applications for HS-PON that is in the order of ms [90], regardless of the optical emitter of the 50G-PON channel. Therefore, the FIR-based equalizers do not introduce excessive equalization delay over the HS-PON DSP-based architecture.

In figures 4.15-4.18, the impulse responses obtained with the simulation parameters $ROP = -24$ dBm, $N_F = 12$, $N_B = 3$ and $\Delta = 4$ in FF and FB sections are illustrated, respectively. Figure 4.15 illustrates the DFE impulse response obtained through the setup EML ++ 25G Rx.

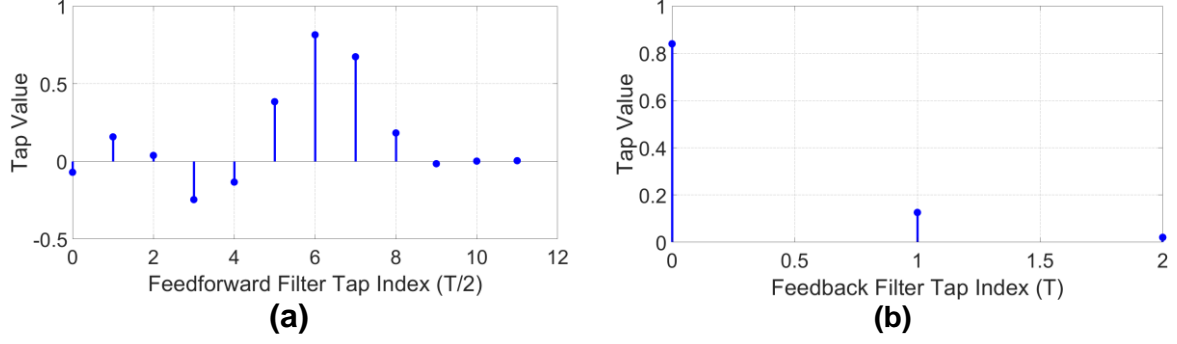


Figure 4.15: MMSE-DFE impulse response over channel EML + 25G Rx (a) feedforward filter and (b) feedback filter.

Considering $N_F = 12$ taps, most of the energy is concentrated between taps 3 to 8, hence $T_{span} = 6 \times \frac{T}{2} = 3T$ symbols periods span over the FF section. Considering the feedback filter, taps 0 and 1 contain most of the total energy, hence the FB filter spans $T_{span} = 2T$ symbols periods. Thus, $N_{DFE} = (N_F = 6, N_B = 2)$ taps are expected for best-effort LMS-DFE performances.

Figure 4.16 illustrates the impulse response of the MMSE-DFE, obtained through the channel EML + 50G Rx.

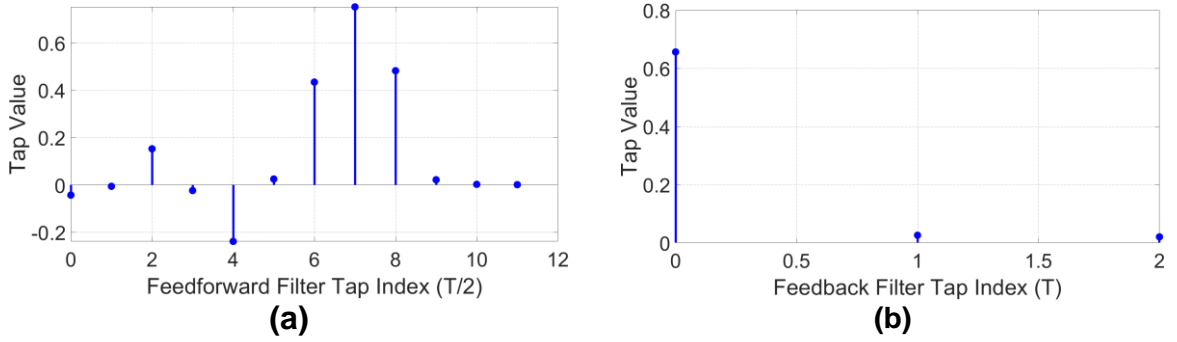


Figure 4.16: MMSE-DFE impulse response over channel EML + 50G Rx (a) feedforward filter and (b) feedback filter.

The non-negligible energy is distributed from taps 2 to 8, hence it is concentrated in a window with $N_W = 7$ fractionally spaced taps, consequently the FF filter span $T_{span} = 7 \times \frac{T}{2} = 3.5T$ symbols periods. Most of the energy is concentrated into the first tap of the feedback filter, therefore it spans a symbol period. Therefore $N_{DFE} = (N_F = 7, N_B = 1)$ taps are expected in the LMS-DFE implementation to reduce most of the combined channel distortion and noise.

Figure 4.17 illustrates the impulse response of the MMSE-DFE, obtained through the channel DML + 25G Rx.

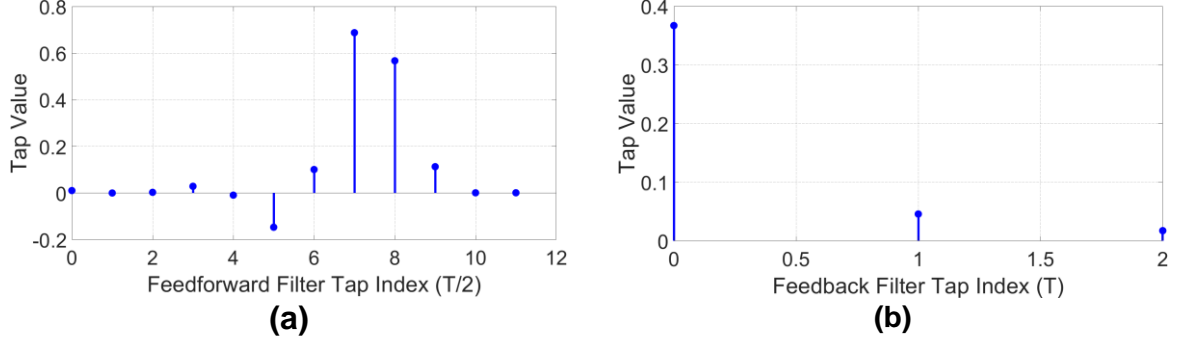


Figure 4.17: MMSE-DFE impulse response over channel DML + 25G Rx (a) feedforward filter and (b) feedback filter.

The feedforward section has the highest energy taps centered between taps 5 and 9, hence the FF filter spans $T_{span} = 5 \times \frac{T}{2} = 2.5T$ symbol periods. Feedback section span a single $T_{span} = T$ symbol period since the relative energy in the first tap. Then, $N_{DFE} = (N_F = 5, N_B = 1)$ taps are expected in the LMS-DFE implementation to mitigate most channel distortion.

Figure 4.18 illustrates the impulse response of the MMSE-DFE, obtained through the DML + 50G Rx.

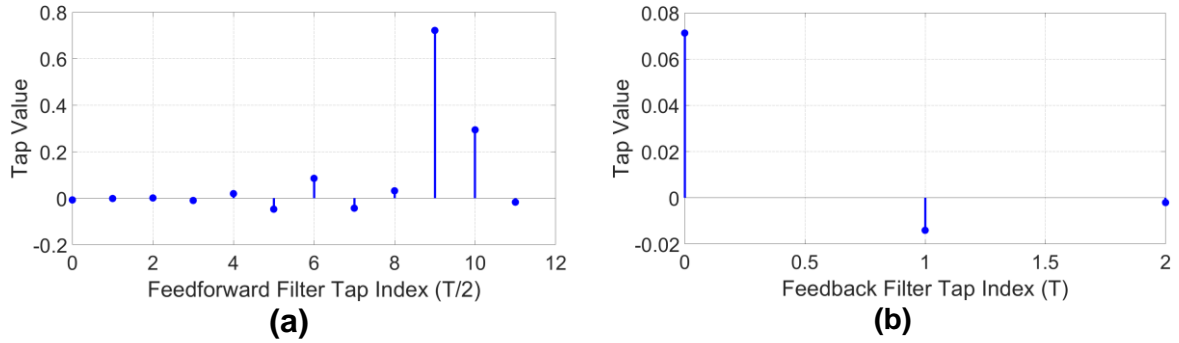


Figure 4.18: MMSE-DFE impulse response over channel DML + 50G Rx (a) Feedforward filter taps (b) Feedback filter taps

As observed with the MMSE-LE in section 3.5, this channel is practically ISI-free. Only taps 9 and 10 present essential energy, thus the FF filter spans a single symbol period $T_{span} = 2 \times \frac{T}{2} = T$. The FB also spans a single symbol period, and we also observe that the order of magnitude of the FB taps is 100 times smaller than the previously obtained FB filters. $N_{DFE} = (N_F = 2, N_B = 1)$ taps are expected in the LMS-DFE implementation for top-tier equalization performance.

Table 4.1 summarizes the obtained results through the MMSE-DFE closed-form equations.

Table 4.1: Closed-form predictions of the MMSE-DFE over EML and DML based channels.

Channel	MMSE-DFE	SNR _{EQ} (dB)	Predicted sensitivity (dBm)
EML + 25G Rx	$N_F = 2, N_B = 1, \Delta = 0$	11.9	-26.0
	$N_F = 4, N_B = 2, \Delta = 1$	12.5	-27.0
	$N_F = 6, N_B = 1, \Delta = 2$	12.9	-27.0
EML + 50G Rx	$N_F = 2, N_B = 1, \Delta = 0$	11.1	-25.0
	$N_F = 8, N_B = 1, \Delta = 2$	12.3	-27.0
DML + 25G Rx	$N_F = 2, N_B = 1, \Delta = 0$	13.9	-26.0
	$N_F = 4, N_B = 2, \Delta = 1$	14.2	-28.0
DML + 50G Rx	$N_F = 2, N_B = 1, \Delta = 0$	13.3	-27.0

The MMSE-DFE predictions suggest that the equalizer can achieve the ITU-T recommended sensitivity with only 2 taps in the FF filter and one tap at the FB filter, considering EML and DML-based emitters. The two analysis based on the theoretical BER and the observation of taps values show the set of taps to reach the best performances with the DFE.

The following section compares closed-form predictions to the simulated LMS-DFE performance. Also, we compare the LMS-LE and LMS-DFE best-effort performances.

4.7 Simulated performance of the LMS-DFE and LMS-LE over the 50G HS-PON based on EML and DML

4.7.1 The EML + 25G Rx channel

Figure 4.17 illustrates the performance of the EML + 25G Rx channel with the LMS-DFE integrated into the receiver.

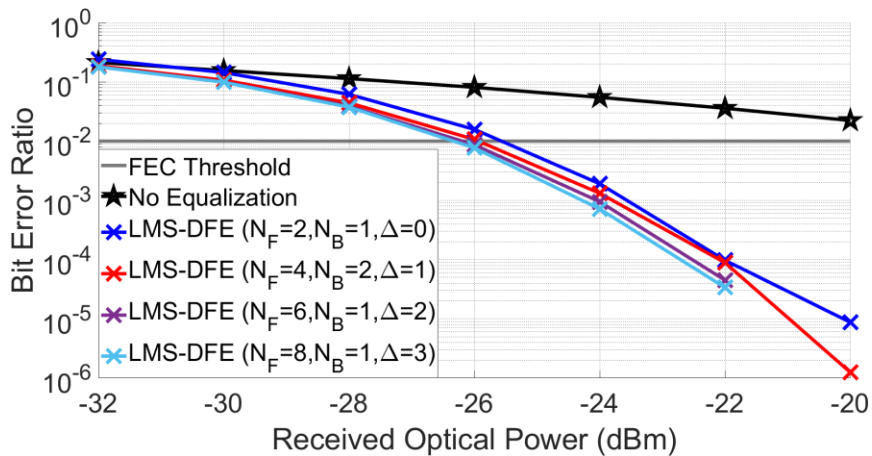


Figure 4.19: measured BER vs ROP over channel EML + 25G Rx at the output of the LMS-DFE.

The gain provided by the low-complexity DFE set $N_{DFE} = (N_F = 2, N_B = 1)$ to the receiver is remarkable. It compensates for severe ISI with a minimal number of taps.

With more taps, the improvement is small. Therefore, most of the EML + 25G Rx ISI was already compensated. The good balance and best-effort performance is obtained with $N_{DFE} = (N_F = 4, N_B = 2)$

Figure 4.20 shows the best performance of the LMS-LE and LMS-DFE over the EML + 25G Rx channel.

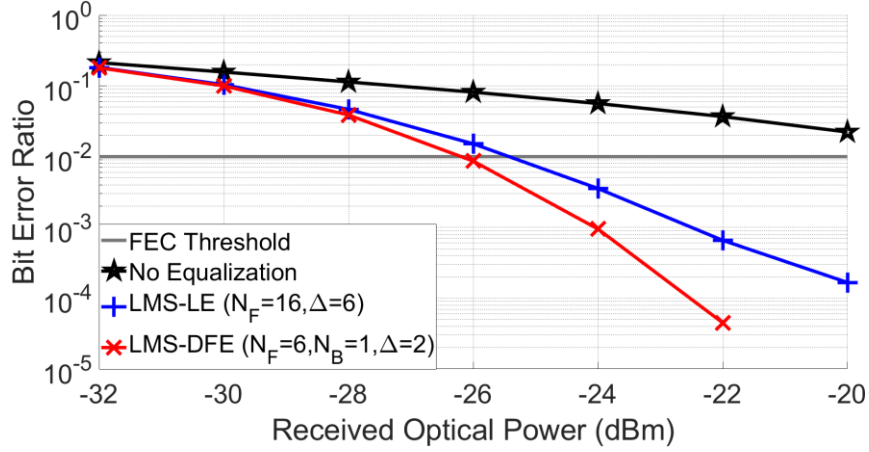


Figure 4.20: measured BER vs ROP over channel EML + 25G Rx at the output of the LMS-DFE and LMS-LE with best effort performance parameters.

The LMS-DFE achieves better performance than the LMS-LE. It requires less number of taps and improves the receiver sensitivity by 1dB with respect to the LE. For ROPs higher than -24 dBm, the improvement through DFE tends to increase more than the LE. Hence, the LMS-DFE is the recommended equalizer for the EML + 25G Rx channel, mainly because the DFE compensates the severe channel ISI due to spectral notch without critical error propagation and less number of taps.

4.7.2 The EML + 50G Rx channel

Figure 4.21 illustrates the performance measured with the EML + 50G Rx channel with the LMS-DFE.

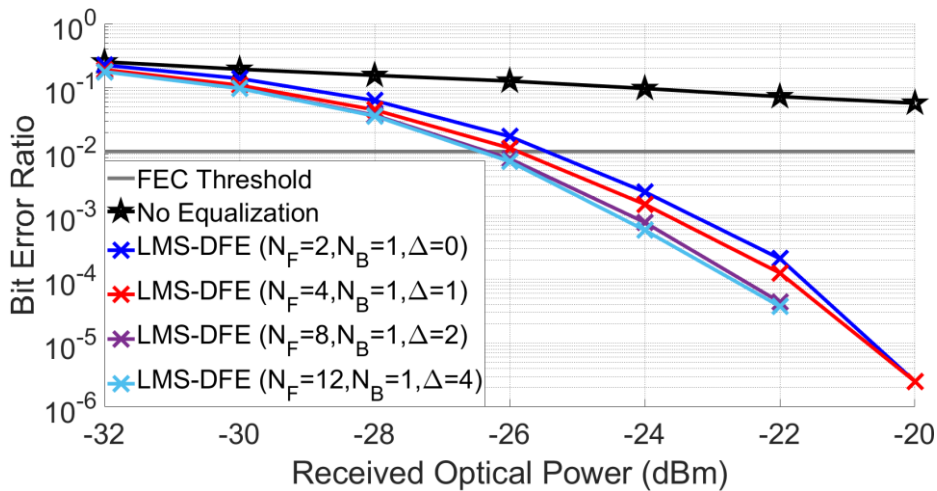


Figure 4.21: measured BER vs ROP over channel EML + 50G Rx at the output of the LMS-DFE.

As mentioned in the simulated performance of the LMS-LE in section 3.8, this channel is less impacted by bandwidth distortion and presents more noise predominance. Naturally, the LMS-DFE demands more taps to reach the same sensitivity of the EML + 25G Rx, but it compensates well for the EML + 50G Rx impairments with a small number of taps. With $N_{DFE} = (N_F = 2, N_B = 1)$ the LMS-DFE achieves low-complexity performance with a sensitivity $S = -25$ dBm. The noise reduces the performance.

Consequently, the good balance performance is obtained with the configuration $N_{DFE} = (N_F = 8, N_B = 1)$. The performance is further improved when the number of feedforward taps is increased to $N_F = 12$, in both good-balance and best-effort cases, the sensitivity of the receiver is improved to $S = -26$ dBm, and the BER is below the error floor for $ROP \geq -22$ dBm.

Figure 4.22 shows the best-effort performances of the LMS-LE and LMS-DFE over the EML + 50G Rx channel.

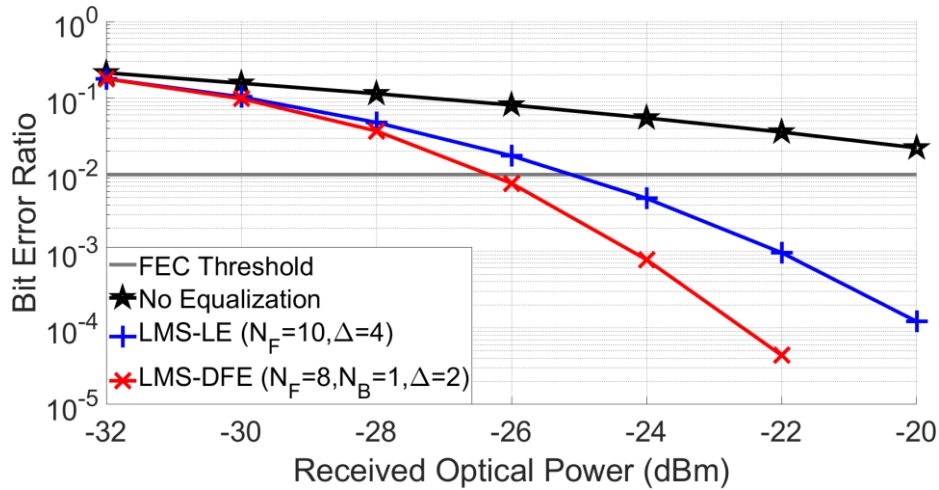


Figure 4.22: measured BER vs ROP over channel EML + 50G Rx at the output of the LMS-DFE and LMS-LE with best effort performance parameters.

The DFE does not suffer from critical error propagation and achieves better performance than the LE with lower computation complexity, hence the LMS-DFE can compensate for amplitude distortion without too much noise enhancement and has better performance in the channel with severe ISI due to frequency notch [91], [92]. Considering both simulated scenarios, the DFE is recommended for channels with EML at transmitter and 25G and 50G APDs, because the LMS-DFE handles well the distortions with small number of taps.

4.7.3 The DML + 25G Rx channel

Figure 4.23 shows the performance of the LMS-DFE with the DML + 25G Rx channel.

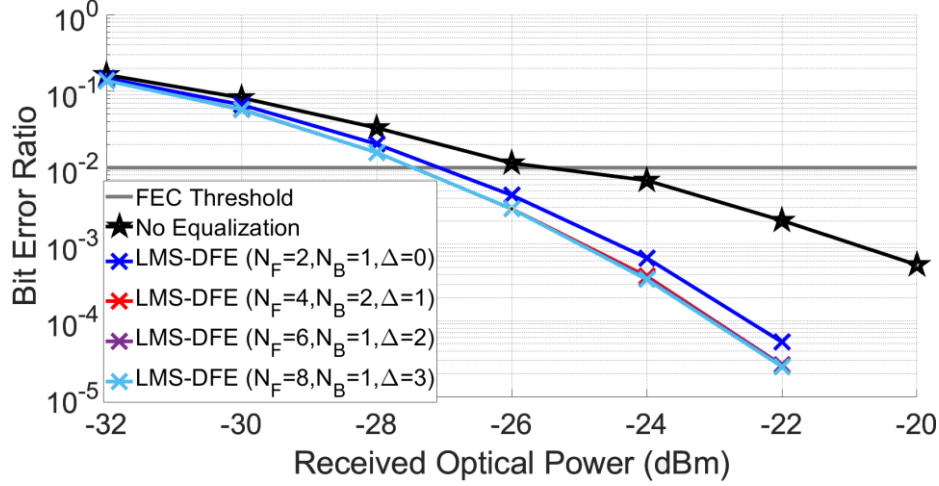


Figure 4.23: measured BER vs ROP over channel DML + 25G Rx at the output of the LMS-DFE.

The performance gain with LMS-DFE is not as substantial as it was with the EML-based channels, which is expected since this channel does not present frequency null. The APD distortion predominates the ISI. The minimal set of taps $N_{DFE} = (N_F = 2, N_B = 1)$ enhances the sensitivity of the receiver to $S = -26$ dBm, the equalization performance is improved with $N_{DFE} = (N_F = 4, N_B = 2)$, but since there is no high channel distortion, the performance is not significantly improved when the taps are increased, as previewed in the closed-form evaluation.

Figure 4.24 shows the best-effort performances of the LMS-LE and LMS-DFE over the DML + 25G Rx channel.

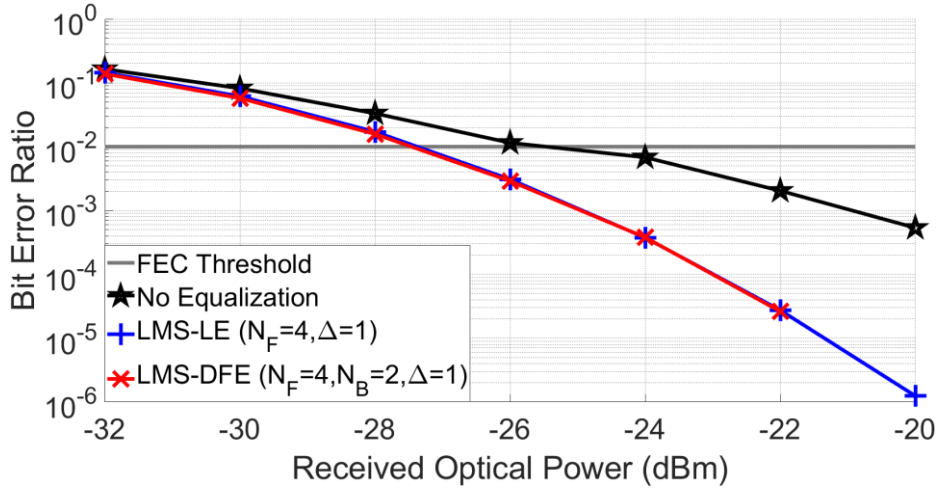


Figure 4.24: measured BER vs ROP over channel DML + 25G Rx at the output of the LMS-DFE and LMS-LE with best effort performance parameters.

The adaptive DFE and LE have the same performance, hence the trailing ISI at the output of FF filter is negligible. The LMS-LE is the recommended choice since it has the best equalization and complexity performance, however the use of MMSE based equalizers is not required.

4.7.4 The DML + 50G Rx channel

Figure 4.25 illustrates the performance of DML + 50G Rx with LMS-DFE.

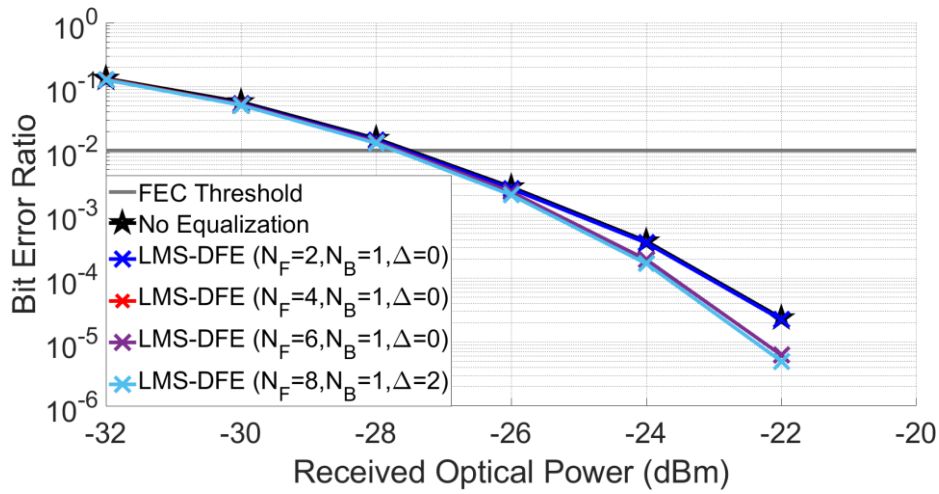


Figure 4.25: measured BER vs ROP over channel DML + 50G Rx at the output of the LMS-DFE.

The LMS-DFE receiver do not increase the performance for the DML + SMF 50G Rx channel since it has an almost ISI-free behavior. It was already evaluated in the closed-form investigation and section 3.8 with the LMS-LE.

Figure 4.25 shows the best-effort performances of the LMS-LE and LMS-DFE over the DML + 50G Rx channel.

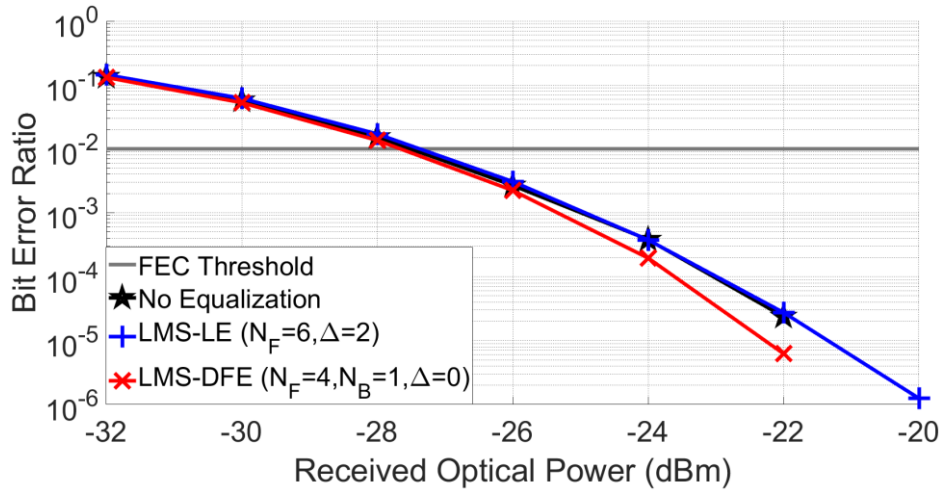


Figure 4.26: measured BER vs ROP over channel DML + 50G Rx at the output of the LMS-DFE and LMS-LE with best effort performance parameters.

The DFE improves the receiver performance when the received optical power is higher than $ROP = -26$ dBm. However, the sensitivity is not enhanced regardless of the MMSE-based equalizer.

Hence, using MMSE-equalization in practice would only add complexity to the 50G receiver. The use of nonlinear compensation may be interesting to compensate the chirp-related distortion of the DML.

4.7.5 Transient analysis of the LMS-DFE

Figures 4.27 and 4.28 illustrates the transient MSE vs iteration curve obtained with the EML and DML based channels which $ROP = -24$ dBm with the best-effort equalization parameters. $N_{DA} = 200 \times 10^3$ and $N_{DD} = 800 \times 10^3$ symbols were used during the training and tracking phase, respectively.

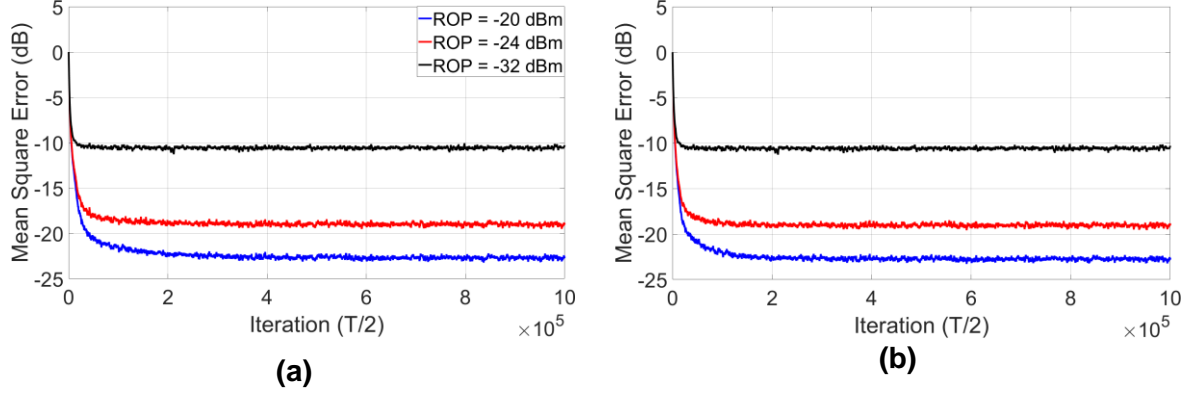


Figure 4.27: MSE vs iteration over channels EML + SMF + (a) 25G Rx and (b) 50G Rx.

The LMS-DFE MSE curves of both EML-based channels are very similar. Hence the DFE is not very sensible to the change of the APD bandwidth, as verified in the BER vs ROP presented curves. Here, we see that the obtained MSE at the end of the tracking phase is the same.

Also, each ROP's measured BER has approximated values in both cases. For instance, considering the scenario whose ROP is -24 dBm, at both cases the MSE obtained at the end of the tracking phase is -19dB, and the measured bit error ratio is $BER = 9 \times 10^{-4}$. $N_{sy} = 100 \times 10^3$ symbols are necessary to obtain the optimal FF and FB filter taps. Considering the symbol period $T = \frac{1}{50E9} = 20$ ps, the learning period is $T_{LP} = 100 \times 10^3 \times 20$ ps = 2.0 μ s. We noticed that the LMS-DFE achieves better MSE at the end of the tracking phase than the LMS-LE.

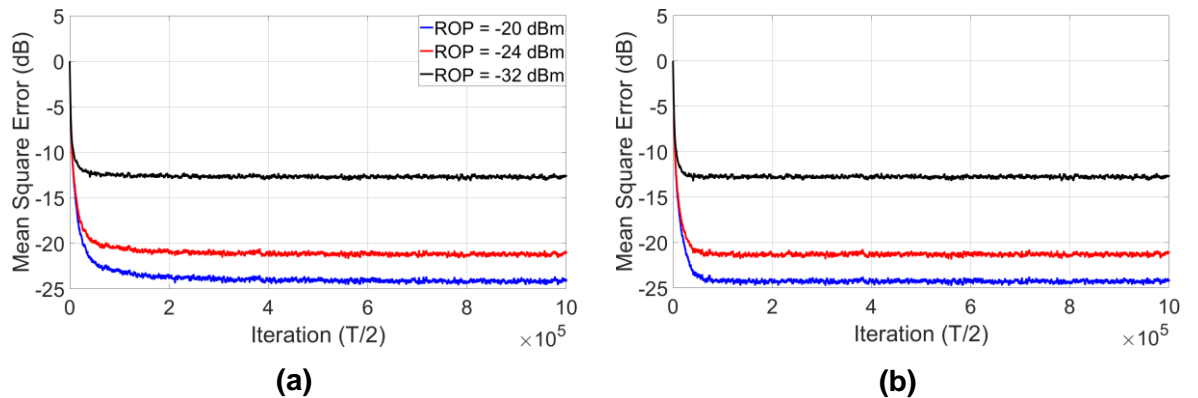


Figure 4.28: MSE vs iteration over channels DML + SMF + (a) 25G Rx and (b) 50G Rx.

We observe the same trend as the previous LMS-DFE-based receivers, and both MSE curves converge after 2 μ s and the BER after equalization has a good correspondence between measured MSE at the end of the tracking phase with both receivers.

Both LMS-DFE and LMS-LE (verified in section 3.8) present a negligible adaptation period in the order of μ s, considering HS-PON latency requirements in the order of ms. The equalization delay is not critical considering the ITU-T recommendations, i.e., the FIR-based equalizer receivers achieve the required sensitivity respecting the needed latency for the HS-PON services such as voice, internet, and advanced video services [1].

4.8 Main results of the DFE

Table 4.2 exhibits the use-case performances demonstrated during this chapter.

Table 4.2: Main results obtained with MMSE-DFE.

Channel	MMSE-DFE	Predicted sensitivity (dBm)	Simulated sensitivity (dBm)	Optical budget (dB)
EML + 25G Rx	$N_F = 2, N_B = 1, \Delta = 0$	-26	-25	35
	$N_F = 4, N_B = 2, \Delta = 1$	-27	-25	35
	$N_F = 6, N_B = 1, \Delta = 2$	-27	-26	36
EML + 50G Rx	$N_F = 2, N_B = 1, \Delta = 0$	-25	-25	35
	$N_F = 8, N_B = 1, \Delta = 2$	-26	-26	36
DML + 25G Rx	$N_F = 2, N_B = 1, \Delta = 0$	-26	-27	36
	$N_F = 4, N_B = 2, \Delta = 1$	-28	-27	36
DML+ SMF + 50G Rx	$N_F = 2, N_B = 1, \Delta = 0$	-27	-27	36

It was possible to predict the number of taps in FF and FB filters and achieve the required sensitivity through closed-form equations $S \leq -24$ dBm over all channels. Compared to the LMS-DFE implementation performance, the closed-form predictions were accurate enough to determine when the MMSE-DFE achieves low-complexity and best-effort performances.

The predicted sensitivity in the EML + 50G Rx and DML + 50G Rx channels were identical and in line with what we obtained with the LMS-DFE configuration. However, there is a margin of at least 1 dB between predicted and measured sensitivity. Therefore the channel estimations do not account for all the optical channel impacts. Which is a consequence when the low number of taps is used to estimate the channel performance of an optical channel with severe ISI. The corrected closed-form equations considering the OOK alphabet are sufficient to assess the channel performance, although the penalty of the optical emitter based on E_s and the optical extinction ratio.

The MMSE-DFE-based receivers for both EML and DML meet the maximal optical path loss recommendation C+ (32 dB) with only $N_F = 2$ taps in the $T/2$ spaced FF filter and $N_B = 1$ T spaced tap in the FB filter, it also achieves the maximum optical path loss of class C+ (32 dB).

Table 4.3 highlights the results obtained with the LMS FIR-based equalizers.

Table 4.3: Main results obtained with LE and DFE.

Channel	LMS-LE		LMS-DFE	
	Parameter	Measured sensitivity (dBm)	Parameter	Measured sensitivity (dBm)
EML + 25G Rx	$N_F = 4, \Delta = 3$	-23	$N_F = 2, N_B = 1, \Delta = 0$	-25
	$N_F = 6, \Delta = 3$	-24	$N_F = 4, N_B = 2, \Delta = 1$	-25
	$N_F = 16, \Delta = 6$	-25	$N_F = 6, N_B = 1, \Delta = 2$	-26
EML + 50G Rx	$N_F = 6, \Delta = 3$	-23	$N_F = 2, N_B = 1, \Delta = 0$	-25
	$N_F = 8, \Delta = 3$	-24	$N_F = 8, N_B = 1, \Delta = 2$	-26
DML + 25G Rx	$N_F = 4, \Delta = 1$	-25	$N_F = 2, N_B = 1, \Delta = 0$	-27
	$N_F = 8, \Delta = 4$	-27	$N_F = 4, N_B = 2, \Delta = 1$	-27
DML+SMF + 50G Rx	$N_F = 8, \Delta = 4$	-27	$N_F = 2, N_B = 1, \Delta = 0$	-27

The table clarifies that the performance of the LMS-DFE is superior to the LMS-LE in terms of total number of taps, delay of equalization, and sensitivity. The LMS-DFE is more indicated for the HS-PON 50G downstream channel for both EML and DML. The use of LMS-LE may only increase the complexity of the receiver since for $-32 \leq ROP \leq 20$ dBm, the signal-to-noise ratio at the receiver input is sufficiently high to the DFE not be impact by critical error decision. In other words, the LMS-DFE is more indicated for the EML channel because it presents frequency nulls and it compensate well for the severe ISI. It is also recommended for the DML channel because the performance is still as good as the LMS-LE, regardless of the ROP.

4.9 Concluding remarks

The decision feedback equalization is a PON solution for the 50G-PON. Since the DFE was not impacted by critical decision errors in the simulations, and the channel present high frequency selectivity, the DFE is a good choice for PON.

This chapter introduced the concept, the advantages, and the disadvantages of the MMSE-DFE. The closed-form equations explained how to calculate the performance of the DFE, the FF, and FB filters taps, especially for zero-mean and OOK alphabet, considering the MMSE criterion. It demonstrated the LMS version of the MMSE-DFE and an approach to minimize the number of taps of the DFE maintaining the target sensitivity at receiver. Finally, the closed-form equations were used to predict the performance of the MMSE-DFE through 50G channels based on EML and DML emitters. Then the LMS-DFE was implemented, considering the use cases proposed in the MMSE-DFE evaluation.

The results shows that the MMSE-DFE closed-form OOK based equations are well-suited to predict performance of low-complexity, good-balance, and best-effort with a difference of 2 dB at maximum to the simulated performance. The LMS-DFE

only need $N_F = 2$ taps in the fractionally spaced FF filter and $N_B = 1$ tap in the T-spaced FB filter to guarantee transmissions with sensitivity $S \leq -25$ dBm at 50Gbit/s for the downstream HS-PON, without equalization delay. It shows that the presented severe ISI IM/DD channel is effectively compensated with a feedforward filter $N_F = 8$ taps in FF filter that spans 4 symbols, and $N_B = 2$ taps in FB filter, which spans 2 symbols, in the EML + 25G channel, which was the worst case of ISI. The equalization delay is very small $0 \leq \Delta \leq 120$ ps, compared to the predicted latency of the next HS-PON services. With the standard LMS-DFE no more than $N_{DA} = 100 \times 10^3$ symbols are necessary to the training of the equalizer, with negligible learning period with $T_{LP} = 2$ μ s, considering the recommended latency demanded for advanced services by ITU-T, in the order of 1 ms.

Overall, the LMS-DFE achieves better performances in terms of number of taps, delay and sensitivity. The LMS-DFE is not critically impacted in the operation region $20 \leq ROP \leq -32$ dBm, so the LMS-DFE is more advantageous than the LMS-LE. Both equalizers do not improve the performance of the DML + 50G Rx channel, so the FIR-equalization is not suitable for this channel, and nonlinear compensation may be used for this channel.

This chapter ends the FIR-based equalization investigation for HS-PON channels at 50G. The next chapter investigates trellis-based equalization, mainly to deal with the nonlinear distortions of the IM/DD PON channel.

5 Maximum Likelihood Sequence Estimation: An Optimal Solution for the 50G-PON

5.1 Introduction

The Maximum Likelihood Sequence Estimation (MLSE) based receiver is optimal. It is a receiver capable of compensating distortions that are not perceived by the previously presented MMSE-based receivers. In PON it may be interesting to use it because the optical emitter and receiver introduces nonlinear distortions.

Chapters 3 and 4 introduced the FIR-based equalizers to compensate for the HS-PON 50G channel distortions. The receiver with MMSE-LE and MMSE-DFE achieved the recommended optical budget and sensitivity required by ITU-T. Both receivers are memoryless and output a symbol z_n , which is supposed to be close to the information sequence $x_{n-\Delta}$.

This chapter describes the sequence-based detector architecture comprising Maximum Likelihood Sequence Estimation. Here, two versions of the MLSE are introduced and evaluated through the EML and DML based optical channel simulations.

This chapter is organized as follows, in section 5.2, the concept of sequence detection, the Finite-State Machine (FSM) model, and the criterion used by the MLSE are introduced. Then, section 5.3 describes the two versions of the MLSE, one based on a linear gaussian channel model and the generalized version of the MLSE based on the conditional probability distribution function (PDF) of the received sequences considered. Section 5.4 develops the implementation of the Viterbi Algorithm (VA) and the approach used to reduce the number of states required by the MLSE. Next, section 5.5 discusses the results and channel estimation. Also, the MLSE and MMSE-based equalizers are compared. Finally, section 5.6 summarizes the main contents of the chapter.

5.2 The sequence detection

Chapters 3 and 4 considered MMSE equalizers constrained by linear estimation $y_n = \mathbf{H}\mathbf{x}_n + \mathbf{w}_n$. It was verified that MSE reduction enabled HS-PON transmissions to improve the measured BER at the receiver. However, the presented Symbol-by-Symbol (SBS) receivers are constrained since they do not consider the dependency of the symbol of interest z_n with its neighboring symbols. Hence the interest in sequence detection is demonstrated in the thesis.

Here, the channel is modeled through a Finite State Machine (FSM) represented in figure 5.1.

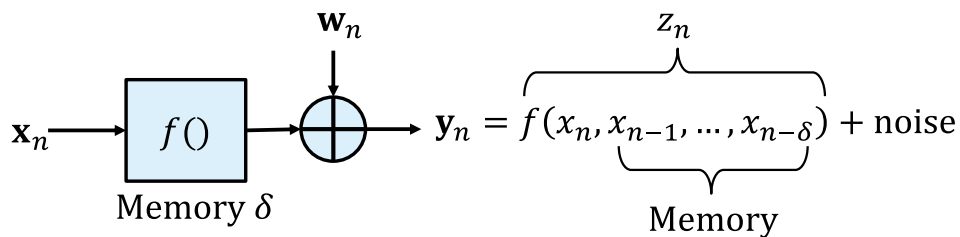


Figure 5.1: The finite state machine model.

The output sequence y_n is a function of the most recent δ inputs that drive the FSM. In other words, the FSM is modeled as a shift register which $N_s = 2^\delta$ states are defined by the last δ inputs $\mathbf{x}_n = [x_n, \dots, x_{n-\delta+1}]$, hence the output sequence is $y_n = f(x_n, x_{n-1}, \dots, x_{n-\delta+1}) + \text{noise} = z_n + \text{noise}$, as described by Forney in [93]. The FSM has $M^\delta = 2^\delta$ states, where M is the emitter alphabet size. The states are stated as S

$$S \equiv [x_n, x_{n-1}, \dots, x_{n-\delta+1}] \quad (5.1)$$

the transitions between a state S' at instant $n-1$ to state S at instant n are illustrated in figure 5.2.

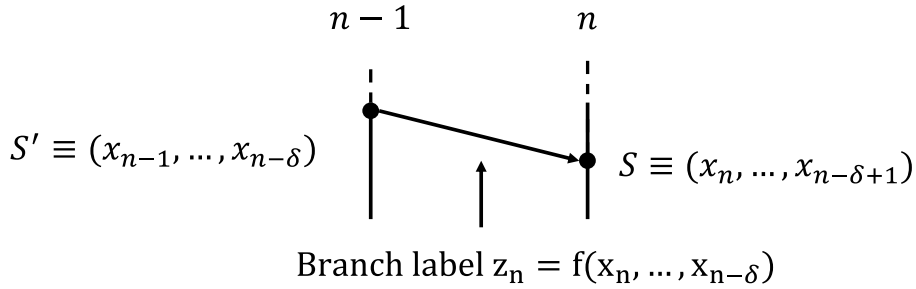


Figure 5.2: The finite state machine transition between states representation.

The state evolution through time can be described graphically through the trellis diagram, as illustrated in figure 5.3.

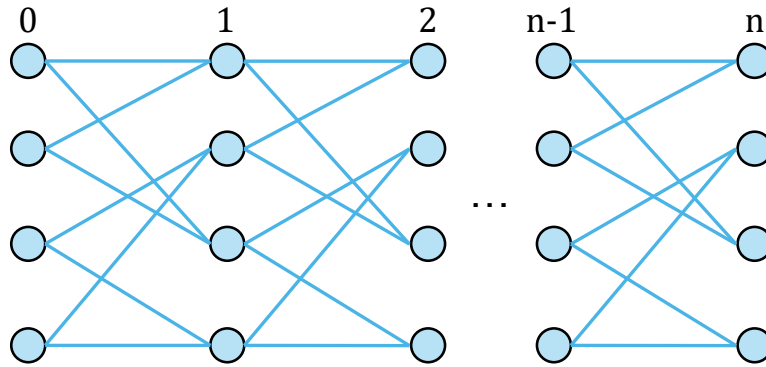


Figure 5.3: The trellis diagram representation.

Each path from 0 to n is associated with a possible symbol sequence $\underline{\mathbf{x}} = (x_1, x_2, \dots, x_N)$ and each state transition is described by a branch. A Branch Metric (BM), also known as weight, is calculated with each transition. The MLSE seeks the path whose sum of weights at the last transition is minimal, in other words, the paths that result in the smaller cost. The sequence-based detection considers that each transmitted symbol x_n will influence the previously $\delta + 1$ previously received symbols $y_n, \dots, y_{n+\delta}$, each of which can, in turn, help to decide on a symbol \hat{x}_n .

5.2.1 The goal of the MLSE

The MLSE looks to minimize the block error probability P_E , assuming the sequence-based detection. Let $P_E = p[\hat{\underline{x}} \neq \underline{x}]$. Then, minimize P_E is equivalent to decide

$$\hat{\underline{x}} = \arg \max_{\underline{x}} p(\underline{y}|\underline{x}) \quad (5.2)$$

over the finite set of all possible sequences $\underline{x} = (x_0, x_1, \dots, x_{N-1})$, considering the received sequence $\underline{y} = [y_0, y_1, \dots, y_{N-1}]$, where each term $y_n = [y_{n,0}, \dots, y_{n,\ell-1}]$ is a ℓ -tuple of the channel output and ℓ is the number of samples per symbol.

N represents the number of transmitted symbols. Considering the received samples independent, given $(x_0, x_1, \dots, x_{N-1})$ the MLSE

$$\hat{\underline{x}} = \arg \max_{\underline{x}} p(\underline{y}|\underline{x}) = p(y_0, \dots, y_{N-1} | x_0, \dots, x_{N-1}) = \prod_{n=0}^{N-1} p(y_n | x_n, \dots, x_{n-\delta+1}) \quad (5.3)$$

seeks for the sequence \underline{x} that maximizes the conditional probability or likelihood function. Since the log is a monotonically increasing function, maximize $p(\underline{y}|\underline{x})$ is equivalent to minimizing $-\ln p(\underline{y}|\underline{x})$

$$\hat{\underline{x}} = \arg \min_{\underline{x}} -\ln p(\underline{y}|\underline{x}) \quad (5.4)$$

hence, search for the minimum weight path in the trellis, where the path weight is $-\ln p(\underline{y}|\underline{x})$. Assuming that in the fractionally spaced scenario with 2 samples per symbol, the number of branch metrics is increased to $\ell = 2$, and equation 5.3 becomes

$$\hat{\underline{x}} = - \left(\sum_{n=0}^{N-1} (\ln p(y_{n,0} | x_0, \dots, x_{n-\delta+1}) + \ln p(y_{n,1} | x_0, \dots, x_{n-\delta+1})) \right) \quad (5.5)$$

The Viterbi algorithm does an efficient search of minimal weight path by taking advantage of the regular structure of the trellis to compute recursively $-\ln p(\underline{y}|\underline{x})$ one trellis step after another, and discard the unlikely paths progressively, keeping only the most likely state.

Under linear gaussian channel assumption, the channel is modeled as a function $f(x_n, \dots, x_{n-\delta+1}) = \sum_{i=0}^{\delta} \hat{h}_i x_{n-i}$, therefore

$$\min -\log p(\underline{y}|\underline{x}) \equiv \min \|\underline{y} - \underline{x}\|^2 \quad (5.6)$$

the Viterbi algorithm searches for the path \underline{x} at minimal Euclidean distance from \underline{y} .

5.3 The variants of the MLSE receiver

Figure 5.4 illustrate the MLSE receiver.

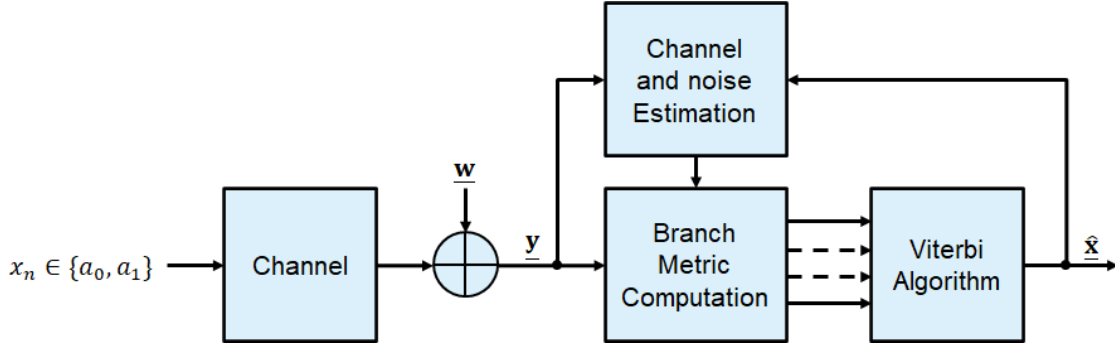


Figure 5.4: The structure of the MLSE-based receiver.

The MLSE-based receivers are optimal for digital communication systems impacted by ISI [51], [93]. In practice, the MLSE is efficiently implemented through the Viterbi algorithm, as mentioned in the last section.

The MLSE implemented in the thesis is fractionally spaced with an interval $T/2$. Two MLSE versions are considered. The branch metric value is based on two different types of channel estimation. One version of the MLSE is constrained to the exact modeling of the channel as the MMSE-LE and the MMSE-DFE, i.e., the channel presents linear ISI $y = \mathbf{H}x + w$ and is impacted by white gaussian noise $w \sim (\mu_0, \frac{N_0}{2})$. Here, the MLSE specialized in the linear gaussian model is entitled MLSE-LIN. The second version of the MLSE does not assume linear modeling. The channel estimation is instead an estimation of the conditional probability density function of the observation y [94]. The less constrained version of the MLSE, therefore, a generalized version of the MLSE, is entitled here MLSE-GEN.

5.3.1 The linear Gaussian channel-based model MLSE

The MLSE-LIN follows a model-based approach where the channel is corrupted by additive Gaussian noise. It considers the channel impulse response and noise in the BM computation.

As mentioned in section 5.2, the output of the z_n is a function of the last δ inputs that drive the FSM. Considering the linear estimation constrained by a filter, the channel output z_n in the absence of noise from instant n to $n + 1$

$$z_n = f(x_n, S \rightarrow S') = \sum_{i=0}^{\delta} h_i x_{n-i} \quad (5.7)$$

is known as a transition symbol, and $\hat{\mathbf{h}} = [\hat{h}_0, \dots, \hat{h}_\delta]$ is the channel impulse response. From equation 5.7, we see that the channel impulse response is necessary. However, in a practical application, the Channel Impulse Response (CIR) is unknown. Therefore,

the use of the FIR filter estimation is commonly used [95]. In this thesis, the response obtained through the data-aided LMS-based algorithm [64] is represented by figure 5.5

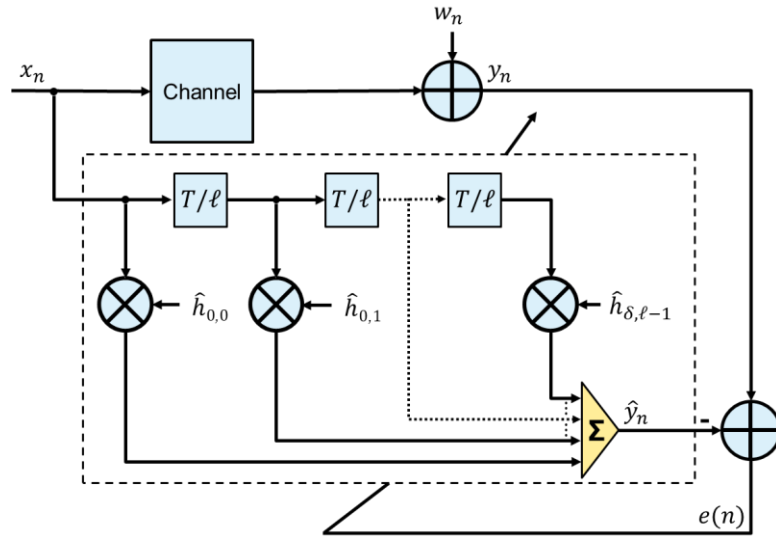


Figure 5.5: The representation of the channel LMS estimator [64].

The estimated CIR is $\hat{\mathbf{h}} = \hat{\mathbf{h}}_{n-1} + \mu x_n e_n$ and the error at instant n is $e_n = y_n - \hat{y}_n$ and $\mu = 0.001$ is the step-size. Once the LMS estimator achieves the steady-state, the estimated T/2 spaced CIR $\hat{\mathbf{h}} = [\hat{h}_{0,0}, \hat{h}_{0,1}, \dots, \hat{h}_{\delta,1}]$ is used in the MLSE-LIN branch metrics computation from a state S at instant n to another S' at instant $n + 1$

$$m(y_n, S \rightarrow S') = \left| \underline{y}_n - z_n(S \rightarrow S') \right|^2 = \sum_{k=1}^{\ell=2} \left| y_{n,k} - \sum_{i=0}^{\delta-1} \hat{h}_{i,k} x_{n-i} \right|^2 \quad (5.8)$$

The MLSE-LIN is evaluated through simulations of the EML and DML channels in section 5.6.

5.3.2 The generalized version of the MLSE

In the previous section, the branch metrics are based on the linear gaussian channel model. However, the PON IM/DD channel may present nonlinearities due to chirp and the APD [40], [96], [97], as mentioned in chapter 2. Also, the noise may not present Gaussian distribution due to optical amplification [96]. The most general MLSE considers the conditional probability density function

$$m = -\ln p(\underline{y}_n | x_n, \dots, x_{n-\delta+1}) \quad (5.9)$$

for each channel output y_n and $(x_1, \dots, x_{n-\delta+1})$. The conditional PDF from equation 5.9 is unknown in practice. Therefore, its estimated by the histogram method here, which is a nonparametric approach [94], [96]. It could be either precomputed or trained online at the system startup based on a training sequence.

Here, the PDF is estimated in a fully data-driven manner. Once the histogram is obtained with sufficient training data, the PDF is estimated. The number of generated histograms is $N_H = M^\delta = 2^\delta$. The number of bins of each histogram depends on the

quantizer resolution. We remind that the receiver presented in chapter 2 has a mid-riser quantifier with a quantization step q_s and the effective number of bits is $\psi = 5$. Thus each constructed histogram has $N_{bins} = M^\psi = 2^5 = 32$ bins, because here we use binary modulation $M = 2$ (Appendix C describe more details on the quantization process).

In the histogram method, each received sample is associated to its respective histogram $y_n = f(x_n, x_{n-1}, \dots, x_{n-\delta+1})$ based on the state $S = (x_n, x_{n-1}, \dots, x_{n-\delta+1})$. In other words, y_n is a combination associated to the training sequence \underline{x} , if each BM was associated with a possible state of the FSM in the MLSE-LIN $m_n \rightarrow S = (x_n, \dots, x_{n-\delta+1})$, here, each histogram is associated with a BM and a state S .

Figure 5.6 shows an example of histogram construction with a single-bit memory $\delta = 1$.

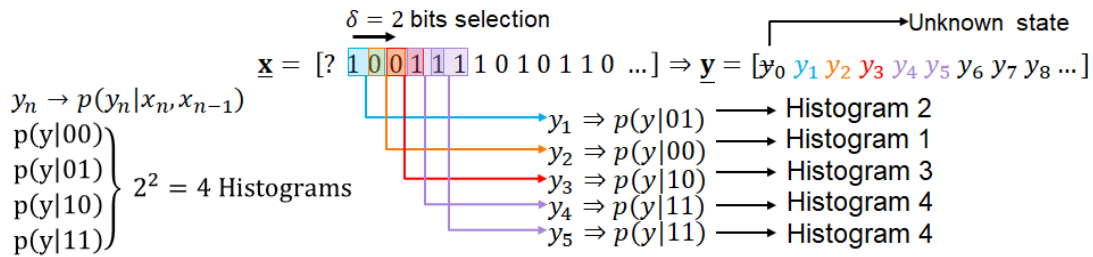


Figure 5.6: an example of the construction of the histogram.

In this example $N_H = 2^2 = 4$ histograms are generated and enumerated from 1 to 4. One may observe that the pair of transmitted bits (states) bits defines to which histogram the received sample will be associated hence $\underline{y}_n \rightarrow p(\underline{y}_n | x_n, x_{n-1})$. The received samples related to unknown states x_i for $i < 0$ are discarded. In the fractionally spaced equalization with $\ell = 2$ the number of generated histograms per BM is $N_{Hist} = \ell \times N_H = 2N_H$ and the fractionally spaced samples $y_{n,0}, y_{n,1}$ are associated with the respective histograms $y_{n,0} \rightarrow p(y_{n,0} | x_n, x_{n-1}, \dots, x_{n-\delta+1})$ and $y_{n,1} \rightarrow p(y_{n,1} | x_n, x_{n-1}, \dots, x_{n-\delta+1})$.

After the histogram construction, the conditional PDF is estimated based on the quantization step q_s and the interval of the bins $0 \leq i \leq 2^\psi - 1$

$$p(\underline{y} | \underline{x}) = \frac{N_i}{N_{tot} \times q_s} \quad (5.10)$$

i is the index in which the quantized observation y_n falls into, N_i is the number of samples collected in bin i and N_{tot} the total number of samples collected for the histogram referenced by \underline{x} .

After the histogram construction and PDF estimation or training phase, the MLSE-GEN is ready to transmit unknown data. Now the received samples y_n values represent a BM of the Viterbi algorithm given by equation 5.9. In other words, each received sample $\underline{y}_n = [y_{n,0}, y_{n,1}]$ have a quantization level that corresponds to a value $m(\underline{y}_n) \rightarrow p(\underline{y}_n | x_n, \dots, x_{n-\delta+1})$ mapped into the estimated PDF. In practice, there are

regions of the histograms without sufficient information. Usually, the extremes of the histograms have unsigned BM. In these cases, we associated a value $m = -20$ dB with the respective BM. This procedure is illustrated in the channel estimation of section 5.6. similar to the MLSE-LIN each BM of the trellis is given by the sum of the fractionally spaced PDFs

$$m = - \left(\sum_{n=0}^{N-1} (\ln p(y_{n,0}|x_n, \dots, x_{n-\delta+1}) + \ln p(y_{n,1}|x_n, \dots, x_{n-\delta+1})) \right) \quad (5.11)$$

We conclude this section reminding that the difference between the MLSE-LIN and MLSE-GEN is the channel model and estimation, therefore the value of branch metric. The MLSE-LIN is based on the channel impulse response estimation through the LMS algorithm, and the MLSE-GEN uses the estimated PDF through the histogram method.

5.4 The Viterbi algorithm implementation

Sections 2 and 3 introduced the sequence detection, the trellis graphic representation, and the MLSE versions of the MLSE implemented during the thesis. This section describes the Viterbi algorithm implementation.

Considering the trellis detection for NRZ-OOK symbols, at each n instant, $N_H = M \times N_s = 2 \times N_s = 2 \times 2^\delta$ branch metrics are calculated, and $M = 2$ branches merge to a single state represented by a node in the trellis. In other words, each transition from state S at time n to another state S' at time $n+1$ is associated with a branch metric $m = f(y_n, S \rightarrow S')$. The N_H branch metrics are stored in a Branch Metric Register (BMR)

$$BMR = [m_0, \dots, m_{N_H-1}] \quad (2N_s \times 1) \text{ vector}$$

the distance between the path and the observation is given by the sum of the branch metrics, known as cumulative path metric (CPM), represented as $c(S, n)$. Figure 5.7 shows a transition $S \rightarrow S'$ considered by the Viterbi algorithm.

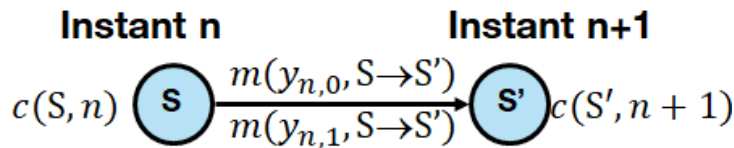


Figure 5.7: The diagram of states of the Viterbi algorithm, based on [98].

When $n=0$ the initialization of trellis occurs, the CPM is fixed to $c(0,0) = 0$ and $c(S, 0) = +\infty$ for any S different from 0. Afterward, the Viterbi algorithm compares at each instant $n > 0$ the $M=2$ incident paths $S' \rightarrow S$, then selects the path with smaller CPM, known as the survivor path.

$$c(S', n) = \min\{c(S, n-1) + m(y_{n-1}, S \rightarrow S')\} \quad (5.12)$$

The CPM is stored in a Cumulated Path Metric Register (CPMR).

$$CPMR = [c(0,0), \dots, c(N_s - 1, N - 1)] \quad (N_s \times N)$$

Matrix

The process of addition, comparison, and selection of CPM is known as Add-Compare-Select (ACS). Hence the ACS process is realized at every $n > 0$ instant which is the most complex process of the MLSE. The survivor path is also stored in a Survivor Path Register (SPR)

$$SPR = [v(0,0), \dots, v(\delta - 1, N - 1)] \quad (\delta \times N - 1)$$

Matrix

Where v designs the stored path at instant n . The MLSE selects the state with a minimum cumulated metric then restitutes the information sequence considering the survivor path, in the end of the trellis window. This process is known as Viterbi traceback or trellis traceback.

5.4.1 The MLSE optimization

The MLSE receiver is implemented in a sliding-window manner [70] since it minimizes the MLSE latency and required memory. The trellis has a length of $N_w \ll N$ stages, hence the CPMR and SPR requires less storage. Basically, the VA is executed, a decoded symbol \hat{x}_n is stored then the sliding window is shifted, this routine is performed progressively from instant $n = 0$ to instant $n = N - N_w + 1$. The length of the sliding window is $N_w = 20 \times \delta$ which is enough to ensure the convergence of the Viterbi algorithm [99], [100].

The assumed channel memory order δ of the MLSE is often smaller than the actual channel memory. Since we aim for an implementation of receivers with the compromise of performance and complexity, the memory δ and thus the number of states $N_s = 2^\delta$ was optimized. An artificial restitution delay $\Delta \leq 5T$ was comprised into the MLSE optimization to consider the channel causality as the MMSE equalizers.

Figure 5.8 shows the procedure used to find the minimum δ and best Δ optimization to reach the target performance $BER \leq 10^{-2}$ at a minimal cost.

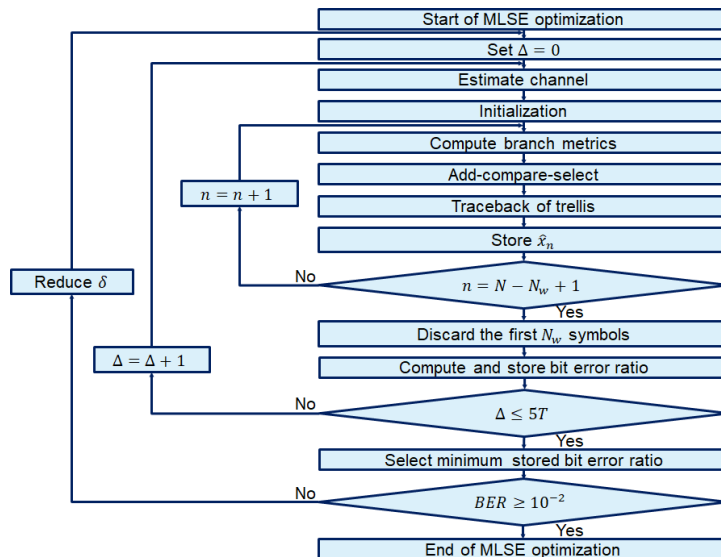


Figure 5.8: The flowchart of the MLSE receiver optimization.

This optimization is used with the MLSE-LIN and the MLSE-GEN receivers. To evaluate the MLSE receivers, a measurement of reference with received optical power $ROP = S_{HS-PON} = -24$ dBm was used to optimize the memory δ and the restitution delay Δ .

5.5 Simulated performance of the MLSE and MMSE receivers over the 50G HS-PON based on EML and DML

This section demonstrates the performance of the MLSE receivers in term of BER and the number of states of the MLSE $N_s = 2^\delta$, therefore the BER is a function of $BER = f_{MLSE}(N_s, \Delta)$. First the channel estimation is studied, afterwards the best performances of the MMSE equalizer and MLSE receivers are compared in terms of BER, then the complexity of each receiver is compared over the HS-PON chain based on EML and DML with 25G and 50G receivers.

5.5.1 Channel estimation

The MLSE-LIN and MLSE-GEN performance depends on the channel estimation. The channel was estimated at each ROP of operation then the branch metrics were calculated. Here it is demonstrated the estimation of the channel impulse response and the PDF whose $N_{tr} = 10^6$ symbols were used for channel estimation.

5.5.1.1 Estimated impulse response through the method LMS

Figure 5.9 shows the estimated impulse response of the EML and DML.

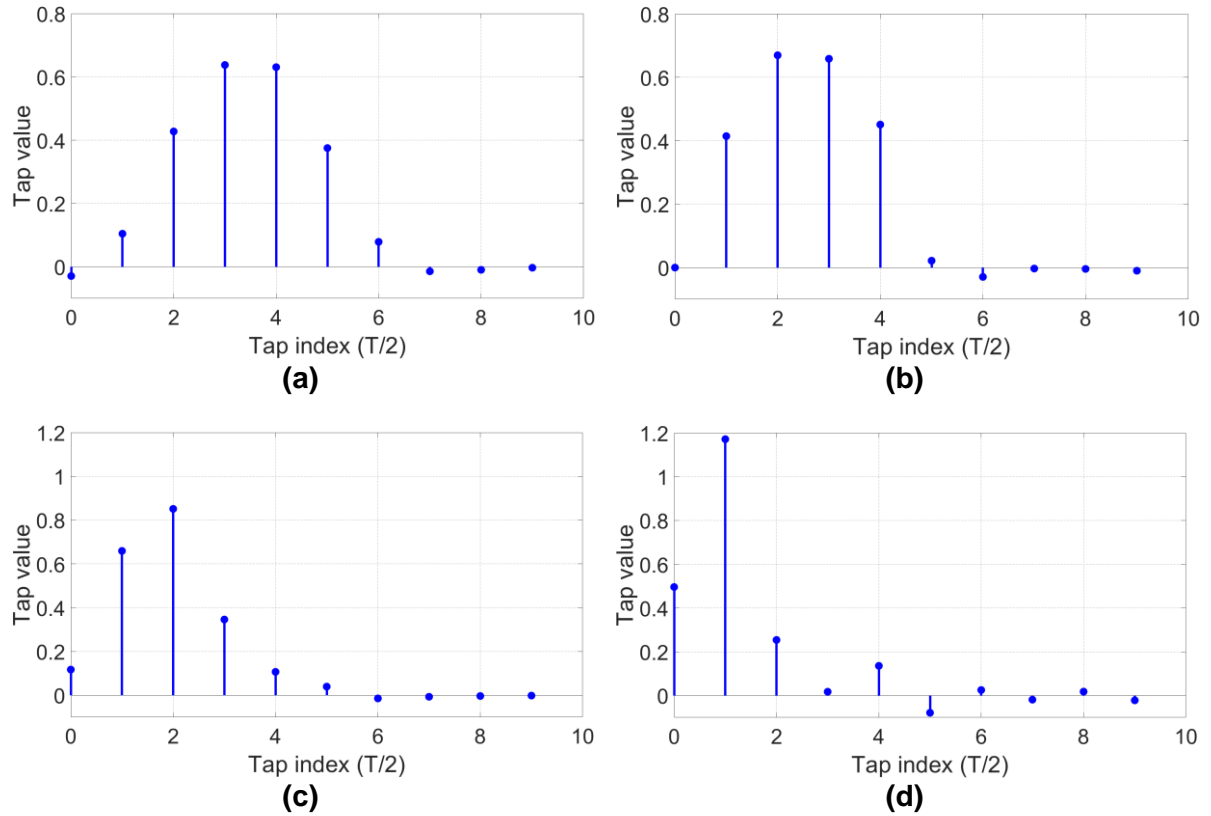


Figure 5.9: Estimated impulse response over channels EML + SMF + (a) 25G Rx and (b) 50G Rx and over the channels DML + SMF + (c) 25G Rx and (d) 50G Rx.

The VOA was disabled here to have an estimation without severe noise impact. The received optical power was $ROP = 3$ dBm through these EML channel estimations and $ROP = 4$ dBm over the DML channel estimation. The EML + 25G Rx spans approximately $\delta = 3$ bits intervals since the energy is concentrated from tap 0 to tap 7 at $T/2$ consequently $N_s = 2^3 = 8$ states may be enough to the MLSE to obtain the most likely transmitted sequence. The EML + 50G Rx has the energy concentrated on the first 6 taps, therefore spans 3 symbols hence $N_s = 4$ states are expected for best-effort performances. The DML + 25G Rx has the energy concentrated in the first 6 taps hence spans 3 symbols, hence $N_s = 4$ states may be enough to MLSE optimal performance. Finally, as the previous channel, the DML + 50G receiver has the most energy concentrated in the first six taps, spanning 3 symbol periods.

5.5.1.2 Transient analysis of the LMS-based estimation

Figure 5.10 shows the *MSE* vs iteration obtained with the EML and DML channels with $ROP = \{-20, -24, -32\}$ dBm as insets.

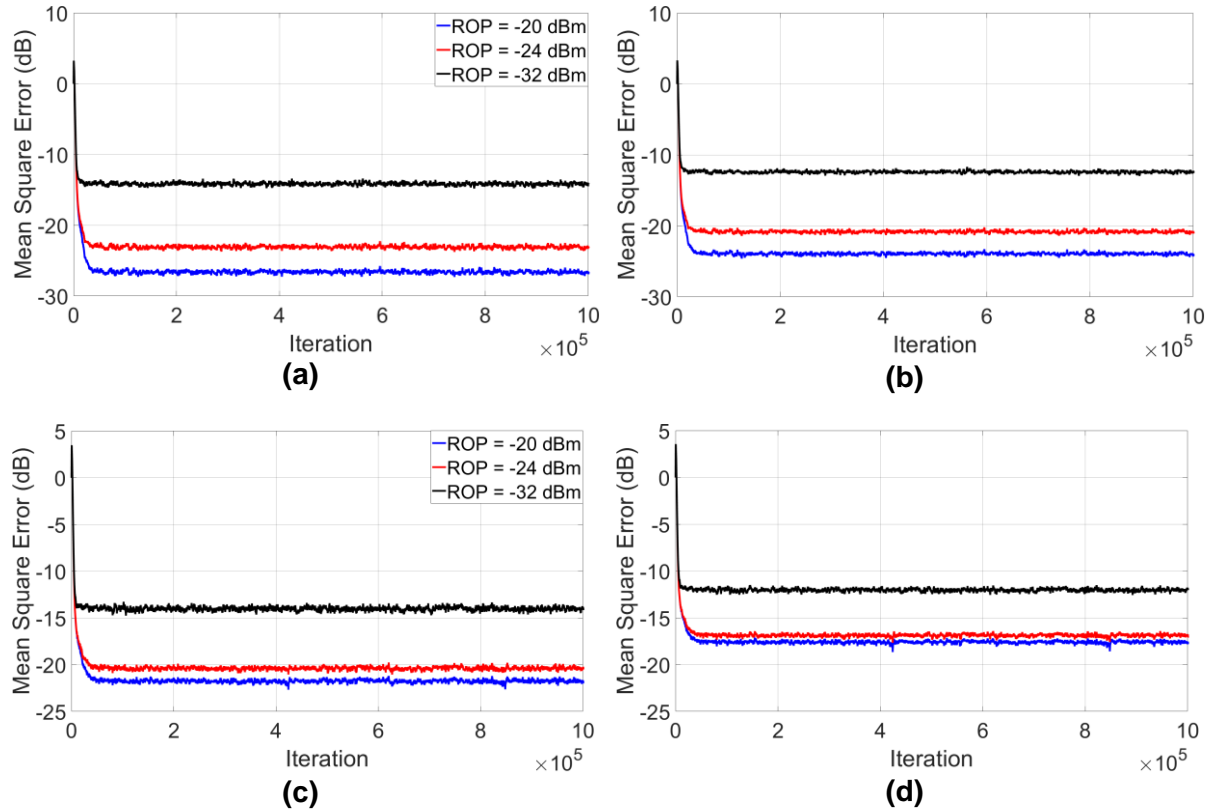


Figure 5.10: learning curve of the LMS-based filter estimator over channels EML + SMF + (a) 25G Rx and (b) 50G Rx and over the DML + SMF + (c) 25G Rx and (d) 50G Rx.

The ROP does not impact severely the number of training symbols for the FIR filter estimation. $N_{tr} = 40 \times 10^3$ symbols are enough to estimate the CIR with all simulated channels. The increase of receiver bandwidth from 18.75GHz to 37.5GHz in both cases may reduce the ISI due to bandwidth limitation however the residual noise at the output of the APD is increased and consequently the MSE is higher, as already verified in chapters 3 and 4.

5.5.1.3 Estimation of the PDF

The PDF estimator considered the receiver quantization resolution, therefore the PDF estimator generated histograms with $2^5 = 32$ bins as mentioned in section 5.3. During the simulations it was verified that the memory of the Viterbi processor does not exceed $1 \leq \delta \leq 3$ as observed with the LMS based estimator in the previous subsection. To estimate the PDFs $N_{tr} = 1 \times 10^6$ symbols were used, however it could be reduced requiring a study of performance. Figure 5.11 shows the estimated PDF of EML and DML channels through an estimator with $\delta = 3$ over simulations with fixed $ROP = -24$ dBm.

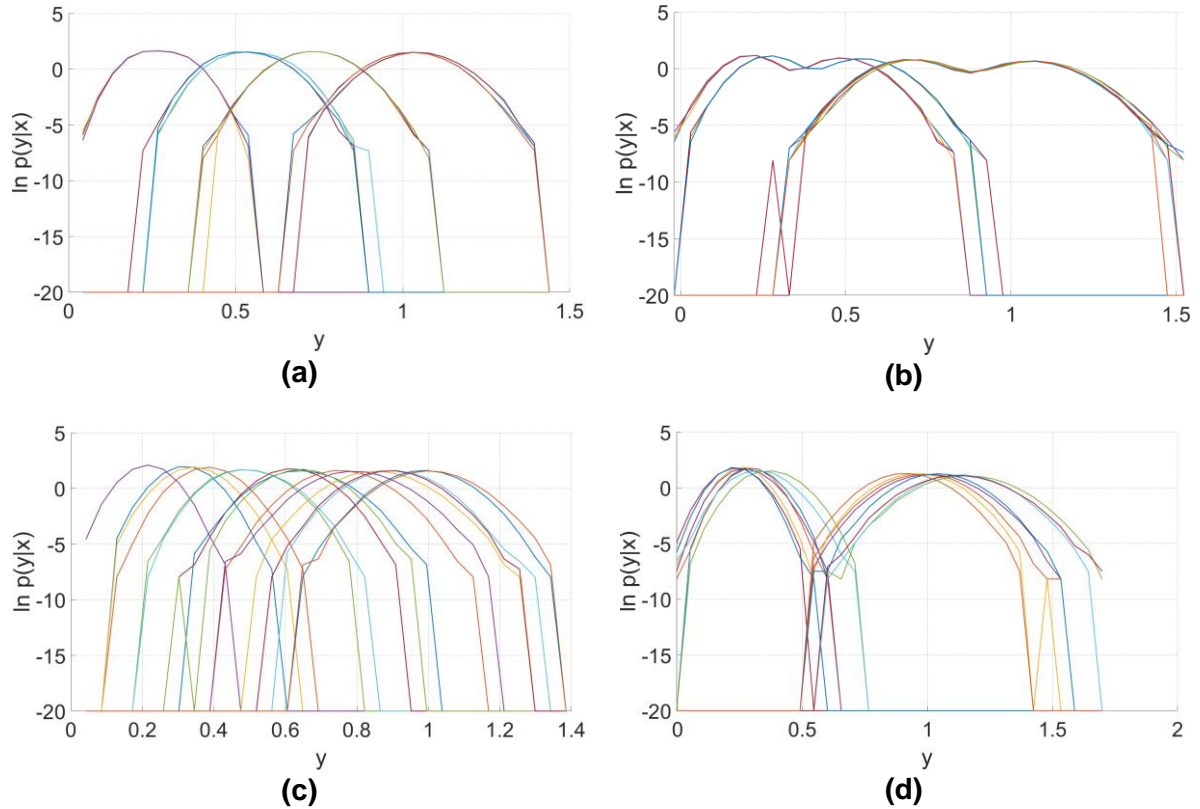


Figure 5.11: Estimated PDF channels EML + SMF + (a) 25G and (b) 50G receivers and over the DML + SMF + (c) 25G and (d) 50G receivers.

Each color represents an estimated PDF in decibels. Comparing the EML-based channels, it is visible that when the bandwidth is increased, the noise variance is increased. As mentioned in section 5.4, the histograms were not entirely obtained, mainly in the extremes of each histogram therefore $\ln p(y|x)$ were associated with -20dB. In other words, the most unlikely received y_n samples are associated with very small probabilities.

5.5.2 The EML + 25G Rx based channel

Figure 5.12 shows the performance of the MLSE-LIN and MLSE-GEN through the EML + 25G Rx channel.

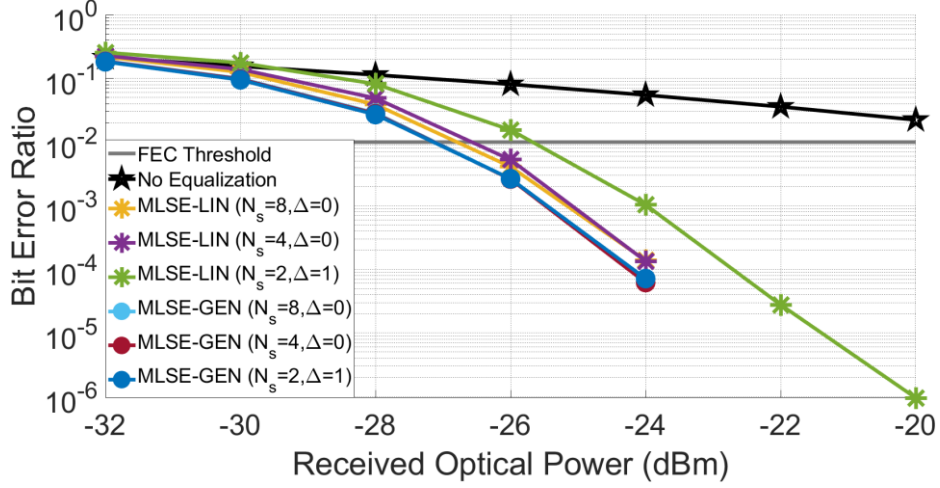


Figure 5.12: The MLSE-LIN and MLSE-GEN performances through the EML + 25G Rx channel.

The MLSE-LIN and MLSE-GEN cope well with the IM/DD channel impairments. They improve the receiver sensitivity regardless of the number of states. The MLSE-GEN handles well the channel distortions because it does not assume linearity, and we remind that the chirp causes nonlinearities.

Both receivers achieve the recommended sensitivity by ITU-T $S_{ITU} \leq -24$ dBm. The MLSE-LIN achieves the sensitivity $S = -26$ dBm with configurations $N_{LIN} = (N_s = 8, \Delta = 0)$ and $N_{LIN} = (N_s = 4, \Delta = 0)$, the best-effort option is the latter because it has almost the same performance as the former but uses fewer states. The low-complexity performance is obtained through $N_{LIN} = (N_s = 2, \Delta = 1)$. In this case, the sensitivity of the receiver is $S = -25$ dBm.

The number of states of the MLSE-LIN agrees with the expected channel memory seen at the beginning of section 5.5. for example, this estimated channel memory is $\delta = 3$, so $N = 2^3 = 8$ states were expected to obtain the best performance.

The MLSE-GEN has almost the same performance through the configurations $N_{GEN} = (N_s = 8, \Delta = 0)$, $N_{GEN} = (N_s = 4, \Delta = 0)$ and $N_{GEN} = (N_s = 2, \Delta = 1)$ with sensitivity $S = -27$ dBm. Hence the latter configuration has the best overall performance with the minimum number of states.

The MLSE-GEN improves the sensitivity by 1 dB more than the MLSE-LIN with fewer states. It demonstrates that the MLSE-GEN compensates better for the channel nonlinearities related to chirp that the MLSE-LIN does not perceive. When two states are considered, the performance of the MLSE-GEN is not degraded as the MLSE-LIN.

Figure 5.13 illustrate the best-effort performances of the MLSE and MMSE-based receivers.

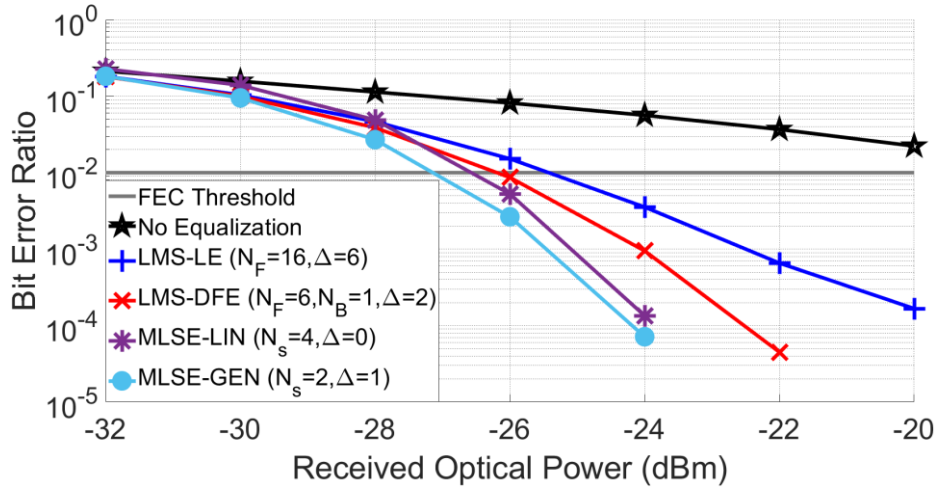


Figure 5.13: The BER vs ROP performances of the MMSE and MLSE based receivers through the EML + 25G Rx channel.

Here, the best choice regarding complexity and performance is the LMS-DFE with sensitivity $S = -26$ dBm. The LMS-LE requires more taps. Therefore it is more complex than the LMS-DFE-based receiver. Otherwise, the MLSE-GEN improves the receiver sensitivity to $S = -27$ dBm with only two states, which is a remarkable performance as it has the lowest computational complexity among the MLSE receivers under test. The MLSE-LIN performs better than the LMS-DFE, but the complexity increase is not enough considering the sensitivity gain.

5.5.3 The EML + 50G Rx based channel

Figure 5.14 shows the performance of the MLSE-LIN and MLSE-GEN over the EML + SMF +50G Rx channel.

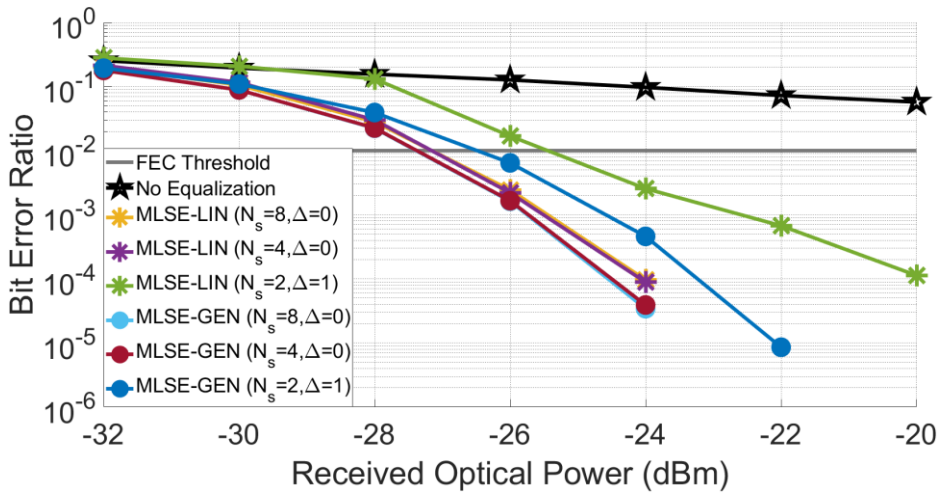


Figure 5.14: The MLSE-LIN and MLSE-GEN performances through the EML + 50G Rx channel.

The MLSE-LIN is more impacted in this channel because the noise dominates more. Hence the linear LMS estimation is constrained. When the number of states is minimal, the linear MLSE suffers critically and cannot maintain the performance obtained with four or eight states.

The set of parameters $N_{LIN} = (N_s = 4, \Delta = 0)$ is the best effort configuration for the MLSE-LIN. It achieves a sensitivity $S = -26$ dBm. $N_{LIN} = (N_s = 2, \Delta = 1)$ is the low complexity configuration with $S = -25$ dBm. The performance with eight states is practically the same as with four states, it is natural considering the channel impulse estimation, $=2$ is enough to capture the non-negligible taps of the channel. The MLSE-GEN follows the same trend, which is expected because this channel does not present a high degree of nonlinearity.

The MLSE-GEN presents better performances with the configurations $N_{GEN} = (N_s = 8, \Delta = 0)$, $N_{GEN} = (N_s = 4, \Delta = 0)$, the latter configuration is enough to achieve the best effort performance with $S = -27$ dBm. When $N_{GEN} = (N_s = 2, \Delta = 1)$ the low-complexity performance is achieved with $S = -26$ dBm.

Comparing the performance degradation from 8 states to 2 states with both MLSE, the MLSE-LIN is relatively more impacted than the MLSE-GEN. Therefore, the approximation of the EML channel with two states is very limited, so the linear estimation does not well model the channel for the MLSE-LIN. The MLSE-GEN solution better captures the behavior of the HS-PON channel and thus better restitutes the data in their integrity, whatever the distortions encountered in this configuration with EML + 20km SMF + 50G.

Figure 5.15 demonstrate the best-effort performance of the MMSE and MLSE based receivers through the EML + 50G Rx channel.

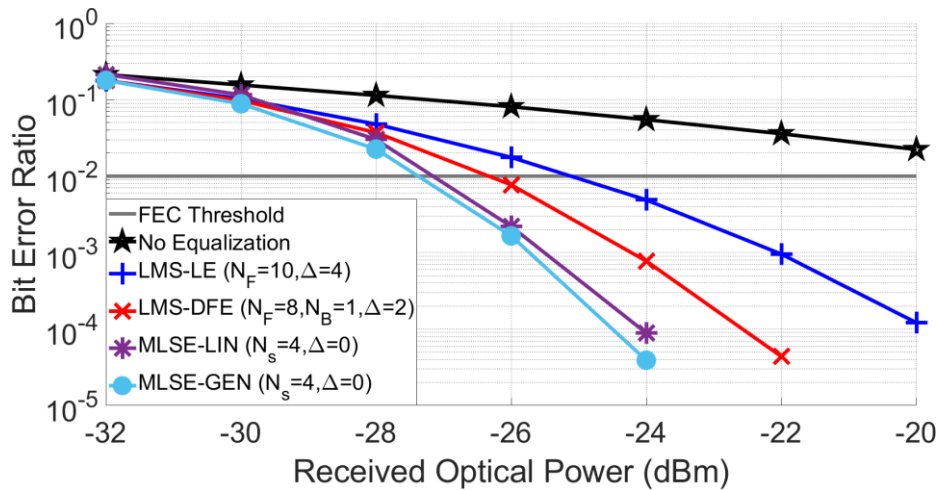


Figure 5.15: The BER vs ROP performances of the MMSE and MLSE based receivers through the EML + 50G Rx channel.

The LMS-DFE achieves $S = -26$ dBm which is 2 dB higher than the recommended sensitivity by ITU and have less complexity than the MLSE receivers. The LMS-LE achieves $S = -25$ dBm however it presents almost the same complexity of the LMS-DFE. At the price of a higher complexity, the MLSE-GEN and MLSE-LIN reach

sensitivities $S = -27$ dBm. Therefore, the LMS-DFE is the most recommended equalizer for the 50G HS-PON in downstream mode with EML.

5.5.4 The DML + 25G Rx based channel

Figure 5.16 shows the performance of the MLSE-LIN and MLSE-GEN over the DML + 25G receiver.

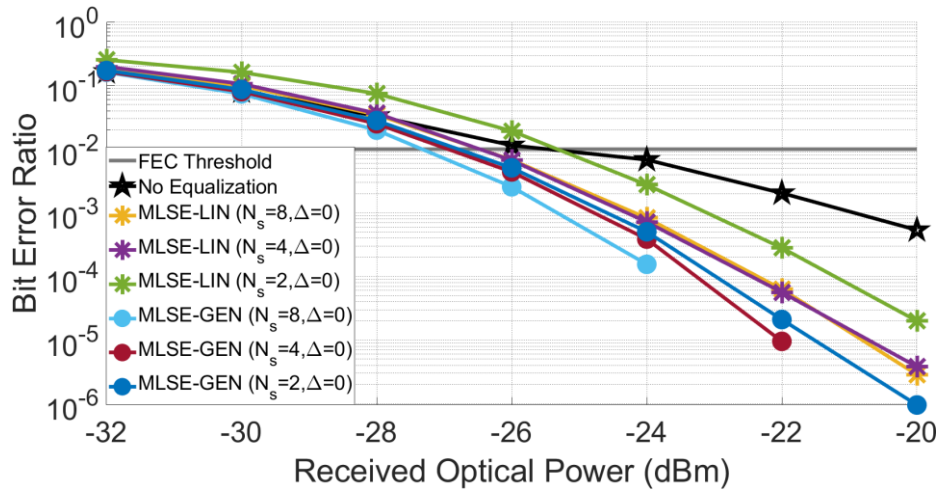


Figure 5.16: The MLSE-LIN and MLSE-GEN performances through the DML + 25G Rx channel.

Both receivers enhance the channel performance. However, the MLSE-LIN performance is critical when two states are considered.

As discussed in section 5.5.1, $N_s = 4$ states are enough for the MLSE-LIN to achieve best-effort performances with sensitivity $S = -26$ dBm. When $N_{LIN} = (N_s = 2, \Delta = 0)$ the performance is severely degraded since the channel is not well-modeled through FIR-based channel estimation since the DML configuration increased nonlinear distortion due to adiabatic and transient chirp. Here the channel estimation problem is very evident because the channel is nonlinear, which reduces the performance of the MLSE-LIN solution.

Otherwise, the MLSE-GEN achieves better performance than the MLSE-LIN, with $N_{GEN} = (N_s = 8, \Delta = 0)$ it reaches the best-effort performance with $S = -27$ dBm hence the MLSE-GEN addresses more nonlinearities of the channel that are not comprised by the MLSE-LIN. The channel linear and nonlinear distortions are well captured through the histogram estimation with only $N_s = 2$ states, with a remarkably low complexity performance.

Figure 5.17 shows the best-effort performance of the MMSE equalizers, and the MLSE based receivers.

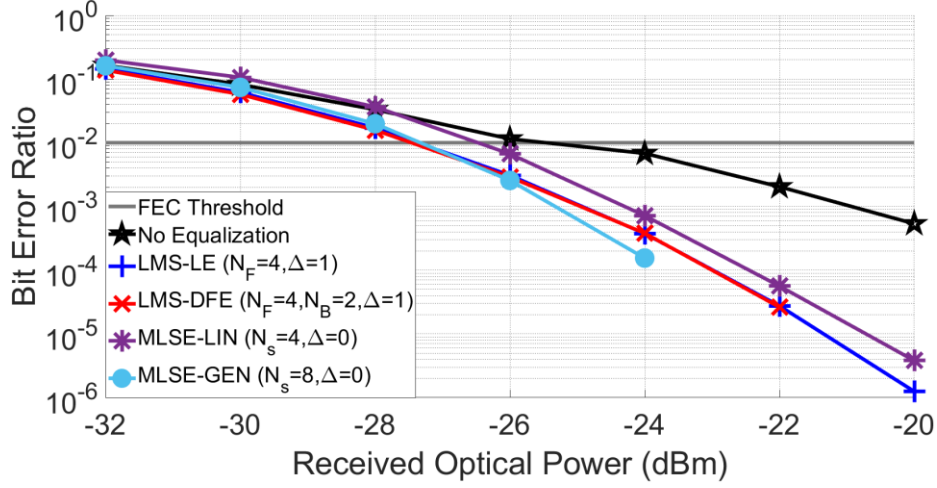


Figure 5.17: The BER vs ROP performances of the MMSE and MLSE based receivers through the DML + 25G Rx channel.

Since the MMSE equalizers have performances as good as the MLSE-GEN over $ROP \geq -24$ dBm, we can confirm that the linear ISI predominates the channel nonlinearities. Consequently, the LMS-LE is the most recommended equalizer because it introduces the smallest complexity, and it achieves the same sensitivity as the MLSE-GEN and the LMS-DFE $S = -27$ dBm. Another conclusion is that when the most crucial impact is ISI only due to bandwidth limitation, the linear equalizer handles better the IM/DD impairments.

The MLSE-GEN performs better when the BER is below the FEC threshold. The MLSE-LIN does not correctly model the DML + 25G channel since it is nonlinear. It achieves worse performance than the other receivers and is not recommended.

5.5.5 The DML + 50G Rx based channel

Figure 5.18 shows the performance of the MLSE based receivers through the DML + 50G Rx.

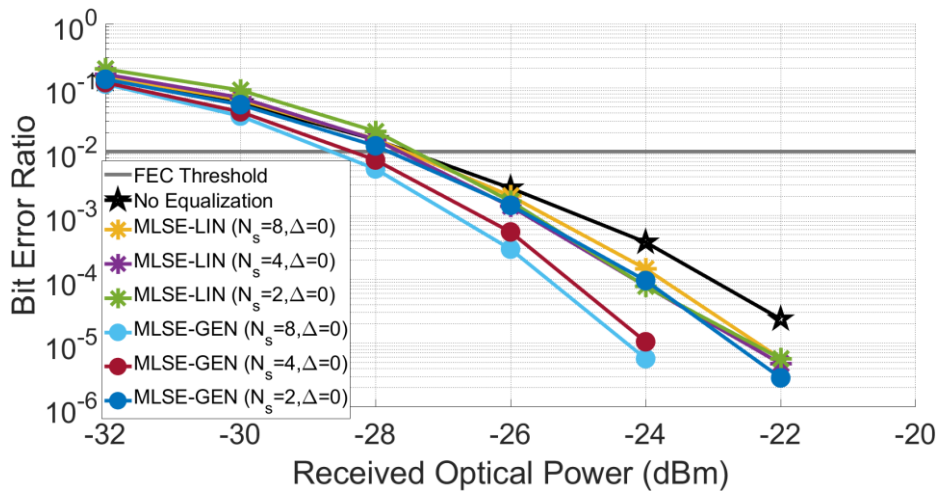


Figure 5.18: The MLSE-LIN and MLSE-GEN performances through the DML + 50G Rx channel.

From the perspective of the MMSE equalizers presented in chapters 3 and 4 or the linear estimator, this is an ISI-free channel with white Gaussian noise. Theoretically, we saw in chapter 2 that this is not entirely true because of nonlinearity induced by chirp. The gain of performance ensured by the MLSE-GEN reveals the nonlinearities of the channel.

Looking into the MLSE-LIN, when $N_s = 4$ states the channel distortions are well addressed. However, the sensitivity of the receiver is not improved. Consequently, the nonlinearities of the channel are transparent to the linear MLSE. The MLSE-GEN perceives the nonlinearities, and it can address them, we can infer it through performance enhancement. The generalized MLSE improves the receiver sensitivity to $S = -28$ dBm with the best-effort configuration $N_{GEN} = (N_s = 4, \Delta = 0)$. In other words, when only nonlinearity manifests, the MLSE-GEN can handle it.

Figure 5.19 compares the performances of the MLSE and MMSE equalizers-based receivers.

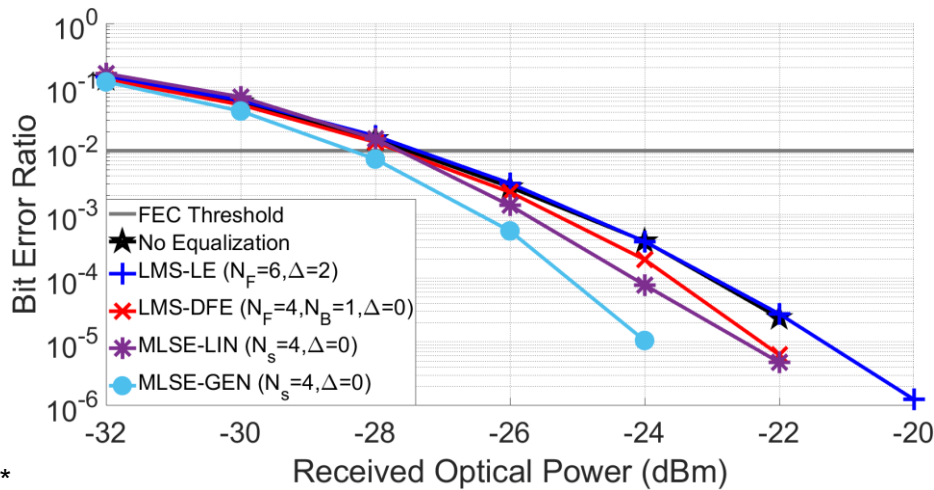


Figure 5.19: The BER vs ROP performances of the MMSE and MLSE based receivers through the DML + 50G Rx channel.

The LMS-LE does not improve the receiver performance. Therefore, it only increases the complexity of the receiver in this simulation. The LMS-DFE and the MLSE-LIN also do not enhance the sensitivity of the receiver, but it improves the performance when the ROP is within $-26 \leq ROP \leq -20$ dBm. The MLSE-GEN outperforms the other developed receivers because it can address the nonlinear channel distortions and improve the sensitivity to $S = -28$ dBm. In conclusion, this channel is effectively ISI-free, but the nonlinearity is present and receivers assuming linear channel are not helpful in this situation.

The delay introduced by the MLSE and MMSE equalizers based receivers is negligible in these 50G-PON simulations transmissions in downstream mode.

5.5.6 Performance comparison of the MMSE and MLSE equalizers

Here the best effort performances of the MMSE and MLSE based receivers are discussed. Table 5.1 summarizes the measured sensitivities over the EML and DML based simulations.

Table 5.1: Main results of the DSP-enabled 50G HS-PON

Calculated sensitivity (dBm)				
Channel	LMS-LE	LMS-DFE	MLSE-LIN	MLSE-GEN
EML + 25G Rx	-25	-26	-26	-27
EML + 50G Rx	-25	-26	-27	-27
DML + 25G Rx	-27	-27	-26	-27
DML + 50G Rx	-27	-27	-27	-28

All the presented receivers enhance the performance of the HS-PON 50G concerning the recommended sensitivity and optical budget by ITU-T [1]. Considering the trade-off between sensitivity and complexity the LMS-DFE is the best choice of equalizer. If the receiver is less constrained by complexity, the MLSE-GEN is the best option since it reaches better sensitivities than the other receivers in all scenarios. During the thesis it was verified that the DSP enabled receivers can be optimized so as to have a minimal number of taps or states while maintaining the target sensitivity.

5.6 Concluding remarks

This chapter introduced the MLSE and its implementation in the 50G-PON. Two versions of the MLSE were introduced, first, the version based on a linear gaussian channel assumption, and second the generalized version based on the histogram of the received signal. The MLSE only requires $2 \leq N_s \leq 8$ states to improve the sensitivity of the receiver based on EML or DML channels.

The MLSE-GEN presented more advantages than the MLSE-LIN in terms of complexity and equalization performance. Therefore, the MLSE-GEN is more suitable for compensating for the HS-PON channel nonlinear distortions and achieving the ITU-T required performance. The MLSE-GEN reached better performances than the MLSE-LIN with fewer states. It could see the nonlinearities of the DML-based channels that were invisible to the linear channel hypothesis-based receivers. Therefore the FIR-based channel estimation (that considers as strong assumption the linearity of the channel) is not well adapted anymore and may impact the performance of receiver, especially when a small number of channel taps $\delta + 1 = 2$ are considered, or the channel presents high adiabatic chirp.

Comparing all equalizers, the LMS-DFE achieves the desired sensitivity without error propagation, and the MLSE-GEN achieves the best performance increasing the receiver sensitivity by more than 1 dB compared to the other receivers. The delay introduced by equalization is negligible, and the number of symbols necessary to train the DSP-enabled receivers is compatible with the HS-PON standards.

6 Experimental Demonstration of the LE, DFE, and MLSE based Receivers

6.1 Introduction

We observed the optical effects of the 50G IM/DD channel in simulations. The small signal regime showed the physical characteristics of the HS-PON, and the large signal model demonstrated the channel impact in transmissions with conditions close to reality. Furthermore, the DSP-based receivers could compensate well for the channel distortions and achieve the recommended performance by ITU-T.

Still, contrasting the simulation and experimental conditions is important to validate the IM/DD model at 50Gbit/s. Here, we demonstrate the applicability of the IM/DD model in an experimental 50Gbit/s setup. Furthermore, the benefits of the fractionally spaced linear equalizer (LMS-LE), the decision feedback equalizer (LMS-DFE), and the maximum likelihood sequence estimation (MLSE-GEN) experimentally in a 50 Gbit/s PON system. The downstream (DS) and upstream (US) chromatic dispersion are emulated in the laboratory, considering the 50G-PON ITU-T conditions, then the captured waveforms were processed offline.

The DS and US directions have different channel behavior and stress the signal differently. This chapter verifies the results and improvements obtained from the previous chapters are also present in real measurements with devices expected in the future 50G-PON.

This chapter is organized as follows: Section 6.2 introduces the experimental setup and parameters used to evaluate the 50G-PON DSP-based receivers in practice. The following section discusses the optimization approach to maximize performance and minimize the DSP complexity. Section 6.4 considers the LMS-LE, LMS-DFE, and MLSE in practice, followed by comparisons to the simulations presented during the thesis. Furthermore, the theoretical frequency considering the small-signal regime discussed in chapter 2 and the experimental frequency response are compared.

6.2 Experimental setup

Figure 6.1 a) shows the setup of our 50 Gbit/s HS-PON experiment.

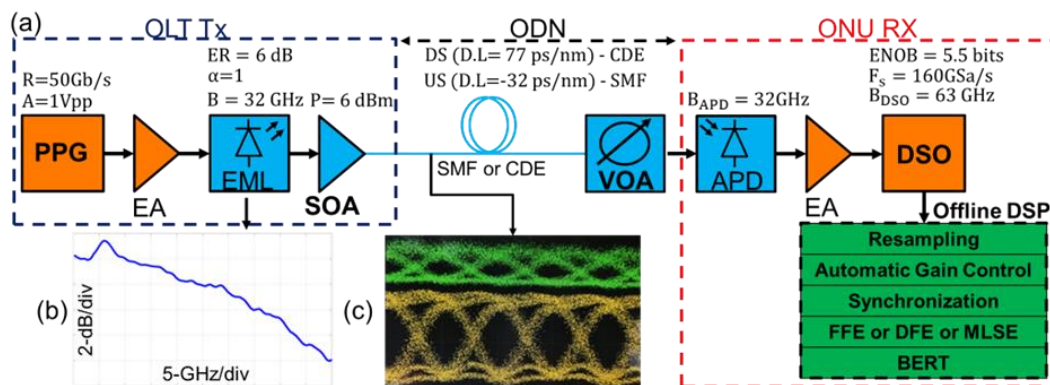


Figure 6.1: 50G-PON (a) Experimental setup of the 50 Gbit/s HS-PON link, (b) S21 of the EML, and (c) eye diagrams at the PPG (yellow color) and SOA (green color) outputs.

A pulse pattern generator (PPG) generates pseudo-random bit sequences (PRBS) of length $2^{15} - 1$ with amplitude $A \sim 1\text{Vpp}$. The signal is amplified by a 55GHz SHF-S807C electrical amplifier (EA) that drives a 56 Gbit/s electro-absorption modulated laser (EML) with 3dB bandwidth $B \sim 32\text{GHz}$ (as shown in Fig. 1b) centered at $\lambda = 1290\text{ nm}$. The EML employs an Indium Phosphide electro-absorption modulator (EAM) that is characterized by a chirp $\alpha \sim 1$ [101]. The optical signal at the EML output is amplified by a Semiconductor Optical Amplifier (SOA) (eye diagram shown in Fig. 1c) in green color) that delivers a power of $\sim 6\text{dBm}$ (corresponding to an optical signal-to-noise ratio higher than $\sim 40\text{dB}$ in 0.1nm) to the 20km link of standard single mode fiber (SMF) with 7dB losses at $\sim 1.3\mu\text{m}$. To mimic the downstream chromatic dispersion at 20km of fiber, a Chromatic Dispersion Emulator (CDE) was used. The cumulated CD was characterized through a network analyzer. The cumulated CD of the 20km link is $D.L = 77\text{ps/nm}$, this configuration is entitled DS. To emulate the cumulated 50G-PON chromatic dispersion in upstream condition, 20 km of SMF fiber (G.652) replaced the CDE, the measured cumulated CD was $D.L = -32\text{ ps/nm}$, this configuration is entitled US.

Afterward, the signal is attenuated by a variable optical attenuator (VOA) which emulates the ODN losses and allows us to plot the bit-error-ratio (BER) versus received optical power (ROP) sensitivity curves. The 50 Gbit/s waveform is finally detected by a SiFotonics Germanium-on-Silicon avalanche photodiode (APD) with 3dB bandwidth $B_{\text{APD}} \sim 32\text{ GHz}$ whose differential outputs are linearly amplified by a 35GHz SHF-D837C RF driver and sampled by a digital storage oscilloscope (DSO) with a vertical resolution (i.e., effective number of bits) $\text{ENOB} \sim 5.5\text{bits}$, sampling frequency $F_s = 160\text{GSa/s}$, and bandwidth $B_{\text{DSO}} = 63\text{GHz}$. Offline digital signal processing (DSP) is performed with MatlabTM at the end of the chain through the following algorithms: (i) resampling, (ii) automatic gain control, (iii) synchronization, (iv) digital equalization and (v) BER testing (BERT). The resampling allows for the use of the fractionally spaced receivers operating at twice the symbol rate. To train the DSP receivers, $N_{tr} = 638 \times 10^3$ symbols were used, i.e., for the training phase of LMS-LE and LMS-DFE, and to obtain the histograms used the branch metrics computation of the MLSE-GEN. Afterward, the tracking phase used $N_{DD} = 10^6$ symbols to evaluate the receivers.

6.3 Receivers optimization methodology

The intersymbol interference of the 50 Gbit/s channel is compensated by one of the above-mentioned digital equalizers: To ensure the highest performance for the DSP-based receivers, we optimized the feedforward taps (N_F), feedback taps (N_B), the number of states (N), the restitution delay Δ , and the number of training symbols (N_{tr}). The adopted approach is almost the same as in chapters 3,4 and 5. The difference is that the delay was optimized over each ROP with the LMS-LE and LMS-DFE, hence $\Delta = \Delta_{opt}$, where the optimal delay is within the range $0 \leq \Delta_{opt} \leq N_F$. With the MLSE-GEN, optimizing the Δ for each ROP was not necessary.

6.4 Experimental and simulated performance of the DSP-based receivers over the 50G-PON channel in downstream condition

This section shows the experimental performance of the $T/2$ fractionally spaced receivers in downstream conditions. We implement the previously presented LMS-LE, LMS-DFE, and MLSE on real data emulated by the experimental setup presented in the previous section.

6.4.1 LMS-LE experimental performance over the 50G-PON DS channel

Figure 6.2 shows the system performance without equalization and with the LMS-LE. Without equalization, the receiver does not perform well enough to achieve the FEC threshold ($BER = 10^{-2}$) in any measured received optical power. This result agrees with the EML-based channel simulation results in section 2.6. The LMS-LE copes well with the 20km cumulated chromatic dispersion and the limited bandwidth of the EML and APD. With $N_F = 4$ taps, it achieves a low-complexity performance with sensitivity $S = -19.5$ dBm. With $N_F = 8$ taps, the overall performance of the receiver is enhanced, especially in the range of received power $-14.5 \leq ROP \leq 20.5$ dBm, therefore important ISI is mitigated. With $N_F = 8$ taps, it achieves the good balance performance with the sensitivity of $S = -21$ dBm.

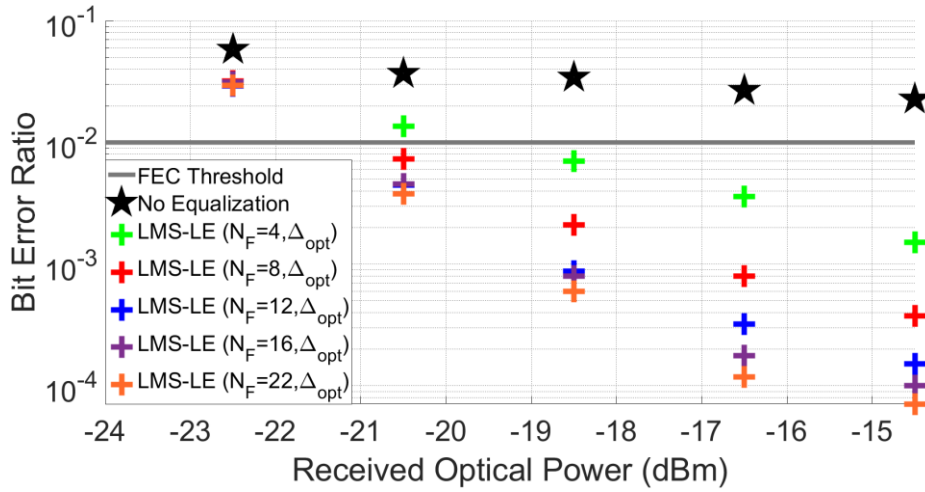


Figure 6.2: measured BER vs ROP over the 50G-PON setup at the output of the LMS-LE.

When more than twelve taps are used the LMS-LE performance is slightly improved. Figure 6.3 displays the impulse response of the LMS-LE with $N_F = 48$ taps and $\Delta = 12$.

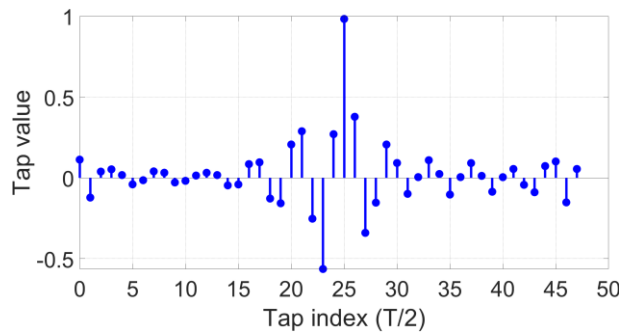


Figure 6.3: measured impulse response of the LMS-LE over the 50G-PON setup in DS configuration.

As observed in the BER vs ROP results, at least $N_F = 12$ taps (from tap index 16 to 28) are necessary to optimally compensate for channel ISI. The other taps outside this range concentrate small energy. Thus, they provide a minor performance gain.

6.4.1.1 Simulated vs experimental performance with the LMS-LE

We compare the experimental and the simulated performance of the LMS-LE in figure 6.4.

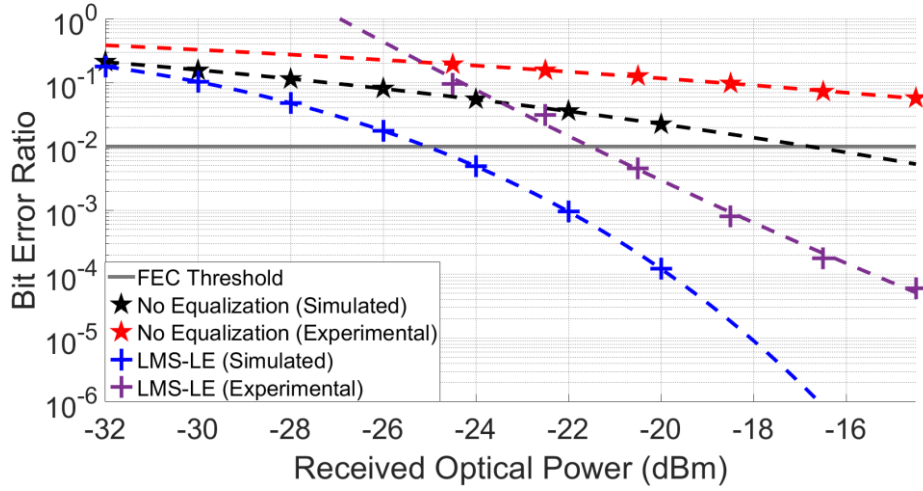


Figure 6.4: BER vs ROP of the LMS-LE with $N_F = 16$ taps in experimental and simulation.

The LMS-LE improves the receiver sensitivity by at least 8 dB in both simulation and experiments. The LMS-LE significantly enhances the overall performance with 16 taps in both cases. However, we see a difference of at least 12 dB between simulation and experiment without equalization. To better understand this behavior, we compared the simulated and experimental signal-to-noise ratio (SNR), as depicted in figure 6.5.

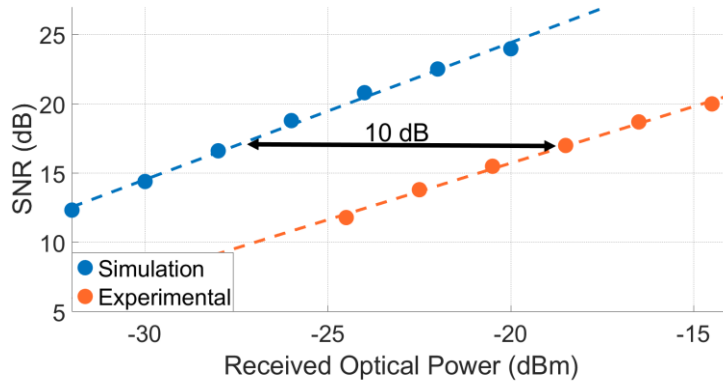


Figure 6.5: The measured and simulated SNR obtained through least mean square estimation at each received optical power.

We obtained a gap of 10 dB between experiments and simulations. Furthermore, the experiment has more devices than the simulations: the electrical drivers and the SOA, which add distortions to the received signal. Hence, a 2dB additional loss is observed in the practical implementation.

6.4.2 LMS-DFE experimental performance over the 50G-PON DS channel

Figure 6.6 shows the LMS-DFE performance over the 50G-PON DS channel

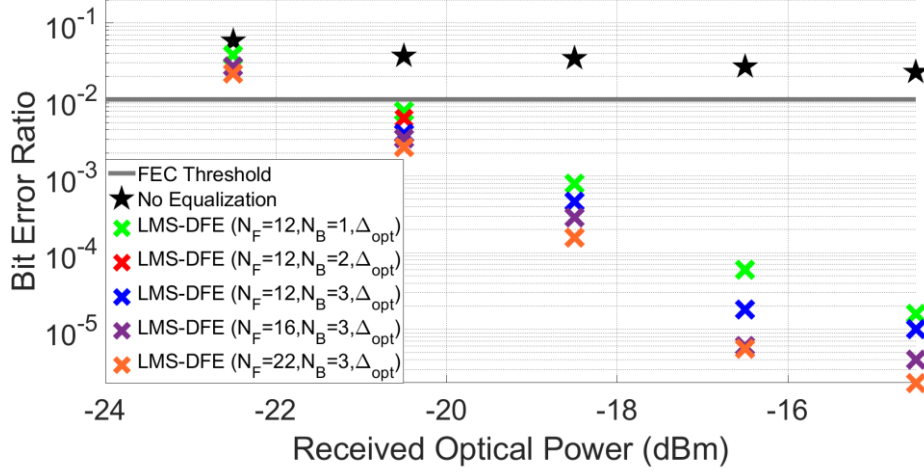


Figure 6.6: measured BER vs ROP over the 50G-PON setup at the output of the LMS-DFE.

The LMS-DFE compensates well for the channel distortions without critical error propagation, even at lower ROP. The better performances are over $ROP \geq -19.5$ dBm. For lower ROP, the performance of the DFE for all sets of taps tends to be the same value. With $N_{DFE} = (N_F = 16, N_B = 3)$ the DFE reaches the best performance with sensitivity $S = -21.5$ dBm. The good balance is obtained with $N_{DFE} = (N_F = 12, N_B = 3)$, with less feedback taps the performance is kept, hence the low-complexity performance is achieved with $N_{DFE} = (N_F = 12, N_B = 2)$, where $S = -21$ dBm.

Figure 6.7 indicates the LMS-DFE impulse response in the feedforward and feedback sections.

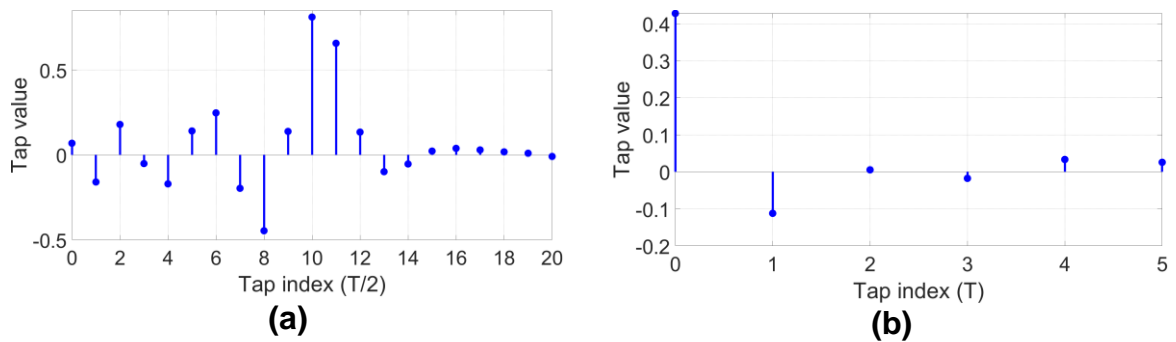


Figure 6.7: LMS-DFE impulse response (a) feedforward filter (b) feedback filter.

As expected, the FF section concentrates the energy in the first $N_F = 16$ taps. According to the BER vs ROP results, the first two taps of the FB section carry most of the energy, which is why we could reduce the number of FB taps from $N_B = 3$ to $N_B = 1$ without high equalization performance penalty.

6.4.2.1 Simulated EML + 50G Rx vs Experimental performance with the LMS-DFE

Comparing the LMS-DFE performance in the simulated (setup EML + 50G Rx) and experimental implementation of figure 6.8 we observe that the LMS-DFE is more penalized in the experimentation. It is natural because the DFE suffers from error propagation (even if it is not critical) in low SNR conditions since it uses the decisions at the output of the feedforward filter to compensate for distortion, as discussed in section 4.2.

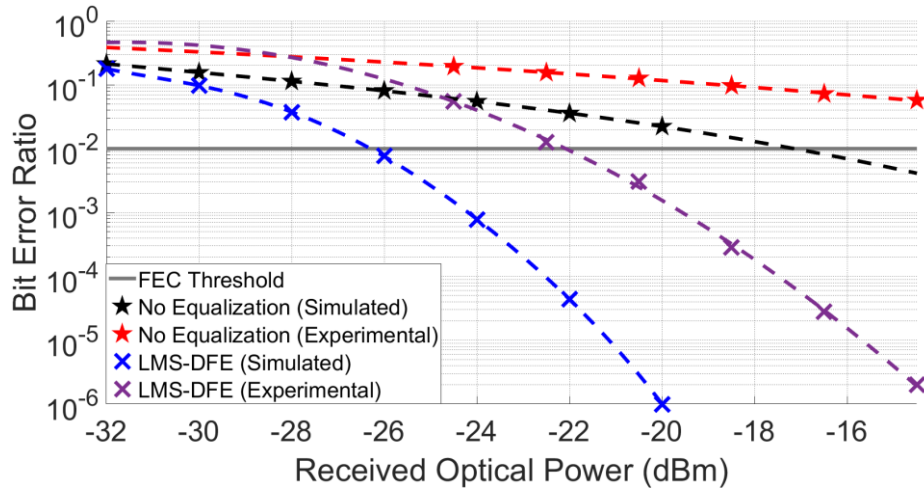


Figure 6.8: BER vs ROP of the LMS-DFE with $N_{DFE} = (N_F = 16, N_B = 3)$ taps in experimental and simulation environment.

6.4.3 MLSE experimental performance over the 50G-PON DS channel

Figure 6.9 shows the performance of the MLSE-GEN and the MLSE-LIN.

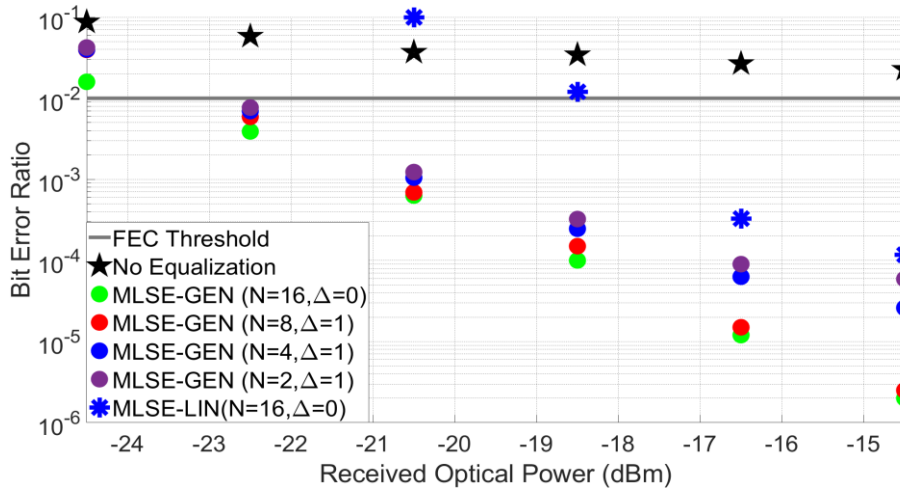


Figure 6.9: measured BER vs ROP over the 50G-PON setup at the output of the MLSE-GEN and the MLSE-LIN with $N = 16$ states.

The MLSE-LIN is not suitable for this experimental setup, as illustrated in the obtained performance from figure 6.9. With $N = 16$ states, it improves the receiver sensitivity,

but the performance is very penalized when compared to the MLSE-GEN. We conclude that the linear Gaussian channel model does not hold in the present case.

The MLSE-GEN makes no such assumption. It improves well the receiver sensitivity without requiring too many states. With $N = 2$ states, it almost achieves $S = -23$ dBm sensitivity and a BER floor of $5 \cdot 10^{-4}$. This is a remarkable performance for a 2-state-only MLSE receiver,. With $N = 4$ states, it performs slightly better. Otherwise, the MLSE-GEN further improves the overall performance with $N = 8$ or $N = 16$ states even at lower SNR. Therefore the MLSE-GEN deals better with the channel constraints with $N = 16$ states, thus obtaining the required sensitivity $S = -24$ dBm by ITU-T without a BER floor in the range $10^{-6} \leq BER \leq 10^{-1}$.

6.4.3.1 Simulated vs Experimental performance with the MLSE-GEN

Now, we compare the best-effort performance of the MLSE-GEN in figure 6.10.

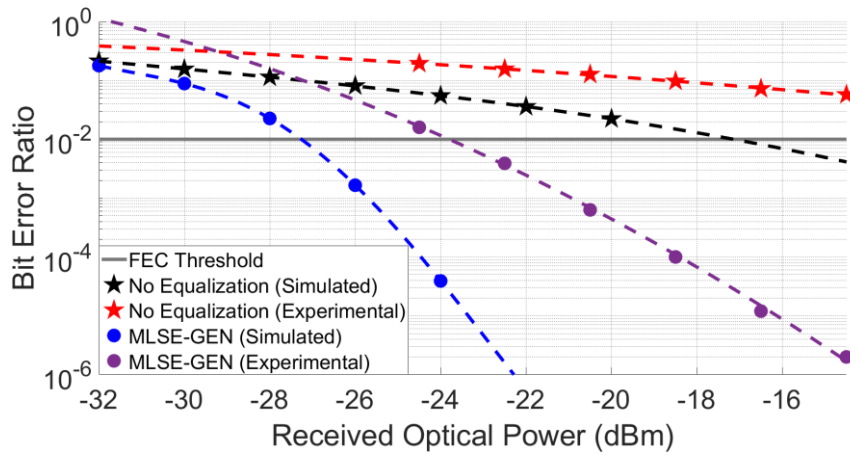


Figure 6.10: BER vs ROP with MLSE-GEN with $N_F = 16$ states in simulation and experiment.

As in the previous cases, the simulated MLSE performance is more optimistic than the measurements because the experimental channel suffers more distortion and the SNR gap of simulation and measurement. Nevertheless, in both cases, the MLSE-GEN dramatically improves the performance. Both achieve the required ITU-T performance levels.

6.4.4 Experimental performance comparison of the MMSE equalizers and MLSE based receivers

Finally, figure 6.11 compares the LMS-LE, the LMS-DFE, and MLSE-GEN with best-effort parameters.

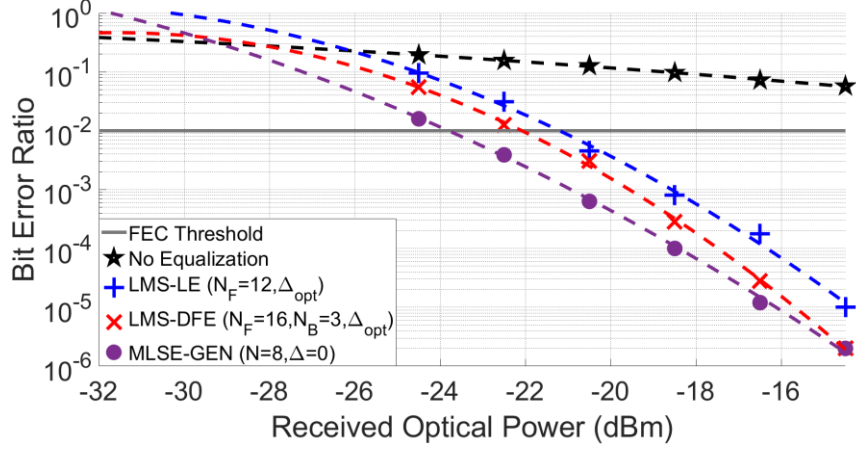


Figure 6.11: BER vs ROP performances of the MMSE and MLSE-based receivers.

All equalizers compensate well for the channel distortions, despite the aggravated noise. The MLSE-GEN has the best performance. It achieves the ITU-T requirements of sensitivity and optical budget, since it is more robust to the channel impairments, as verified in [55]. The improvement of the LMS-LE and LMS-DFE is important, but the SNR breaks down the performance of the MMSE equalizers, especially the DFE, due to decision errors, as mentioned in section 6.4.2. Based on the simulations, the DFE had a great advantage over the LMS-LE. Still, when the noise is increased the DFE performance is more penalized. Since the transmitter power is $P_{Tx} = 6 \text{ dBm}$, the LMS-DFE reaches the required optical budget of 29 dB (N1).

6.4.5 Transient analysis of the MMSE and MLSE-based receivers

Here, we compare the number of symbols required to train the receivers, as shown in figure 6.12. The LMS-LE achieves steady-state after 7.5×10^5 iterations, hence it requires $T_{LP} = 7.5 \times 10^5 \times 20 \text{ ps} = 15 \mu\text{s}$, which is not negligible with respect to the ONU frame of 125 μs .

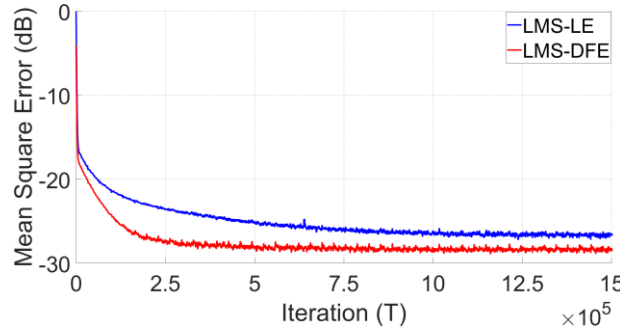


Figure 6.12: MSE vs iteration over the 50G-PON setup at the output of the LMS-LE and LMS-DFE in best-effort condition with $ROP = -20.5 \text{ dBm}$.

The LMS-DFE requires less time. It needs 250.000 symbols to converge, hence $T_{LP} = 5 \mu\text{s}$, at the end of the tracking phase, the measured BER of the LMS-LE is $BER = 0.005$, and for the LMS-DFE, the BER is $BER = 0.003$.

We also looked at the number of symbols necessary to obtain accurate histograms for PDF estimation of the MLSE-GEN. With that objective, we measured

the BER after getting the histograms with $N_{tr} = [50, 100, 150, 200, 250]$ kbits, as illustrated in figure 6.13.

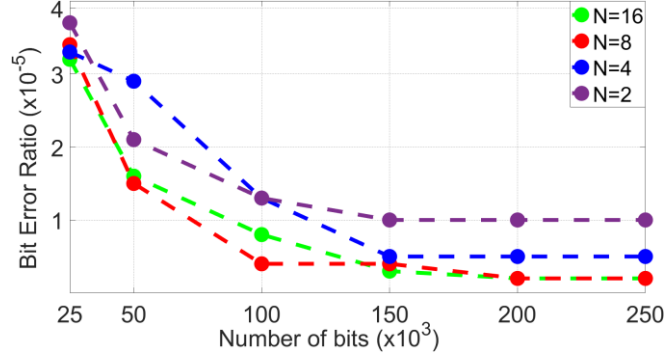


Figure 6.13: MLSE-GEN performance after obtaining the histogram with a limited number of symbols.

As the number of states increases, the number of training symbols increases, especially when the number of states is increased from $N = 8$ to $N = 16$. With the former configuration $N_{tr} = 150$ kbits are necessary, but with $N = 2$, $N = 4$ or $N = 8$ no more than $N_{tr} = 100$ kbits are necessary. Consequently, no more than $T_{LP} = 3 \mu s$ is necessary to train the MLSE-GEN.

6.4.6 Comparison of small-signal and measured frequency response

Figure 6.14 shows the frequency and impulse response of the optical channel. The channel impulse response was estimated through the least mean square method (see Appendix D for more details). Then, we adjusted the parameters of the IM/DD frequency response model proposed in chapter 2.

We see in figure 6.14 a) that the IM/DD model is sufficiently accurate to model the linear impact of the EML-based channel. Both the experimental and the theoretical curves show similar behavior for the frequency response. The small-signal IM/DD model expects more frequency selectivity, but the overall distortion has an excellent agreement.

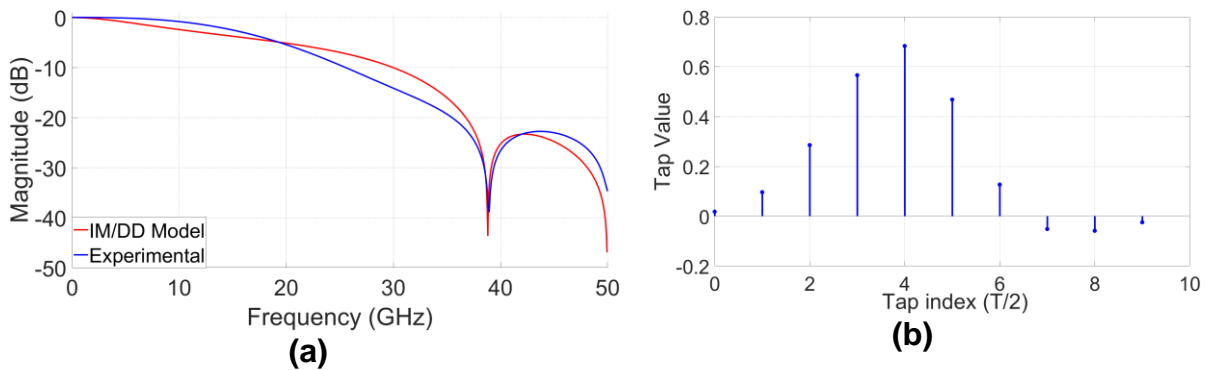


Figure 6.14: The 50G-PON channel (a) frequency response and (b) impulse response

Therefore, the IM/DD model based on the small-signal regime suits the 50 Gbit/s-based PON channel well in the presence of an externally modulated laser. This result supports the applicability of the small-signal model proposed in [50].

Figure 6.14 b) shows the estimated impulse response of the channel. We see that the energy is concentrated in the first eight $T/2$ spaced taps, with the most important in taps 3 to 6. The channel spans at least three symbols intervals $3T = 60$ ps. In the MLSE context, this is relevant. This shows why $\leq N = 2^3 = 8$ states are sufficient to achieve best-effort performance, and two states only still perform well despite the channel impulse response truncation.

6.5 Experimental performance of MLSE and MMSE receivers over the 50G-PON channel in upstream conditions

As mentioned in section 6.2, we evaluated the channel performance in the conditions of upstream chromatic dispersion (D.L = -32 ps/nm) at 50 Gbit/s and in back-to-back configuration. The results are shown in Figure 6.15.

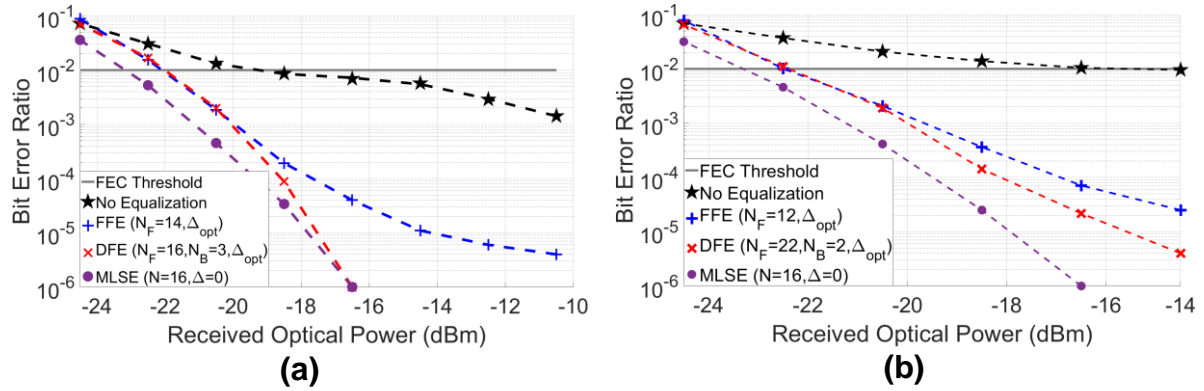


Figure 6.15: Best-effort performance of the LMS-LE, LMS-DFE, and MLSE-GEN in (a) Back-to-back and (b) upstream configuration.

In both cases, the receivers significantly improve the receiver sensitivity. In the back-to-back, without equalization, they achieve the sensitivity of $S = -18$ dBm, and the US reaches $S = -16$ dBm. The MLSE-GEN is the most recommended receiver for attaining the target ITU-T optical budget. It outperforms the MMSE equalizers, especially because the noise is high here. Still, comparing the DFE and LE, the latter has better performance because it is more robust to noise. For instance, when $ROP < -20$ dBm, in both setups, the SNR is too low for the DFE, i.e., due to noise, the decisions at the output of the FF filter are wrong, limiting the DFE performance. Thus, the DFE cannot improve the channel more than the LE. Otherwise, for $ROP \geq -17.5$ dBm, the advantage of the DFE over the LE increases with the evolution of the ROP (consequently the SNR).

6.6 Concluding remarks

This chapter compared the IM/DD simulation to experimental measurements in a 50Gbit/s setup with the EML as optical emitter. We validated that the frequency selectivity due to the chirp, chromatic dispersion and bandwidth limitation expected in the small signal model is also present in experimental implementations.

Also, the improvement of performance through DSP-based receivers were demonstrated. Compared to the configuration without any digital equalization, we showed that the LE, DFE, and MLSE are efficient to cope with the limited bandwidth of electro-optical components and with the interplay between CD and transmitter chirp, in back-to-back, downstream, and upstream conditions

Furthermore, we saw that 1) The simulated performances have a good SNR, so the equalizers and the MLSE can achieve very good sensitivities. Still, in practice, the noise can severely impact the performance of the DSP-based receiver. Without enough SNR, the LE may be the most preferred choice if the noise predominates the ISI, and the equalizers may not achieve the ITU-T requirements, even if the MLSE is more robust to noise. In low distortion scenarios, as in the upstream and back-to-back cases, the LE reached the same sensitivity as the DFE. However, when the ISI was severe, as in the downstream configuration, the DFE could still improve the receiver performance with the at expense of more taps. 2) The IM/DD model based on the small-signal regime is sufficiently accurate to model the linear distortions of an experimental 50G-PON channel based on EML. Consequently, the SNR of the the optical channel impacts a lot the performance of the equalizers and is essential to reach or not the ITU-T HS-PON recommendations. Note that other physical parameters of the 50G PON channel are also important to reach or not the ITU-T requirements, such as the extinction ratio of the transmitter or the intrinsic performance of the APD itself. 3) We have demonstrated the interest of using MLSE detection as an alternative to filter-based equalization techniques in 50G-PON. Even though its computational complexity is higher than that of FFE and DFE, the MLSE implemented here has further improved the receiver sensitivity in both DS and US directions. It allowed a 29dB N1 budget class. The MLSE could be even more attractive if it was combined with a directly modulated laser whose chirp stresses more the 50 Gbit/s channel than an EML, but this remains to be confirmed by further work.

7 Conclusions

We were motivated to show that digital distortion compensation is a key enabling technology for the next generation of passive optical networks.

The leap from 10Gbit/s to 50Gbit/s of PON must happen since the expected data rate demand is vast, and the deployed infrastructure today cannot ensure high-speed transmissions. As discussed in chapter 1, the telecom operators aim to improve the PON system in an organized way through standards and, most of all, with low costs by profiting from the existing infrastructure.

This work started simultaneously as the HS-PON recommendations were being consented. But it was already clear that the use of digital signal processing was required to ensure the expected sensitivity of $S = -24$ dBm with a target bit error ratio of 10^{-2} , thanks to the low-density parity-check coding technique. Furthermore, equalization is essential to compensate for the IM/DD channel impairments and allow the 50G transmission system to reach performance below the FEC threshold.

The central idea here was a PON structure with DSP capability in the end-user side. We focused in Chapter 2 on an ONU architecture with integrated ADC and DSP, the two main optical emitters in the OLT, with EML and DML, and an optimistic and an APD with limited bandwidth. We observed that the phenomena caused by chirp, CD, and bandwidth limitation are limiting for PON at 50G, mainly sensitivity and expected optical budget. Hence, the channel performance needs to be improved, mainly when EML is used, because CD and chirp are the predominant effects. With DML the CD and the chirp are less critical, thanks to the adiabatic chirp. In this case, the main limitation is the receiver bandwidth. Next, receivers with DSP have been investigated to compensate for these distortions.

The MMSE-LE results showed that the channel has enough linear distortion to be compensated, either with EML or DML. The fractional receiver at T/2 with LE was able to reach the performances required by the ITU-T. Also, through the closed-form equations it is possible to predict the channel performance with a margin of error of 1 dB of prediction error, which is another sign that the channel is linear. At least 4 taps are necessary to predict the channel performance well over the EML channel. The LMS-LE required no more than 16 taps to achieve good performances, despite the severe ISI. In DML-based simulations, the LMS-LE only improved the channel with the 25G APD, hence the LE compensates bandwidth limitation well enough.

The MMSE-DFE was the most cost-effective equalizer studied in the thesis. It was able to compensate for the severe ISI due to spectral nulls in simulation. But as we saw in the experimental demonstration, the DFE suffers from error propagation due to incorrect post decisions when the SNR is not high enough. Otherwise, in the DML simulation the DFE handled well the channel the bandwidth limitation. But his efficacy was lower because this channel is less aggressive in terms of ISI. However, with both simulated emitters the DFE reached lower sensitivities than the MMSE-LE with fewer taps, only 2 taps in FF section and a single tap in FB could reach ITU-T expected performances something that is of great importance to reduce the complexity of PON implementation. The predicted performance with the DFE by the closed-form equations was similar to the simulated performance with a margin of error of 1 to 2 dB.

The MLSE-based receiver achieved the best overall performance. With only two states, the generalized version dealt with nonlinear distortions, mainly seen with the

DML due to adiabatic chirp, which was transparent to the FFE and DFE. The nonlinear distortion compensation capability of the MLSE was seen in the setup with DML followed by the 37.5 GHz bandwidth receiver. In this scenario, the worse effect was the nonlinear distortion of the DML. The MLSE improved the receiver performance by 1 dB, something neither the LE nor the DFE could accomplish. With the EML the MLSE could deal well with ISI distortions, the linear version could also achieve efficient performances. We have seen that MLSE models the channel well with only 4 states, but the linear version is limited, so MLSE-GEN is the most recommended option for dealing with all limitations of the PON channel.

All DSP-capable receivers deliver the expected ITU-T physical media dependent performance for HS-PON. In a general analysis, respectively, all the different receivers added sensitivity gains and reached the highest optical budgets expected by ITU-T with a few number of taps or states, in other words No more than 12 taps at $T/2$ are needed for LE, and fewer than 8 for DFE, either with EML or DML. We can summarize that the overall performance was $S_{MLSE} > S_{DFE} - 1dB > S_{FFE} - 1dB$. In all scenarios, a few tens of kilobits, hence a few μs are needed to train the receivers, something that is not critical considering the time of an ONU frame.

The objective of this work was to show the performance gains of digital equalization to the future passive optical networks at the rate of 50Gbit/s. Thanks to the LE, DFE, and MLSE a 50G HS-PON achieves the sensitivity and optical budget recommended by the recently consented ITU-T PMD requirements. The main contribution of this work was to show that receivers with equalization or maximum likelihood detection can effectively deal with the distortions of the 50G-PON IM/DD channel. Thanks to these devices, we see that future DSP-based PON are able to achieve ITU-T recommendations in downstream transmission scenarios under the worst conditions of chromatic dispersion, chirp, and bandwidth limitation, considering the available transceivers to be deployed in the 50G-PON infrastructure. This work focused on the downlink direction while the ITU-T consented to the 50G-PON downstream recommendations. Nowadays, research and standardization works consider the operation of HS-PON in 50G upstream. Otherwise, the research of 100Gbit/s PON has already started.

Future perspectives

The evaluation presented in the thesis is based on a low-cost PON IM/DD. Digital signal processing and higher transmission bandwidths are needed to address power budget and sensitivity requirements. For the future PON on a single wavelength, with rates beyond 100Gbit/s, the IM/DD technology also starts to suffer from the bottleneck, the severe frequency distortion due to high cumulated CD and direct detection causes severe ISI hence the use of coherent detection techniques is one of the most logical paths to be followed in future optical access networks.

Otherwise, the use of pulse amplitude modulation with 4 levels (PAM-4) combined with optical transceivers of higher extinction ratio may increase the line rate throughput.

Furthermore, Machine Learning (ML) is a powerful technology to compensate the nonlinearities. With enough DSP capabilities on the PON infrastructure, it would be a good choice, especially when the channel nonlinearities are high.

Finally, the use of DSP for upstream transmission should be further investigated to profit from the potential of the DSP-enabled PON in the two senses of the OLT to ONU communication.

Appendix A

The statistics of the generated symbols

The emitted symbols consider the physical characteristics of the optical emitter. They are based on the extinction ratio ER and the energy of the emitted symbols E_x , hence the emitted symbols have a binary dictionary $x_n \in \{a_0, a_1\}$. Consequently, a generated symbol is a function $x_n = f(ER, E_s)$. To calculate the symbol values, the energy of the emitted symbols is the same as the NRZ-OOK alphabet.

$$E_x = \mathbb{E}\{|x_n|^2\} = 0.5$$

The range of values of the generated symbols are shown in Figure A.1.

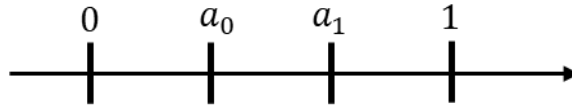


Figure A.1: The emitter constellation.

The extinction ratio directly defines the Euclidean distance between the symbol associated with level low level a_0 and the symbol associated with high level a_1 . The generated symbols are given by:

$$\begin{cases} E_s = \frac{1}{2}(a_0^2 + a_1^2) \\ ER = \frac{a_1^2}{a_0^2} \\ ER_{dB} = 10 \log_{10}(ER) \end{cases}$$

or

$$x_n = \begin{cases} a_0^2 = \frac{2E_s}{(1 + 10^{\frac{2ER}{10}})} \\ a_1^2 = 2E_s - a_0^2 \end{cases}$$

The receiver recreated the reference symbols for the bit error ratio computation, also the training of the LMS-based equalizers.

Appendix B

Automatic gain control

The automatic gain control controlled the amplitude of the received discrete waveform at the channel output to be at the level of the quantizer present in the receiver. Figure B.1 shows the simplified scheme of the AGC-based channel:

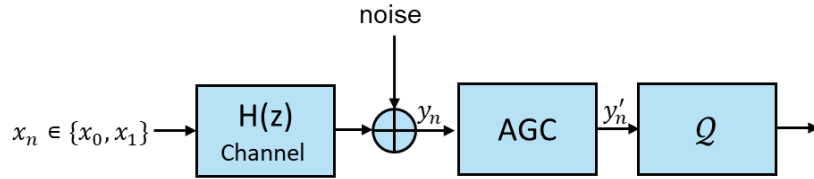


Figure B.1: The diagram of the automatic gain control based receiver.

The symbol Q represents the quantization device. The energy of the received waveform y_n is represented by E_y . The AGC scaled the received waveform y_n using the energy of the NRZ-OOK transmitted symbols $E_x = 0.5$ as reference. Basically, y_n is multiplied by a factor α

$$\alpha = \sqrt{\frac{E_x}{E_y}}$$

to guarantee that the AGC output

$$y'_n = \alpha y_n$$

the target energy $E_{tgt} = 0.5$. Furthermore, this process facilitated the use of the least mean square based equalizers since the emitted and received waveforms had the same energy.

Appendix C

Mid riser quantization

The mid-rise quantization was used to simulate analog-to-digital conversion. This approach was inspired by [39], [102] . The uniform quantization had a fixed dynamic range x_q with clipping value V based on a low V_L and high amplitude value V_H .

$$V = V_H - V_L$$

The quantizer presented the quantization resolution B , hence 2^B symmetric quantization levels with quantization step

$$q = \frac{V}{2^B}$$

with dynamic quantization range

$$x_q = Q(x) \in \left[V_L + \frac{q}{2}, V_H - \frac{q}{2} \right]$$

with each quantization level described by

$$q_n = V_L + \frac{q}{2} \times (2n + 1)$$

for $n = 0, 1, \dots, 2^B - 1$.

Furthermore, the bins of the generated histograms were equal to the quantization levels. This information was helpful in the training phase of the generalized version of the MLSE.

Appendix D

Least mean square estimation

The least mean square estimation was very useful for channel and noise estimation. It was based on section 6.3 of the book [64]. During the estimation, the N symbols of the transmitted $\mathbf{x} = [x_0, x_1, \dots, x_{N-1}]$ and received sequence $\mathbf{y} = [y_0, y_1, \dots, y_{N-1}]$ are known. The channel is modelled as:

$$\mathbf{y} = \mathbf{X}\hat{\mathbf{h}} + \mathbf{w}$$

the estimated impulse response of the channel is $\hat{\mathbf{h}} = [\hat{h}_0, \dots, \hat{h}_{L-1}]$, the transmitted symbols matrix is \mathbf{X} , and L is the assumed channel length. The matricial representation of the channel is

$$\begin{bmatrix} y_0 \\ y_1 \\ \vdots \\ y_N \end{bmatrix} = \begin{bmatrix} x_0 & 0 & \dots & \dots & 0 \\ x_1 & x_0 & \dots & \vdots & \vdots \\ \vdots & \vdots & \ddots & \vdots & \vdots \\ \vdots & \vdots & \dots & \ddots & \vdots \\ x_N & x_{N-1} & \dots & \dots & x_{N-L+1} \end{bmatrix} \hat{\mathbf{h}} + \begin{bmatrix} w_0 \\ w_1 \\ \vdots \\ w_N \end{bmatrix}$$

The estimated channel taps are given by

$$\hat{\mathbf{h}} = (\mathbf{X}^H \mathbf{X})^{-1} \mathbf{X}^H \mathbf{y}$$

the noise variance is

$$\hat{\sigma}_w^2 = \frac{1}{N+1} \|\mathbf{y} - \mathbf{X}\hat{\mathbf{h}}\|^2$$

where the operator $\|\cdot\|$ represents the Euclidean norm. The least mean square estimation was also helpful in 1) obtaining the signal-to-noise ratio, since the variance of the emitted symbols was known, 2) the theoretical predictions of the MMSE-based equalizers were based on the taps and SNR estimation, and 3) the estimation of the channel taps in the experimental demonstration.

Bibliography

- [1] ITU-T G.9804 Series of Recs, “Higher Speed Passive Optical Networks.” Nov. 22, 2019. Accessed: Jul. 11, 2022. [Online]. Available: <https://www.itu.int/rec/T-REC-G.9804.1-201911-l/en>
- [2] “History of the Internet,” *Wikipedia*. Nov. 10, 2022. Accessed: Nov. 24, 2022. [Online]. Available: https://en.wikipedia.org/w/index.php?title=History_of_the_Internet&oldid=1121166082#cite_note-35
- [3] N. S. Cisco, “Cisco Annual Internet Report (2018–2023) White Paper.” Accessed: Nov. 23, 2022. [Online]. Available: <https://www.cisco.com/c/en/us/solutions/collateral/executive-perspectives/annual-internet-report/white-paper-c11-741490.html>
- [4] S. E. Landero, I. F. de Jauregui Ruiz, A. Ferrari, D. L. Gac, Y. Frignac, and G. Charlet, “Link Power Optimization for S+C+L Multi-band WDM Coherent Transmission Systems,” in *2022 Optical Fiber Communications Conference and Exhibition (OFC)*, Mar. 2022, pp. 1–3.
- [5] S. Barthomeuf, “Augmentation de la capacité des interfaces PONs TDMA au-delà de 10Gbit/s dans les réseaux d’accès en fibres optiques,” 2019.
- [6] S. Gorshe, “A Tutorial on ITU-T G.709 Optical Transport Networks (OTN),” no. 1, p. 77.
- [7] Netflix, “Internet connection speed recommendations.” Accessed: Nov. 27, 2022. [Online]. Available: <https://help.netflix.com/en/node/306#:~:text=To%20watch%20Netflix%20in%20Full,set%20to%20Auto%20or%20High>
- [8] F. Senat, “Projet de loi de finances pour 2023 : Économie.” [Online]. Available: <http://www.senat.fr/rap/l22-115-312/l22-115-3126.html>
- [9] J. Prat, *Bext-Generation FTTH Passive Optical Networks Research Towards Unlimited Bandwidth Access*. Springer, 2008.
- [10] L. Xue, “Key Signal Processing Technologies for High-speed Passive Optical Networks,” Chalmers University of Technology, 2021.
- [11] J. S. Wey 魏君珊, “The Outlook for PON Standardization: A Tutorial,” *J. Light. Technol.*, vol. 38, no. 1, pp. 31–42, Jan. 2020, doi: 10.1109/JLT.2019.2950889.
- [12] P. Torres-Ferrera, F. Effenberger, M. S. Faruk, S. J. Savory, and R. Gaudino, “Overview of high-speed TDM-PON beyond 50 Gbps per wavelength using digital signal processing [Invited Tutorial],” *J. Opt. Commun. Netw.*, vol. 14, no. 12, pp. 982–996, Dec. 2022, doi: 10.1364/JOCN.468920.
- [13] V. Houtsma, D. van Veen, and E. Harstead, “Recent Progress on Standardization of Next-Generation 25, 50, and 100G EPON,” *J. Light. Technol.*, vol. 35, no. 6, pp. 1228–1234, Mar. 2017, doi: 10.1109/JLT.2016.2637825.
- [14] FSN, “Full Service Access Network.” [Online]. Available: <https://www.fsan.org/>

- [15] ITU-T, "ITU-T standards - progress and recent activities," 2020. Accessed: Nov. 28, 2022. [Online]. Available: https://www.itu.int/en/ITU-T/studygroups/2017-2020/15/Documents/OFC2018-2-Q2_v5.pdf
- [16] "G.983.1 : Broadband optical access systems based on Passive Optical Networks (PON)." <https://www.itu.int/rec/T-REC-G.983.1/en> (accessed Nov. 28, 2022).
- [17] IEEE Computer Society, "802.3ah." Accessed: Nov. 28, 2022. [Online]. Available: https://www.ieee802.org/21/doctree/2006_Meeting_Docs/2006-11_meeting_docs/802.3ah-2004.pdf
- [18] "IEEE Standards Association," *IEEE Standards Association*. <https://standards.ieee.org> (accessed Nov. 29, 2022).
- [19] "G.987.1 : 10-Gigabit-capable passive optical networks (XG-PON): General requirements." <https://www.itu.int/rec/T-REC-G.987.1-201603-l/en> (accessed Nov. 29, 2022).
- [20] "G.989 : 40-Gigabit-capable passive optical networks (NG-PON2): Definitions, abbreviations and acronyms." <https://www.itu.int/rec/T-REC-G.989/> (accessed Nov. 29, 2022).
- [21] "IEEE P802.3ca 100G-EPON Task Force." <https://www.ieee802.org/3/ca/> (accessed Nov. 30, 2022).
- [22] C. Hong *et al.*, "High Speed Ge/Si Avalanche Photodiode with High Sensitivity for 50Gbit/s and 100Gbit/s Optical Access Systems," in *2022 Optical Fiber Communications Conference and Exhibition (OFC)*, Mar. 2022, pp. 1–3.
- [23] J. Potet *et al.*, "Assessment of an SOA for Burst Mode Pre-Amplification in Higher Speed PON reaching 30dB of Optical Budget," in *2021 Optical Fiber Communications Conference and Exhibition (OFC)*, Jun. 2021, pp. 1–3.
- [24] A. Mahadevan, Y. Lefevre, E. Harstead, W. van Hoof, D. van Veen, and V. Houtsma, "Flexible Upstream FEC for Higher Throughput, Efficiency, and Robustness for 50G PON," in *2022 Optical Fiber Communications Conference and Exhibition (OFC)*, Mar. 2022, pp. 1–3.
- [25] R. Bonk *et al.*, "50G-PON: The First ITU-T Higher-Speed PON System," *IEEE Commun. Mag.*, vol. 60, no. 3, pp. 48–54, Mar. 2022, doi: 10.1109/MCOM.001.2100441.
- [26] N. Genay, F. Bougart, F. Nogueira Sampaio, and E. Pincemin, "50G-PON Standardisation: Orange's Contribution,"
- [27] D. Zhang, D. Liu, X. Wu, and D. Nessel, "Progress of ITU-T higher speed passive optical network (50G-PON) standardization," *J. Opt. Commun. Netw.*, vol. 12, no. 10, pp. D99–D108, Oct. 2020, doi: 10.1364/JOCN.391830.
- [28] N. H. Zhu *et al.*, "Directly Modulated Semiconductor Lasers," *IEEE J. Sel. Top. Quantum Electron.*, vol. 24, no. 1, pp. 1–19, Jan. 2018, doi: 10.1109/JSTQE.2017.2720959.
- [29] J. E. Bowers, "High speed semiconductor laser design and performance," *Solid-State Electron.*, vol. 30, no. 1, pp. 1–11, Jan. 1987, doi: 10.1016/0038-1101(87)90023-2.

- [30] L. Anet Neto *et al.*, "Simple Estimation of Fiber Dispersion and Laser Chirp Parameters Using the Downhill Simplex Fitting Algorithm," *J. Light. Technol.*, vol. 31, no. 2, pp. 334–342, Jan. 2013, doi: 10.1109/JLT.2012.2226704.
- [31] Y. Zhu *et al.*, "Comparative study of cost-effective coherent and direct detection schemes for 100 Gb/s/λ PON," *J. Opt. Commun. Netw.*, vol. 12, no. 9, pp. D36–D47, Sep. 2020, doi: 10.1364/JOCN.390911.
- [32] L. A. Neto, J. Maes, P. Larsson-Edefors, J. Nakagawa, K. Onohara, and S. J. Trowbridge, "Considerations on the Use of Digital Signal Processing in Future Optical Access Networks," *J. Light. Technol.*, vol. 38, no. 3, pp. 598–607, Feb. 2020, doi: 10.1109/JLT.2019.2946687.
- [33] M. Jha, R. Dhawan, R. Parihar, and A. Choudhary, "Frequency Response Tailoring of a Phase Modulated Link With Stimulated Brillouin Scattering," *IEEE Photonics Technol. Lett.*, vol. 34, no. 19, pp. 1054–1057, Oct. 2022, doi: 10.1109/LPT.2022.3199586.
- [34] "G.652 : Characteristics of a single-mode optical fibre and cable." <https://www.itu.int/rec/T-REC-G.652-201611-I/en> (accessed Dec. 04, 2022).
- [35] Giovind P. Agrawal, *Fiber-Optic Communication Systems*, Third Edition. in Wiley-Interscience. 2002.
- [36] J. Armstrong, B. J. C. Schmidt, D. Kalra, H. A. Suraweera, and A. J. Lowery, "SPC07-4: Performance of Asymmetrically Clipped Optical OFDM in AWGN for an Intensity Modulated Direct Detection System," in *IEEE Globecom 2006*, Nov. 2006, pp. 1–5. doi: 10.1109/GLOCOM.2006.571.
- [37] J. M. Kahn and J. R. Barry, "wireless infrared communications," *Proc. IEEE*, vol. 85, pp. 265–298, 1997.
- [38] Christophe Peucheret, "Direct Current Modulation of Semiconductor Lasers - Introduction to Optical Communications." Technical University of Denmark, Jul. 14, 2011.
- [39] D. G. Manolakis and V. K. Ingle, *Applied Digital Signal Processing*, Cambridge University Press. 2011.
- [40] K. Zhang, Q. Zhuge, H. Xin, W. Hu, and D. V. Plant, "Performance comparison of DML, EML and MZM in dispersion-unmanaged short reach transmissions with digital signal processing," *Opt. Express*, vol. 26, no. 26, pp. 34288–34304, Dec. 2018, doi: 10.1364/OE.26.034288.
- [41] Luiz Anet Neto, "Étude des potentialités des techniques de modulation multiporteuse pour les futurs réseaux d'accès optique wdm et tdm pon," Université de Limoges, Lannion, 2012.
- [42] G. Agrawal, *Nonlinear Fiber Optics*, Fourth Edition. Academic Press, 2006.
- [43] L. Bjerkan, A. Royset, L. Hafskjaer, and D. Myhre, "Measurement of laser parameters for simulation of high-speed fiberoptic systems," *J. Light. Technol.*, vol. 14, no. 5, pp. 839–850, May 1996, doi: 10.1109/50.495166.
- [44] J. Wang and K. Petermann, "Small signal analysis for dispersive optical fiber communication systems," *J. Light. Technol.*, vol. 10, no. 1, pp. 96–100, Jan. 1992, doi: 10.1109/50.108743.

- [45] Rongqing Hui and Maurice O' Sullivan, *Fiber Optic Measurement Techniques*, 1st ed. Elsevier Academic Press, 2008.
- [46] B. Li *et al.*, "DSP enabled next generation 50G TDM-PON," *J. Opt. Commun. Netw.*, vol. 12, no. 9, pp. D1–D8, Sep. 2020, doi: 10.1364/JOCN.391904.
- [47] W. R. Bennett, *Electrical Noise*. New York: McGraw-Hill, 1960.
- [48] D. K. C. MacDonald, *Noise and Fluctuations: An Introduction*. New York: Wiley, 1962.
- [49] F. N. H. Robinson, *Noise and Fluctuations in electronic Devices and Circuits*. Oxford: University press, 1974.
- [50] S. P. O'Duill, Y. Lin, P. Sheridan, and L. P. Barry, "Applicability of small-signal laser and fiber models for passive optical networks operating at the 1550 nm window," *Opt. Fiber Technol.*, vol. 56, p. 102203, May 2020, doi: 10.1016/j.yofte.2020.102203.
- [51] R. L. Bidan, "Turbo-Equalization for bandwidth-efficient digital communications over frequency-selective channels," Thesis, INSA de Rennes, 2003. Accessed: Jun. 23, 2022. [Online]. Available: <https://tel.archives-ouvertes.fr/tel-00110853>
- [52] R. M. Gray, "Toeplitz and Circulant Matrices: A review." 2021. Accessed: Nov. 20, 2022. [Online]. Available: <http://www-ee.stanford.edu/~gray/toeplitz.pdf>
- [53] S. H. Bae, H. Kim, and Y. C. Chung, "Transmission of 51.56-Gb/s OOK signal using 1.55- μ m directly modulated laser and duobinary electrical equalizer," *Opt. Express*, vol. 24, no. 20, pp. 22555–22562, Oct. 2016, doi: 10.1364/OE.24.022555.
- [54] B. G. Kim, S. Hyun Bae, and Y. C. Chung, "Requirement of DML's Chirp Parameters for RoF-based Mobile Fronthaul Networks," in *2018 23rd Opto-Electronics and Communications Conference (OECC)*, Jul. 2018, pp. 1–2. doi: 10.1109/OECC.2018.8729950.
- [55] W. Liang, H. Wang, J. Wei, J. Zhou, D. Guo, and W. Liu, "DSP-enabled 50G OOK-PON with beyond 29 dB power budget using O-band 10G DML and 10G APD," *Opt. Commun.*, vol. 504, p. 127486, Feb. 2022, doi: 10.1016/j.optcom.2021.127486.
- [56] F. A. N. Sampaio, E. Pincemin, N. Genay, L. A. Neto, R. Le Bidan, and Y. Jaouen, "An analysis of linear digital equalization in 50Gbit/s HS-PONs to compensate the combined effect of chirp and chromatic dispersion," in *2021 Conference on Lasers and Electro-Optics Europe & European Quantum Electronics Conference (CLEO/Europe-EQEC)*, Jun. 2021, pp. 1–1. doi: 10.1109/CLEO/Europe-EQEC52157.2021.9541738.
- [57] VPI Transmission Maker, "Laser Pulsed - VPI component maker, user's manual, photonic modules reference manuals." Accessed: 10 Jan. 2022. [Online]. Available: [http:// www.vpiphotonics.com](http://www.vpiphotonics.com).
- [58] VPI Transmission Maker, "Laser Rate Equation (Single Mode) - VPI component maker, user's manual, photonic modules reference manuals." Accessed: 10 Jan. 2022. [Online]. Available: <http:// www.vpiphotonics.com>.

- [59] VPI Transmission Maker, "Electroabsorption Modulator - VPI component maker, user's manual, photonic modules reference manuals." Accessed: 10 Jan. 2022. [Online]. Available: [http:// www.vpiphotonics.com](http://www.vpiphotonics.com).
- [60] P. Torres-Ferrera, F. Effenberger, M. S. Faruk, S. J. Savory, and R. Gaudino, "Overview of high-speed TDM-PON beyond 50 Gbps per wavelength using digital signal processing [Invited Tutorial]," *J. Opt. Commun. Netw.*, vol. 14, no. 12, p. 982, Dec. 2022, doi: 10.1364/JOCN.468920.
- [61] C. A. Belfiore and J. H. Park, "Decision feedback equalization," *Proc. IEEE*, vol. 67, no. 8, pp. 1143–1156, Aug. 1979, doi: 10.1109/PROC.1979.11409.
- [62] M. Aaron and D. Tufts, "Intersymbol interference and error probability," *IEEE Trans. Inf. Theory*, vol. 12, no. 1, pp. 26–34, Jan. 1966, doi: 10.1109/TIT.1966.1053842.
- [63] "G.9804.1 : Higher speed passive optical networks - Requirements." <https://www.itu.int/rec/T-REC-G.9804.1-201911-l/en> (accessed Jul. 11, 2022).
- [64] A. H. Sayed, *Adaptive Filters*. John Wiley & Sons, 2011.
- [65] P. Galko and S. Pasupathy, "Optimal linear receiver filters for binary digital signals," vol. 1, p. 1H.6, Jan. 1982.
- [66] C.-C. Yeh and J. R. Barry, "Adaptive minimum bit-error rate equalization for binary signaling," *IEEE Trans. Commun.*, vol. 48, no. 7, pp. 1226–1235, Jul. 2000, doi: 10.1109/26.855530.
- [67] J. Levendovszky, L. Kovacs, and E. C. van der Meulen, "Minimum Probability of Error-Based Equalization Algorithms for Fading Channels," *EURASIP J. Wirel. Commun. Netw.*, vol. 2007, no. 1, Art. no. 1, Dec. 2007, doi: 10.1155/2007/14683.
- [68] J. G. Proakis, *Digital Communications*. McGraw-Hill, 2008.
- [69] S. U. H. Qureshi, "Adaptive equalization," *Proc. IEEE*, vol. 73, no. 9, pp. 1349–1387, Sep. 1985, doi: 10.1109/PROC.1985.13298.
- [70] R. W. Lucky, "Automatic equalization for digital communication," *Bell Syst. Tech. J.*, vol. 44, no. 4, pp. 547–588, Apr. 1965, doi: 10.1002/j.1538-7305.1965.tb01678.x.
- [71] D. W. Tufts, "Nyquist's problem—The joint optimization of transmitter and receiver in pulse amplitude modulation," *Proc. IEEE*, vol. 53, no. 3, pp. 248–259, Mar. 1965, doi: 10.1109/PROC.1965.3682.
- [72] F. A. N. Sampaio, E. Pincemin, N. Genay, L. A. Neto, R. Le Bidan, and Y. Jaouen, "An analysis of linear digital equalization in 50Gbit/s HS-PONs to compensate the combined effect of chirp and chromatic dispersion," in *2021 Conference on Lasers and Electro-Optics Europe & European Quantum Electronics Conference (CLEO/Europe-EQEC)*, Jun. 2021, pp. 1–1. doi: 10.1109/CLEO/Europe-EQEC52157.2021.9541738.
- [73] J. M. Cioffi, "Chapter 3: Equalization," in *Digital Communication: Signal Processing*, Stanford University. Accessed: Jul. 07, 2022. [Online]. Available: <https://cioffi-group.stanford.edu/doc/book/chap3.pdf>
- [74] R. D. Gitlin and S. B. Weinstein, "Fractionally-spaced equalization: An improved digital transversal equalizer," *Bell Syst. Tech. J.*, vol. 60, no. 2, pp. 275–296, Feb. 1981, doi: 10.1002/j.1538-7305.1981.tb00240.x.

- [75] N. Al-Dhahir and J. M. Cioffi, "Efficient computation of the delay-optimized finite length MMSE-DFE," *IEEE Trans. Signal Process.*, vol. 44, no. 5, pp. 1288–1292, May 1996, doi: 10.1109/78.502344.
- [76] Raphaël Le Bidan, "Notes on MMSE linear and decision-feedback equalizers for OOK," Dept MEE,IMT Atlantique, Bretagne-Pays de la Loire École Mines Télécom, Dept MEE,IMT Atlantique, Bretagne-Pays de la Loire École Mines Télécom, Oct. 2021.
- [77] B. Widrow, J. M. McCool, M. G. Larimore, and C. R. Johnson, "Stationary and nonstationary learning characteristics of the LMS adaptive filter," *Proc. IEEE*, vol. 64, no. 8, pp. 1151–1162, Aug. 1976, doi: 10.1109/PROC.1976.10286.
- [78] "Statistical Theory of Signal Detection - 2nd Edition." <https://www.elsevier.com/books/statistical-theory-of-signal-detection/helstrom/978-0-08-013265-5> (accessed Aug. 20, 2022).
- [79] G. Ungerboeck, "Fractional Tap-Spacing Equalizer and Consequences for Clock Recovery in Data Modems," *IEEE Trans. Commun.*, vol. 24, no. 8, pp. 856–864, Aug. 1976, doi: 10.1109/TCOM.1976.1093381.
- [80] R. Chang and J. Hancock, "On receiver structures for channels having memory," *IEEE Trans. Inf. Theory*, vol. 12, no. 4, pp. 463–468, Oct. 1966, doi: 10.1109/TIT.1966.1053923.
- [81] K. Abend and B. D. Fritchman, "Statistical detection for communication channels with intersymbol interference," *Proc. IEEE*, vol. 58, no. 5, pp. 779–785, May 1970, doi: 10.1109/PROC.1970.7732.
- [82] S. Qureshi and E. Newhall, "Adaptive receiver for data transmission over time-dispersive channels," *IEEE Trans. Inf. Theory*, vol. 19, no. 4, pp. 448–457, Jul. 1973, doi: 10.1109/TIT.1973.1055046.
- [83] M. Austin, "Decision-feedback equalization for digital communication over dispersive channels.," *undefined*, 1967, Accessed: Aug. 08, 2022. [Online]. Available: <https://www.semanticscholar.org/paper/Decision-feedback-equalization-for-digital-over-Austin/50cb8faaef3c898e0952a4cbe7af1e2a3e389eaf>
- [84] P. Monsen, "Feedback equalization for fading dispersive channels," *IEEE Trans. Inf. Theory*, vol. 17, no. 1, pp. 56–64, Jan. 1971, doi: 10.1109/TIT.1971.1054575.
- [85] P. S. Bednarz and J. M. Cioffi, "Decision feedback equalization for channels with error correcting capabilities," in *Proceedings of ICC'97 - International Conference on Communications*, Jun. 1997, pp. 1607–1612 vol.3. doi: 10.1109/ICC.1997.595059.
- [86] J. E. Smee and N. C. Beaulieu, "Error-rate evaluation of linear equalization and decision feedback equalization with error propagation," *IEEE Trans. Commun.*, vol. 46, no. 5, pp. 656–665, May 1998, doi: 10.1109/26.668737.
- [87] S. A. Altekhar and N. C. Beaulieu, "Upper bounds to the error probability of decision feedback equalization," *IEEE Trans. Inf. Theory*, vol. 39, no. 1, pp. 145–156, Jan. 1993, doi: 10.1109/18.179351.
- [88] V. Houtsma and D. van Veen, "A Study of Options for High-Speed TDM-PON Beyond 10G," *J. Light. Technol.*, vol. 35, no. 4, pp. 1059–1066, Feb. 2017, doi: 10.1109/JLT.2016.2638121.

- [89] Golub Gebe H., Van Loan Charles F., *Matrix Computations*, 3rd ed. Baltimore: John Hopkins, 1996.
- [90] "White Paper on 50G-PON Technology," p. 26.
- [91] F. A. N. Sampaio, N. Genay, E. Pincemin, R. L. Bidan, Y. Jaouen, and F. Bourgart, "Study of Minimum Mean Square Error Optimal Equalizers for 50Gbit/s High Speed Passive Optical Networks," in *OSA Advanced Photonics Congress 2021 (2021)*, paper SpF1E.2, Optica Publishing Group, Jul. 2021, p. SpF1E.2. doi: 10.1364/SPPCOM.2021.SpF1E.2.
- [92] M. S.-B. Hossain *et al.*, "Transmission Beyond 200 Gbit/s With IM/DD System for Campus and Intra-Datacenter Network Applications," *IEEE Photonics Technol. Lett.*, vol. 33, no. 5, pp. 263–266, Mar. 2021, doi: 10.1109/LPT.2021.3056005.
- [93] G. Forney, "Maximum-likelihood sequence estimation of digital sequences in the presence of intersymbol interference," *IEEE Trans. Inf. Theory*, vol. 18, no. 3, pp. 363–378, May 1972, doi: 10.1109/TIT.1972.1054829.
- [94] G. Bosco, P. Poggiolini, and M. Visintin, "Performance Analysis of MLSE Receivers Based on the Square-Root Metric," *J. Light. Technol.*, vol. 26, no. 14, pp. 2098–2109, Jul. 2008, doi: 10.1109/JLT.2008.920135.
- [95] W.-H. Sheen and G. L. Stuber, "MLSE equalization and decoding for multipath-fading channels," *IEEE Trans. Commun.*, vol. 39, no. 10, pp. 1455–1464, Oct. 1991, doi: 10.1109/26.103040.
- [96] O. E. Agazzi, M. R. Hueda, H. S. Carrer, and D. E. Crivelli, "Maximum-likelihood sequence estimation in dispersive optical channels," *J. Light. Technol.*, vol. 23, no. 2, pp. 749–763, Feb. 2005, doi: 10.1109/JLT.2004.838870.
- [97] R. Rosales *et al.*, "Achieving high budget classes in the downstream link of 50G-PON," *J. Opt. Commun. Netw.*, vol. 13, no. 8, pp. D13–D21, Aug. 2021, doi: 10.1364/JOCN.426009.
- [98] Raphaël Le Bidan, "Algorithmes de détection en présence d'interférence entre symboles," France Telecom, France Telecom, May 03, 2008.
- [99] G. D. Forney, "The viterbi algorithm," *Proc. IEEE*, vol. 61, no. 3, pp. 268–278, Mar. 1973, doi: 10.1109/PROC.1973.9030.
- [100] I. Stamoulias, K. Georgoulakis, S. Blionas, and G. O. Glentis, "FPGA implementation of an MLSE equalizer in 10Gb/s optical links," in *2015 IEEE International Conference on Digital Signal Processing (DSP)*, Jul. 2015, pp. 794–798. doi: 10.1109/ICDSP.2015.7251985.
- [101] Fraunhofer, "Electroabsorption-Modulated Lasers (EML) for 100G/400G." [Online]. Available: https://www.hhi.fraunhofer.de/fileadmin/PDF/PC/LAS/20200107_Electroabsorption-modulated_lasers__EML__for_100G400G_NEU.pdf
- [102] R. Le Bidan, "Performance of MMSE-AE with quantized inputs," Dept MEE, IMT Atlantique, Bretagne-Pays de la Loire École Mines Télécom, Dept MEE, IMT Atlantique, Bretagne-Pays de la Loire École Mines Télécom, Jun. 16, 2021.

Titre: Etude des techniques de compensation numérique pour les réseaux d'accès optique 50G-PON

Mots clés : égalisation, modulation d'intensité, réseau optique passif.

Résumé : Au cours des prochaines années, les débits requis pour les réseaux d'accès seront immenses en raison de l'augmentation massive des appareils connectés et du nombre d'applications gourmandes en bande passante. Les réseaux optiques passifs (PON) sont le choix classique pour les réseaux d'accès car ils allient un faible coût et une capacité de débit de transmission élevée. Les chercheurs de l'industrie travaillent au sein des groupes de normalisation ITU-T et IEEE à augmenter la capacité d'un canal optique de 10 Gbit/s vers 25 Gbit/s, 50 Gbit/s et même 100 Gbit/s. Cette thèse se concentre sur les techniques de compensation numérique pour le 50G-PON parce que c'est l'évolution qui devrait être déployée en premier sur le terrain et que le canal optique est gravement impacté par la dispersion chromatique, le chirp, la limitation de la bande passante et l'atténuation. Le travail a été organisé comme suit :

- Nous avons étudié la compensation des interférences intersymbole (ISI) via l'égalisation linéaire, l'égalisation à retour de décision (LE et DFE respectivement) basées sur le critère d'erreur quadratique moyenne minimale (MMSE), et montré comment prédire les performances de l'égaliseur au moyen d'équations simples, sur la base d'un modèle du canal. Ensuite, l'utilisation d'un récepteur optimal au sens du maximum de vraisemblance (MLSE).
- Enfin, nous avons réalisé des transmissions expérimentales dans le laboratoire 50Gbit/s d'Orange ensuite le traitement numérique des signaux obtenus. Les mesures expérimentales ont conforté le modèle IM/DD simulé, et les trois récepteurs basés sur le DSP ont été évalués en conditions réelles.

Title: Study of digital compensation techniques for 50G-PON optical access networks

Keywords : equalization, intensity modulation, passive optical network.

Abstract : Over the next years, the required bit rates for access networks are immense due to the massive increase of connected devices and bandwidth-hungry applications. Passive Optical Networks (PON) are the conventional choice for access works because they ally low cost and have high transmission rate capacity. As industry researchers participating in standardization committees ITU-T and IEEE target increasing the single channel capacity from 10 Gbit/s to 25Gbit/s, 50Gbit/s, and even 100 Gbit/s, this thesis focuses on digital compensation techniques for the 50G-PON since the optical channel is critically impaired by chromatic dispersion, chirp, bandwidth limitation, and attenuation. The work was organized as follows:

- We used two models that approximate the real conditions of a PON based on Intensity Modulation and Direct Detection (IM/DD), a small-signal model constructed in MATLAB© and a large signal model via VPI Transmission Maker™.
- We perform Intersymbol Interference (ISI) compensation through Minimum Mean Square Error (MMSE) based equalization and Maximum Likelihood Sequence Detection (MLSE). Also, closed-form equations were used to predict the performance of the equalizers.
- Finally, we realized experimental transmissions in Orange's 50Gbit/s laboratory followed by offline processing. The experimental measurements were compared to the simulated IM/DD model, and the three DSP-based receivers were evaluated in practice.